

CHAPTER 3

INTENSIVE STUDIES OF SIERRA CLOUDWATER  
CHEMISTRY AND ITS  
RELATIONSHIP TO PRECURSOR  
AEROSOL AND GAS CONCENTRATIONS

## Introduction

The initial chemical composition of cloudwater has been shown to be determined largely by the composition of the aerosol that serve as condensation nuclei and the ambient concentrations of soluble gases (Jacob et al., 1985, 1986, a, b, 1987). The composition is altered as additional aerosol is scavenged and chemical reactions take place within the droplet. In order to understand what influences cloudwater chemistry at a particular location, therefore, it is necessary to understand the processes that control local concentrations of aerosol and gases, particularly during the period immediately preceding cloud formation. These processes include emission rates, atmospheric reactions, transport routes, and deposition.

Concentrations of most inorganic aerosol and gas phase species in the southern and central Sierra Nevada of California are controlled primarily by meteorological conditions affecting transport from distant sources. Figure 1 illustrates the location of the Sierra relative to the population centers of central California. Both the San Joaquin Valley and the San Francisco Bay area are thought to be important pollutant source regions affecting air quality in the central and southern Sierra. Local Sierra sources of species such as  $\text{SO}_2$ ,  $\text{NO}_x$ , and  $\text{NH}_3$  are relatively unimportant by comparison.

A conceptual model of transport within the San Joaquin Valley has been described by Smith et al. (1981). Meteorology is normally dominated by the presence of high mountains that border the valley on three sides. Net air flow into the valley is from the northwest for all months except January and February. Mass continuity requires the existence of a compensating flow out of the valley. The most

effective exit transport mechanism is thought to be a continuation of the northwesterly flow over the Tehachapi Mountains at the southeastern end of the valley. Afternoon upslope flows on both sides of the valley, induced by preferential heating of the air along the mountain slopes, are thought to play a secondary role in transporting air out of the valley. The upslope flows form the primary mechanism for transport of air parcels from the Valley floor up to the slopes of the Sierra.

Temperature inversions in the air mass above the San Joaquin Valley floor are strongest in the winter, but occur frequently throughout the year (Smith et al., 1981). The presence of the mountains surrounding the valley combines with an inversion to trap pollutants within the valley. The passage of frontal systems through the valley can serve to alleviate this condition by eliminating the temperature inversion, thus permitting pollutants to mix up to elevations where they may exit over the Tehachapi Mountains. Increased wind speeds often associated with the fronts also aid in the removal of valley pollutants. Frontal systems may also change the direction of predominant air flow within the valley from northwesterly to southerly, thereby altering the importance of various regional emissions to Sierra air quality.

Past studies have indicated that pollutant concentrations at Lower Kaweah (elev. 6240 feet) in Sequoia National Park (see Figure 1) are significantly affected by the passage of cold fronts. Collett et al. (1989) observed increasing concentrations of aerosols and gases as a cold front approached (see also Chapter 1). It was speculated that the increases were due, at least in part, to increases in vertical mixing within the valley. Cahill et al. (1986) observed a similar trend for concentrations of fine particle sulfur, and attributed the increase to synoptic scale changes accompanying the cold front which led to increased southerly air flow from

the Bakersfield area. Large quantities of  $\text{SO}_2$  are released to the atmosphere in conjunction with oil field activities in the vicinity of Bakersfield.

Increases in aerosol and gas concentrations with the advance of cold fronts may significantly affect the chemical composition of the cloudwater produced in the storm system. The mechanism by which these increases occur (e.g. increased vertical mixing, increased southerly flow, or both) may affect the balance between different species (e.g.  $\text{NO}_3^-$  vs.  $\text{SO}_4^{2-}$ , or acids vs. bases) in the air mass and in the cloudwater, since different pollutant source regions have different emission signatures.

This chapter describes the results of a study to investigate more completely the behavior of aerosol and gas concentrations at Lower Kaweah in conjunction with the advance of a cold front through the region, and how those concentrations were reflected in the chemistry of the cloudwater associated with the front. The study also was designed to examine the composition of cloudwater collected simultaneously at two different elevations. The results of that investigation are described here as well, including a discussion of concentrations of organic acids, carbonyls, S(IV), and  $\text{H}_2\text{O}_2$  in the cloudwater.

## Experimental Procedure

In order to investigate spatial and temporal variations of aerosol and gas concentrations during the study, three sampling stations were established: Visalia (elev. 300 feet), Ash Mountain (1800 feet), and Lower Kaweah (6240 feet). Aerosol and gas phase samples were collected using a filter pack technique. Teflon filters (Gelman Zefluor, 1  $\mu\text{m}$  pore size) were used to collect aerosol for determination of

major ions. A pair of oxalic acid-impregnated quartz fiber backup filters was used to collect  $\text{NH}_3$ . A nylon filter was used to collect  $\text{HNO}_3$ . Each of the stations was equipped with two automated aerosol collectors (see Figure 2) to enable simultaneous collection of samples at all three sites. Each collector can hold up to three sets of filter packs at one time and features a programmable timer to enable automated sampling during three separate time periods. Flow rates through the filter packs ( $10.8 \text{ l} \cdot \text{min}^{-1}$ ) are controlled by critical orifices.

Consecutive six-hour samples were collected continuously at the three sites during the period from 0100 PST on April 26, 1988 to 1300 PST on April 29, 1988, except for the morning of April 28, when the schedule was altered at Lower Kaweah due to the presence of intercepting clouds. Filters were picked up from Visalia and Ash Mountain between 1100 and 1300 PST daily. Those at Lower Kaweah were retrieved at least twice daily. Retrieved filters were placed individually in covered petri dishes and stored in sealed plastic bags at  $4^\circ\text{C}$  until analyzed. The quartz filters were extracted in distilled de-ionized water ( $\text{D}^2\text{H}_2\text{O}$ ); the Teflon filters were wetted with ethanol and extracted in  $\text{D}^2\text{H}_2\text{O}$ ; the nylon filters were extracted in a bicarbonate/carbonate solution. Filter extracts were analyzed by the methods described below for the analysis of cloudwater samples.

Cloudwater samples were collected with two Caltech Active Strand Cloudwater Collectors (CASCC). A complete description of the CASCC (Daube et al., 1987) is given in Chapter 5. One CASCC was co-located at the Lower Kaweah research site with the regular automated cloudwater sampling system (see Chapter 2) and the automated aerosol collector. This CASCC, equipped with a rain-excluding inlet, was powered by a 12 V power supply. The second CASCC was operated using a 12 V deep-cycle marine battery, enabling a second sampling

location to be selected during a cloud interception event without power requirement restrictions. The site selected is located at approximately 6450 feet elevation near Moro Rock, 1.5 miles southeast of Lower Kaweah. The second CASCC was operated without a rain-excluding inlet. Samplers at both sites were operated manually. Samples were collected over half-hour intervals.

Cloudwater samples were weighed immediately after collection to determine their volume. An aliquot of each sample was removed to determine sample pH. A Radiometer PHM80 Standard pH meter with a GK2320C semi-micro combination electrode calibrated with pH 4 and 7 buffers was used to measure the pH. Small aliquots of sample also were removed and treated to stabilize reactive species. S(IV) was stabilized as the hydroxymethanesulfonate by adding buffered  $\text{CH}_2\text{O}$  (Dasgupta et al., 1980).  $\text{CH}_2\text{O}$  was reacted with  $\text{NH}_4^+$ -acetylacetone (Nash, 1953) to form 3,5-dihydro-1,4-dihydrolutidine (DDL), which is stable for several weeks (Reitz, 1980). A buffered solution of p-OH phenylacetic acid (POPA) and peroxidase was used to preserve peroxides (Lazrus et al., 1985) by formation of the dimer. Carboxylic acids were preserved by addition of chloroform (Keene et al., 1984). Carbonyls were derivatized with 2,4-dinitro-phenylhydrazine (DNPH) in acidic solution (Grosjean and Wright, 1983). Samples and aliquots were stored at 4 °C until analysis.

The major ions,  $\text{Cl}^-$ ,  $\text{NO}_3^-$ , and  $\text{SO}_4^{2-}$ , were measured in our laboratory using a Dionex 2020i ion chromatograph with a Dionex AS4A column and a 2.8 mM  $\text{HCO}_3^-$ /2.2 mM  $\text{CO}_3^{2-}$  eluent.  $\text{Na}^+$ ,  $\text{Ca}^{2+}$ ,  $\text{Mg}^{2+}$ , and  $\text{K}^+$  concentrations were measured using a Varian Techtron AA6 atomic absorption spectrophotometer. An air/acetylene flame was used for  $\text{Na}^+$  and  $\text{K}^+$ ;  $\text{N}_2\text{O}$ /acetylene was used for  $\text{Ca}^{2+}$  and  $\text{Mg}^{2+}$  to minimize interferences.  $\text{NH}_4^+$  was measured by the phenol-hypochlorite

method (Solorzano, 1967) using an Alpkem flow injection analyzer.

The stabilized  $\text{CH}_2\text{O}$  was measured by absorption at 412 nm, after addition of  $\text{I}_2$  to accelerate the decomposition of sulfonates (Smith and Erhardt, 1975).  $\text{S(IV)}$  was analyzed by the pararosaniline method (Dasgupta, 1981). This method was adapted for flow injection analysis. Peroxide was measured by the fluorescence of the POPA dimer (Lazrus et al., 1985). This method is sensitive to both  $\text{H}_2\text{O}_2$  and some organic peroxides; however, the significantly lower Henry's Law coefficients of  $\text{CH}_3\text{OOH}$  and peroxyacetic acid suggest that they will not be found at significant concentrations in cloudwater (Lazrus et al., 1985). Carboxylic acids were measured using ion exclusion chromatography. A Dionex ICE-AS1 column was employed with dilute HCl as the eluent.

The dinitrophenylhydrazone derivatives of carbonyls were extracted three times in 60/40 (v/v) hexane/dichloromethane after adding cyclohexanone 2,4-dinitrophenylhydrazone (Aldrich) as an internal standard. The organic fraction was washed with  $\text{D}^2\text{H}_2\text{O}$  to remove excess acid and unreacted DNPH, and then evaporated to dryness under a stream of  $\text{N}_2$ . The extracted and dried hydrazones were refrigerated until analysis. Previous work has shown that the derivatives are stable during storage (Munger et al., 1989). Immediately before analysis the residue was dissolved in tetrahydrofuran (THF). The derivatized carbonyls were separated by HPLC on a C18 column (Alltech Spherisorb ODS-2), using 45/27.5/27.5 (v/v/v)  $\text{H}_2\text{O}/\text{CH}_3\text{CN}/\text{THF}$  as the mobile phase. Aldehydes and ketones were determined by absorbance at 365 nm; each analysis was repeated at 430 nm to determine the dicarbonyls, which absorb at a higher wavelength. Standards were prepared from carbonyl hydrazones that were previously synthesized and purified.

## Results and Discussion

### *Aerosol and Gases*

The dominant species observed in the aerosol at Visalia, Ash Mountain, and Lower Kaweah were  $\text{NO}_3^-$ ,  $\text{SO}_4^{2-}$ , and  $\text{NH}_4^+$  (see Table 1). Smaller concentrations of  $\text{Na}^+$ ,  $\text{K}^+$ ,  $\text{Ca}^{2+}$ ,  $\text{Mg}^{2+}$ , and  $\text{Cl}^-$  also were observed. No attempt was made to measure organic aerosol in this study. By comparing the ratio of  $\text{NH}_4^+$  to the sum of  $\text{NO}_3^-$  and  $\text{SO}_4^{2-}$ , the relative neutrality of the aerosol, with respect to the dominant species, may be examined. The results of this calculation, presented in Figure 3, indicate that the aerosol at all three sampling locations was essentially neutral during the period studied.

Figure 4 presents the results for a similar acid-base balance that has been expanded to include gas phase concentrations of  $\text{NH}_3$  and  $\text{HNO}_3$ . When these gas phase concentrations are included, the air mass at Visalia is seen to be consistently basic, due to large inputs of  $\text{NH}_3$ . Excess acid neutralizing capacity at Visalia, in the form of  $\text{NH}_3$ , has been observed in past investigations (Jacob et al., 1986); during the same study, fogwater formed in the region was found to consistently have a very high pH (range: 5.5-7.2), due to the high  $\text{NH}_3$  inputs. The high density of cattle feed-lots surrounding Visalia (see Figure 5) are most likely the predominant source of  $\text{NH}_3$  for the region. The air masses sampled at both Ash Mountain and Lower Kaweah were found to be considerably less basic than those observed at Visalia during the study period. However, samples from both sites were observed to be somewhat basic, with those from Ash Mountain more basic than Lower Kaweah samples.

Excess base in samples collected at Visalia exceeded excess base in samples at Ash Mountain on both an absolute basis and a relative basis (see Figure 6). The same is true of the comparison between Ash Mountain and Lower Kaweah, for those samples collected during the first two-thirds of the study period. The samples collected after sunrise on April 28, however, had essentially equivalent ratios of base to acid. The difference in base/acid ratios between sampling locations is one indication that the air mass observed at the upper site, in each comparison, is not simply a diluted version of the air mass observed at the lower site. Either some other change is taking place as air is transported from Visalia to Ash Mountain to Lower Kaweah on the upslope breezes (e.g. preferential deposition of gas phase  $\text{NH}_3$ , or gas phase production of  $\text{SO}_4^{2-}$  or  $\text{NO}_3^-$ ), or the air masses sampled at the upper two sites have at least some contribution from other source regions.

Examination of the ratio of N(V) to S(VI) also indicates that a simple dilution of air from the Visalia area, as it is transported in the upslope flow, does not account for the air mass compositions observed at the upper two sites (see Figure 7). The N(V)/S(VI) ratio was calculated as the sum of gas phase  $\text{HNO}_3$  ( $\text{nmole}\cdot\text{m}^{-3}$ ) and aerosol  $\text{NO}_3^-$  ( $\text{neq}\cdot\text{m}^{-3}$ ), divided by aerosol  $\text{SO}_4^{2-}$  ( $\text{neq}\cdot\text{m}^{-3}$ ). The measured ratios at Ash Mountain and Lower Kaweah were quite similar during most of the sampling periods, typically hovering around one-half during the night and morning hours, when downslope winds predominate. During the daylight hours, the ratio often was observed to lie closer to one. The N(V)/S(VI) ratio at Visalia, meanwhile, was never observed to fall significantly below one and was often found to approach three. The observations at Visalia, like those at the other two sites, also indicated that the ratio shifted toward a predominance of N(V) during the daytime hours.

Surface winds at Visalia typically blew out of the northwest during the daytime and out of the southeast at night, throughout the study period (see Figure 8). Southerly winds have been observed at night on numerous occasions along the eastern edge of the San Joaquin Valley (Smith et al., 1981), and are believed to be the result of terrain-blocking of the predominant northwesterly flow at the valley's southern boundary. Increased vertical stability at night prevents the flow from exiting over the Tehachapi Mountains and forces it to return northward along the eastern valley boundary, establishing what has come to be known as the Fresno eddy. Since large emissions of  $\text{SO}_2$  occur in the southern San Joaquin Valley due to extensive oil field activity, a shift to southerly winds at night might be expected to result in an enrichment of  $\text{SO}_4^{2-}$  in nighttime aerosol at locations farther north, including Visalia. Concentrations of aerosol  $\text{SO}_4^{2-}$  at Visalia, however, were observed to be relatively constant over the study period (see Figure 9) and exhibited no strong correlation with either wind direction or time of day.

The changes in the ratio of N(V) to S(VI) at Visalia are actually the result of daytime increases in both aerosol  $\text{NO}_3^-$  concentrations and  $\text{HNO}_3$  concentrations. Concentrations of these species are depicted in Figure 10. These increases are most likely due to photochemical oxidation of  $\text{NO}_x$  emitted by morning traffic, both locally and in the larger cities located to the north.

An examination of the concentration vs. time profiles for the major aerosol species measured at Lower Kaweah reveals a substantial increase in concentrations on April 28, compared to the levels seen during the preceding two days. This is illustrated in Figures 11 through 13 for  $\text{NO}_3^-$ ,  $\text{SO}_4^{2-}$ , and  $\text{NH}_4^+$ . A similar pattern is apparent in the concentration profiles of these three species at Ash Mountain as well. Perhaps most notable is that concentrations of  $\text{NO}_3^-$ ,  $\text{SO}_4^{2-}$ , and  $\text{NH}_4^+$  in the

aerosol were consistently higher at Visalia than at the other two sites, until the afternoon of April 28. During that sampling period, concentrations of all three species essentially were equivalent at the three locations, possibly indicating that the air mass over the valley had become well mixed up to at least 6,000 feet.

At 1000 PDT on the morning of April 28, clouds were sighted below Lower Kaweah with an upper boundary of approximately 4,500 feet. These clouds, associated with the approach of a slow-moving cold front, gradually rose over the next few hours, enveloping the two cloudwater sampling locations. The approach of the frontal system appeared to increase mixing in the atmosphere above the valley floor. Vertical temperature profiles measured in the atmosphere over both Bakersfield and Fresno (Figure 14) indicated a substantial reduction in early morning stability on April 28, relative to the previous two days. These observations are consistent with the hypothesis that a decrease in atmospheric stability over the valley enabled pollutants, previously trapped near the valley floor, to mix up to higher elevations, consequently increasing pollutant loadings observed at both Ash Mountain and Lower Kaweah.

Gas phase concentrations of both  $\text{NH}_3$  and  $\text{HNO}_3$  at Lower Kaweah and Ash Mountain on the afternoon of April 28, however, were much lower than those observed at Visalia (see Figures 15 and 16). In fact, unlike the aerosol concentrations, they did not increase substantially above peak afternoon levels observed earlier in the week. This is not sufficient evidence, however, to conclude that these species were not mixed from the valley floor up to Lower Kaweah. Gas phase concentrations of both species are controlled by equilibrium with an aerosol phase. The equilibrium strongly depends on temperature and relative humidity. The high temperature observed on April 28 in Visalia was 27 °C (NOAA, 1988a),

and relative humidities along the length of the valley ranged from 45 to 55% during the afternoon and early evening (NOAA, 1988b, c). Based on these observations, along with the aerosol and gas phase data from Visalia, equilibrium predictions for the  $\text{H}_2\text{SO}_4\text{-NH}_3\text{-HNO}_3$  system indicate that 72% of the  $\text{NH}_3$  and 58% of the  $\text{HNO}_3$  should have resided in the gas phase (Pilinis and Seinfeld, 1987). The observations indicated 70% and 53%, respectively, resided in the gas phase; in good agreement with the equilibrium predictions. At Lower Kaweah, afternoon temperatures were approximately 5 °C; relative humidities exceeded the deliquescence point of  $\text{NH}_4\text{NO}_3$  ( $\approx 74\%$  at 278 K; Seinfeld, 1986) throughout the afternoon. Equilibrium calculations, utilizing these conditions and the observed aerosol and gas phase concentrations at the site, predict that 11% of the  $\text{NH}_3$  and 6% of the  $\text{HNO}_3$  should reside in the gas phase. The observations are once again in good agreement with these predictions: 11%  $\text{NH}_3$  and 7%  $\text{HNO}_3$ . The large differences in  $\text{NH}_3$  and  $\text{HNO}_3$  concentrations between Visalia and Lower Kaweah are not surprising in view of these circumstances.

Variations in the  $\text{HNO}_3\text{-NH}_3$  system aerosol-gas partition coefficients, as a function of temperature and relative humidity, imply that intersite comparisons of gas phase concentrations of  $\text{NH}_3$  and  $\text{HNO}_3$ , or aerosol concentrations of  $\text{NH}_4^+$  and  $\text{NO}_3^-$ , are not very meaningful under conditions experienced in this study. Given the large differences in temperature and relative humidity between the sampling locations, it is better to compare total concentrations of  $\text{N(-III)}$ , given by the sum of  $\text{NH}_3$  and  $\text{NH}_4^+$ , and  $\text{N(V)}$ , given by the sum of  $\text{HNO}_3$  and  $\text{NO}_3^-$ . Figure 17 illustrates the concentration vs. time profiles of  $\text{N(V)}$  for the three sites. While  $\text{N(V)}$  concentrations are seen to peak on the afternoon of April 28, as was observed for  $\text{NO}_3^-$  aerosol concentrations, differences in concentrations are maintained between the three sites.  $\text{N(-III)}$  concentrations at Lower Kaweah also are observed

to peak during the same period (see Figure 18), although the increase above levels seen earlier in the week is not as great as was observed in the case of N(V). Similar to N(V) concentrations, N(-III) concentrations maintain an elevational gradient, with Visalia exhibiting the highest concentrations. Concentration differences between the three sites, however, are significantly reduced for both N(V) and N(-III) on the afternoon of April 28.

While the vertical N(V) and N(-III) concentration profiles indicate that the air over the valley was not well-mixed to 6,000 feet, the observed decrease in atmospheric stability on April 28 still may have contributed significantly to the rise in pollutant levels observed both at Ash Mountain and Lower Kaweah. Both the velocity of the upslope flow, and the flow depth, have been found to increase with distance upward along the slope (Smith et al., 1981). These increases were attributed to contributions of heat and buoyancy by the sunlit slope to the flow. Increasing depth and velocity increase the total flux in the upslope flow, requiring entrainment of additional air from above the valley floor. Since the air in higher elevation layers is generally cleaner than air near the valley floor, the concentration of pollutants within the slope flow should decrease with elevation. A decrease in vertical stability above the valley floor, which allows pollutants previously trapped near the surface to mix up to higher elevations, will increase the concentrations of pollutants in the "dilution" air, preventing pollutant concentration levels in the upslope flow from decreasing as rapidly.

It is important to examine the behavior of wind patterns in the valley during this period to evaluate their potential for influencing pollutant levels at Lower Kaweah. Winds at Lower Kaweah typically follow a very predictable pattern (upslope flow during the day, downslope flow at night), driven by slope heating

effects. On at least one occasion, a break in this pattern has been observed, leading to continued upslope flow, even at night. This breakdown was observed in association with the passage of a strong frontal system. Disruption of the upslope-downslope flow pattern could account for increased pollutant loadings at elevated sites, particularly during the night and early morning, as was observed in past work (Collett et al., 1989). During this study, however, no significant breakdown was observed in the diurnal upslope-downslope flow pattern (see Figure 19). In fact, a slight decrease in the velocity of the daytime upslope flow was observed at Lower Kaweah, probably due to reduced solar heating of the slopes in the presence of cloud cover.

As indicated previously, increases in fine particle sulfur concentrations at Lower Kaweah have been observed in conjunction with the approach of a cold front (Cahill et al., 1986). The increase, observed at night during downslope flow conditions, was attributed to generation of southerly winds by the frontal system. In the current study, an increase in aerosol  $\text{SO}_4^{2-}$  was observed as the cold front approached. In this case, however, the April 28 rise in  $\text{SO}_4^{2-}$  concentrations was observed predominantly during upslope flow. Surface level winds at Visalia (Figure 8) blew from the south for a relatively short period of time on the morning of April 28. A much more extended southerly surface flow pattern was observed the previous morning. Vertical wind profiles measured in the atmosphere above Fresno on the mornings of April 26, 27, and 28 are depicted in Figure 20. These data also indicate that southerly flow was much more predominant at most elevations on April 27 than on April 28. Despite these observations, concentrations of  $\text{SO}_4^{2-}$  measured at Lower Kaweah were higher on April 28 than on April 27. This suggests that the increase in aerosol  $\text{SO}_4^{2-}$  observed in this study is not attributable predominantly to increased southerly flow from Bakersfield and the southern San

Joaquin Valley. Increased vertical mixing at Bakersfield, observed on the morning of April 28 (see Figure 14), however, may have allowed pollutants to mix up higher in the atmosphere than they could earlier in the study. Since upper level winds in the valley were still blowing from the south (see Figure 20), the increased mixing may have allowed southern San Joaquin Valley emissions to be transported more readily to Lower Kaweah.

Based on the preceding observations, it appears that, at least for the study period in question, the reduction in vertical stability, associated with the approach of the front, was the most important factor contributing to the rise in pollutant levels observed at Lower Kaweah and Ash Mountain. During the passage of a stronger frontal system, changes in wind direction (reflected either by a breakdown of the upslope-downslope flow at Lower Kaweah, or a strong increase in southerly flow) may play a more important role.

#### *Cloudwater*

Clouds began intercepting the hillside at Lower Kaweah at approximately 1100 PDT on April 28. By 1230 they had become dense enough to sample, and collection commenced. The battery powered CASCC was put into operation near Moro Rock at 1130, with the first sample collected from 1145 to 1200. Cloudwater was sampled continuously, in half-hour samples, until 1500 at Lower Kaweah, when the cloud base rose above the site, and until 1600 at Moro Rock, when the clouds dissipated. No rain was observed during the event. Concentrations of major inorganic ions, observed in the cloudwater samples collected at the two sites, are shown in Table 2. Concentrations of species observed in a blank taken by rinsing the collection surfaces of the CASCC at Moro Rock prior to sample collection also

are listed here. Blank concentrations of all species but  $K^+$  were negligible with respect to the concentrations observed in the cloudwater samples. The background concentration of  $1 \mu N K^+$  was significant only because such low concentrations were observed in the cloudwater (2-13  $\mu N$ ).

The pH of the cloudwater dropped continuously over the sampling period at both sites (Figure 21), falling from 4.75 to 4.34 at Moro Rock, and from 4.62 to 4.36 at Lower Kaweah. Comparison of cloudwater pH for those samples collected simultaneously at the two sites reveals that cloudwater sampled at Lower Kaweah had comparable, or slightly higher, free acidity than cloudwater at Moro Rock. The pH levels observed during this event were somewhat lower than those typically observed during the spring at Lower Kaweah (see Chapter 2). The drop in pH at both sites (corresponding to an 82% increase in  $H^+$  at Lower Kaweah and a 157% increase at Moro Rock) coincided with a decrease in the cloudwater ratio of  $NH_4^+$  to the sum of  $NO_3^-$  and  $SO_4^{2-}$ .

The composition of the cloudwater collected at both sites was dominated by concentrations of  $NO_3^-$ ,  $SO_4^{2-}$ , and  $NH_4^+$ . These ions were observed to be the dominant contributors in all of the samples collected at Lower Kaweah (see Chapter 2).  $NO_3^-$  and  $SO_4^{2-}$  concentrations represent the major inorganic contributions to atmospheric acidity provided by  $HNO_3$  and  $H_2SO_4$ .  $NH_4^+$  concentrations are indicative of the major inorganic contribution to neutralization of atmospheric acidity by  $NH_3$ . Concentrations of all three species are plotted in Figures 22 and 23 for samples collected at Lower Kaweah and Moro Rock, respectively. Concentrations at both sites were observed to rise toward the end of the sampling period. The rise in concentrations corresponded to an increase in visibility, and a decrease in the collection rate of the CASCC, at each site. Since the collection rate

of the CASCC depends on the liquid water content (LWC) of the clouds being sampled (see Chapter 5), it is possible that a decrease in cloud LWC may have been the cause of the concentration increases. This seems particularly likely since the concentrations at the two sites did not increase simultaneously, despite the fact that the sites are located relatively close to one another.

Calculated values of the cloud LWC, based on the theoretical collection efficiency of the CASCC and the observed cloudwater collection rate, are listed in Table 2. The performance of the two CASCCs used in the study differed slightly because of the use of a rain-excluding inlet on the Lower Kaweah collector. Corrections have been made to the estimates of LWC for each collector, utilizing laboratory measurements of the velocity across the impaction surface in the two collector configurations. Calculated values of LWC are averages over the length of each sample collection period. They range from 0.08 to 0.25 ml·m<sup>-3</sup> at Lower Kaweah and from 0.15 to 0.37 ml·m<sup>-3</sup> at Moro Rock.

By multiplying the cloudwater concentration of a species by the LWC, it is possible to obtain an estimate of the loading of that cloudwater species in the air mass sampled. Units of cloudwater loading are concentration per volume of air. Cloudwater loadings of NO<sub>3</sub><sup>-</sup>, SO<sub>4</sub><sup>2-</sup>, and NH<sub>4</sub><sup>+</sup> are presented in Figures 24 through 26. The loadings are fairly constant during the middle of the sampling period at both sites. Some fluctuations are apparent, however, near the beginning and the end of the event. These fluctuations appear to be correlated with changes in LWC. During periods of higher LWC, the cloudwater loadings of the three species increase; when LWC drops, the cloudwater loadings generally drop. This trend suggests that scavenging of N(V), S(VI), and N(-III) from the aerosol and gas phases may have been more efficient at higher LWC. Loadings observed at Moro Rock were

somewhat higher than those at Lower Kaweah. Since observed LWCs were also higher at Moro Rock, the differences in cloudwater loadings at the two sites are consistent with the hypothesis that higher LWC was responsible for more efficient scavenging by the cloudwater.

It is not unreasonable to expect that scavenging of small aerosol particles, which contain much of the  $\text{NH}_4^+$ ,  $\text{NO}_3^-$ , and  $\text{SO}_4^{2-}$  (Seinfeld, 1986), will be affected by changes in LWC. Variations in LWC observed during the event were most likely the product of changes in supersaturation of the air mass (increased supersaturation leading to increased LWC). At a given supersaturation, there is a critical minimum size for aerosol nucleation. Aerosol smaller than this size, about  $0.1 \mu\text{m}$  for typical cloud conditions (Mason, 1971), are scavenged through impaction and diffusion processes, which are less efficient than nucleation. As supersaturation in the cloud is increased, the critical size for nucleation is decreased, and small aerosol is scavenged with increased efficiency. This can lead to an increase in cloudwater loadings of those species contained in the small aerosol. Scavenging of  $\text{NH}_3$  and  $\text{HNO}_3$  from the gas phase is quite efficient at the pH values observed during this event and probably was not affected significantly by the changes in LWC.

It is important to point out that the observed changes in cloudwater loadings of  $\text{NO}_3^-$ ,  $\text{SO}_4^{2-}$ , and  $\text{NH}_4^+$  may have been due to causes other than variations in aerosol scavenging efficiency. The values of LWC are calculated using the cloudwater collection rate of the CASCC, assuming a collection efficiency that is independent of LWC. Past observations have revealed that clouds with higher LWC typically have a higher mass median droplet diameter (Best, 1951). Since the collection efficiency of the CASCC is greater for larger droplets, this implies that cloudwater in higher LWC clouds should be collected more efficiently. The error

associated with neglecting this effect introduces a bias into the estimates of LWC and, hence, cloudwater loadings. At higher LWC, the loadings tend to be overestimated; at lower LWC, they are underestimated. The magnitude of this error, however, is less than 5% over the range of LWC observed in the study, assuming that the droplet size distribution being sampled was not highly unusual. The fluctuations in cloudwater loadings significantly exceeded 5%.

Intermittent sampling of clear air parcels tends to reduce the half-hour average values of LWC and therefore leads to underestimation of values of cloudwater loading in the cloudy parcels of interest. Such a situation can occur when the clouds being sampled become "patchy", with interspersed volumes of cloudy and clear air, and is common at the upper and lower boundaries of a cloud. Visual observations during the study indicated that this phenomenon may have been important during the last half-hour of sampling at Lower Kaweah, when the lower cloud boundary was approaching the elevation of the site, but not during any other periods. No periods of "patchiness" were observed while sampling at Moro Rock. Lower estimates of LWC at Moro Rock toward the end of the sampling period, however, may partially be due to a decrease in the sampling efficiency of the CASCC, as the battery voltage dropped. The fan which draws the air through the CASCC was observed to slow somewhat during the final sampling period. The possible effects of patchiness at Lower Kaweah, and dropping battery voltage at Moro Rock, are limited primarily to the final half-hour sample at each site and do not affect the hypothesis of variations in aerosol scavenging efficiency during the rest of the sampling period.

Another potential explanation of the observed variations in values of cloudwater loading of the major species lies in the possibility that aerosol and gas

phase concentrations of these species, entering the bottom of the cloud in the upslope flow, may not have been constant. Indeed, data presented above illustrate that these concentrations vary considerably throughout the course of a day. However, the likelihood of the half-hour average concentrations varying by 20% from one period to the next, with no consistent trend, seems small given the regularity of the upslope flow in the region and the distance from emission sources. In addition, it seems more than mere coincidence that the variations in cloudwater loading are correlated so well with cloud LWC. Nevertheless, in the absence of short term aerosol and gas phase measurements, it is not possible to rule out variations in clear air loadings of these species as a source of variation in cloudwater loadings.

Total atmospheric loadings of N(V), S(VI), and N(-III), respectively, measured prior to, and following, the cloud interception event, are illustrated in Figures 24 through 26, along with the values of each species' cloudwater loading. (Measurements made during the cloud interception event have not been included due to uneven deposition of cloudwater droplets on the filter surfaces. The irregular pattern of deposition, associated with the orientation of the filters relative to the wind direction during periods of moderate to high wind speed, is a common problem in such environments). Comparison of the cloudwater loading of all three major species with these clear air loadings suggests that a large fraction of each species was incorporated into the cloudwater. Once again, in the absence of reliable short term aerosol and gas measurements during the sampling period, it is not possible to calculate accurate scavenging ratios.

Measurements of peroxide concentrations in cloudwater at the two sites ranged from 15 to 47  $\mu\text{M}$ , with those at Lower Kaweah consistently higher than

those at Moro Rock (see Table 3). As indicated previously, these concentrations are believed to represent primarily  $\text{H}_2\text{O}_2$ . Cloudwater loadings of  $\text{H}_2\text{O}_2$  are presented in Figure 27. During the first hour and a half of sampling, the loading was observed to increase substantially.  $\text{H}_2\text{O}_2$  loadings drop off, toward the end of the sampling period, at both sites. These drops, however, may be due largely to biases in the estimate of LWC toward the end of the event at each site, as discussed above. The high Henry's Law coefficient for  $\text{H}_2\text{O}_2$ ,  $1.4 \times 10^5 \text{ M} \cdot \text{atm}^{-1}$  at 293 K (Yoshizumi et al., 1984), indicates that  $\text{H}_2\text{O}_2$  will be scavenged almost entirely from the gas phase. Cloudwater loadings of  $\text{H}_2\text{O}_2$ , therefore, are good indicators of the total concentration of  $\text{H}_2\text{O}_2$  in the air mass. This implies that the increases in the total amount of  $\text{H}_2\text{O}_2$  in the cloudwater, during the first portion of sampling, may reflect increases in gas phase concentrations of  $\text{H}_2\text{O}_2$  entering the bottom of the cloud. Gas phase  $\text{H}_2\text{O}_2$  concentrations have been shown to be positively correlated with photolysis rates under slightly polluted conditions (Stockwell, 1986), so an increase at mid-day should be expected. It also is possible that aqueous phase production of  $\text{H}_2\text{O}_2$  contributed to the increase, although gas phase production typically is thought to dominate, particularly at the pH range observed in the current study (McElroy, 1986).

Aqueous phase oxidation of S(IV) to S(VI) by dissolved  $\text{H}_2\text{O}_2$  is the dominant pathway for production of  $\text{SO}_4^{2-}$  in cloudwater at pH values below 5 (Jacob and Hoffmann, 1983), as long as  $\text{H}_2\text{O}_2$  is available. Cloudwater concentrations of S(IV) at Lower Kaweah and Moro Rock, listed in Table 3, were not observed to be higher than  $6 \mu\text{M}$  in any of the samples. Given that Lower Kaweah was located near the cloud base, this indicates that in-cloud production of  $\text{SO}_4^{2-}$  was probably not important during this event.

Carboxylic acids, found in remote as well as urban areas (Keene et al., 1983), have both natural and anthropogenic sources. These include automotive exhaust, burning of biomass, and atmospheric oxidation of hydrocarbons (Talbot et al., 1988). Oxidation of isoprene, a natural hydrocarbon emitted from vegetation, may be a particularly important source of formic acid (Jacob and Wofsy, 1988), especially in a region like Sequoia National Park. Ratios of formate to acetate in fogwater samples previously collected on the floor of the San Joaquin Valley varied considerably (Munger et al., 1989), depending on sampling location. Samples collected in Visalia exhibited acetate concentrations in excess of formate concentrations, while samples from other locations often were more concentrated in formate. Cloudwater samples collected previously at Lower Kaweah were found to be enriched in formate, relative to acetate (Collett et al., 1989).

Short chain carboxylic acids were found to contribute significantly to the composition of the cloudwater sampled in this study. Formic acid was the predominant carboxylic acid in all of the samples. Concentrations of formic acid ranged from 22 to 24  $\mu\text{M}$ ; acetic acid concentrations ranged from 6 to 9  $\mu\text{M}$ ; and pyruvic acid concentrations ranged from 1 to 5  $\mu\text{M}$ . Differences between the concentrations of each of the species observed at the two sites are not statistically significant.

Concentrations of the conjugate bases (formate, acetate, and pyruvate) are listed in Table 4. These were calculated using the measured pH of each sample and the acid dissociation constant for each acid, adjusted for the ambient temperature. Due to the low  $\text{pK}_a$  values of formic and pyruvic acid, both of these species exist almost entirely in the deprotonated form in the pH range observed. Since the pH of the cloudwater was near the  $\text{pK}_a$  of acetic acid, approximately half the acetic acid

should exist in the samples as acetate.

The sum of the concentrations of formate, acetate, and pyruvate in each sample can be compared to the  $H^+$  concentration to estimate the maximum possible contribution of these weak acids to free acidity in the cloudwater. Results of this comparison, listed in Table 4, indicate that carboxylate concentrations measured about 200% of the  $H^+$  concentration at the start of the event and fell to about 60% of the  $H^+$  concentration by the end of the event. The maximum contribution of formate, acetate, and pyruvate to free acidity in these samples, therefore, dropped from 100% to 60% over the course of the event. This is a maximum contribution because the free acidity measured in the samples cannot be apportioned between the weak carboxylic acids and the strong mineral acids. In cloudwater from Sequoia National Park, in particular, much of the acidity introduced by these species is neutralized by  $NH_3$ , either in precursor aerosol or in the cloud droplets. Typically,  $H^+$  concentrations are only a small fraction of  $NH_4^+$  concentrations in samples collected in the region (Collett et al., 1989; Chapters 1 and 2).

A variety of carbonyl and dicarbonyl compounds are found in the atmosphere. A review of their chemistry has been provided recently by Finlayson-Pitts and Pitts (1986). Primary sources of carbonyl compounds include emissions from animal excretion, forest fires, and incomplete combustion processes (Carlier et al., 1986). While emission as primary compounds is common, the bulk of the total concentrations of these species in the atmosphere is believed to come from secondary sources. Formaldehyde, frequently observed at significant levels in fog and cloudwater (Munger et al., 1989), is a product of the oxidation of naturally occurring hydrocarbons including isoprene, while acetaldehyde is formed from the oxidation of amines, propene, and 2-butene (Finlayson-Pitts and Pitts, 1986).

Benzaldehyde, glyoxal, and methylglyoxal are formed from the oxidation of simple aromatic hydrocarbons such as toluene (Carrier et al., 1986, Finlayson-Pitts and Pitts, 1986), produced in engine exhaust. Glyoxal and methylglyoxal have been found, along with formaldehyde, at significant concentrations in fog samples collected in the mountains surrounding Los Angeles (Steinberg and Kaplan, 1984).

Concentrations of carbonyl and dicarbonyl compounds observed in the cloudwater samples collected at Moro Rock and Lower Kaweah are indicated in Table 5. During most periods, formaldehyde was the dominant species, with concentrations ranging from 8 to 14  $\mu\text{M}$ ; much lower than previously observed on the valley floor (6 to 498  $\mu\text{M}$ ; Munger et al., 1989). Second in importance was glyoxal, measured at concentrations between 5 and 13  $\mu\text{M}$ . Smaller concentrations of acetaldehyde, methylglyoxal, and benzaldehyde also were observed. A peak in the output of the ion chromatograph with a retention time matching the retention time of propanal in the standards was observed in most of the samples, but not in the blank. The peak was not definitely identified as a propanal peak, however, and may represent a combination of responses from three-carbon species in the samples. The area of these peaks indicated concentrations as high as 5  $\mu\text{M}$  in some of the samples, based on the propanal response in the standards. These concentrations are surprisingly high in view of the low solubility of these species in water, indicating that equilibrium gas phase concentrations must have been much higher than would normally be expected.

Glyoxal and methylglyoxal concentrations were at least two times less than those reported for fog by Steinberg and Kaplan (1984), although acetaldehyde concentrations were comparable. Benzaldehyde was only observed toward the end of the sampling period, at both sites, suggesting that it may have been associated

with emissions from morning traffic in the valley below, which require a few hours to be transported by the upslope flow to the elevation of the sampling sites.

## Conclusions

Measurements of major inorganic aerosol species are presented for three sites in central California during a four day period in April, 1988. Measurements were made at Visalia (elev. 300 feet), Ash Mountain (1800 feet) and Lower Kaweah (6240 feet). Concentrations of  $\text{NH}_3$  and  $\text{HNO}_3$  also were measured at these locations. Aerosol compositions were nearly neutral at all locations; however, large concentrations of  $\text{NH}_3$  at Visalia contributed significantly to the alkalinity of the total air mass there. Concentrations of all major species were observed to decrease from Visalia to Ash Mountain to Lower Kaweah during most of the sampling periods. Ratios of N(V) to S(VI) at Ash Mountain and Lower Kaweah were markedly different than those observed at Visalia, suggesting that at least some contribution to air quality at the higher elevations must come from another source area.

Concentrations at Ash Mountain and Lower Kaweah exhibited diurnal fluctuations, with peaks in the late afternoon, consistent with the transport of pollutants from San Joaquin Valley sources by daytime upslope winds. Concentrations of most of these species reached a maximum at Ash Mountain and Lower Kaweah on April 28, increasing as a weak cold front approached. Concentrations at Visalia were somewhat lower on April 28 than earlier in the week. A reduction in atmospheric stability above the valley on April 28, associated with the approach of the storm system, appears to have contributed to the increased concentrations observed at the upper two sites by allowing pollutants previously

trapped near the valley floor to mix up to higher elevations. Upper level wind data indicate that at least part of the air mass sampled at Lower Kaweah and Ash Mountain on April 28 may have passed over the southern San Joaquin Valley.

Clouds began intercepting the hillside at Lower Kaweah at approximately 1100 PDT on April 28. Five cloudwater samples were collected at Lower Kaweah, while nine were obtained at a second site 1.5 miles southeast and 200 feet higher in elevation (Moro Rock). The pH of the cloudwater at both sites was observed to fall throughout the course of the event, dropping as low as 4.34.  $\text{NO}_3^-$ ,  $\text{SO}_4^{2-}$ , and  $\text{NH}_4^+$  were the major inorganic species observed in the cloudwater. The cloudwater pH drop coincided with an increase in the ratio of  $\text{NH}_4^+$  to the sum of  $\text{NO}_3^-$  and  $\text{SO}_4^{2-}$ .

The clouds sampled at Moro Rock were more dense than those sampled at Lower Kaweah. Concentrations of major ions were correspondingly lower at Moro Rock. The clouds appeared to scavenge a large fraction of the aerosol  $\text{NO}_3^-$ ,  $\text{SO}_4^{2-}$ , and  $\text{NH}_4^+$ , as well as the gas phase  $\text{HNO}_3$  and  $\text{NH}_3$ . Total loadings of  $\text{NO}_3^-$ ,  $\text{SO}_4^{2-}$ , and  $\text{NH}_4^+$  in the cloudwater were positively correlated with cloud liquid water content, suggesting that scavenging efficiencies for these particles may have been similarly correlated. Short term aerosol and gas measurements needed to confirm this hypothesis are not available.

$\text{H}_2\text{O}_2$  was observed at significant concentrations in the cloudwater, ranging from 15 to 47  $\mu\text{M}$ . S(IV) concentrations were  $\leq 6 \mu\text{M}$  in all samples, even near cloud base, indicating that aqueous phase production of  $\text{SO}_4^{2-}$  was probably not important during this event. Significant concentrations of formic and acetic acids were observed. Carbonyl concentrations in the cloudwater were dominated by formaldehyde and glyoxal.

## Acknowledgments

We are grateful to the National Park Service, particularly the research staff at Sequoia National Park, for granting us access to sites within the Park. We gratefully acknowledge the California Air Resources Board for providing access to the sampling site in Visalia and for providing financial support for this project (CARB contract #A6-185-32).

## REFERENCES

- Best, A. C. (1951) Drop-size distribution in cloud and fog. *Q. Jl. R. met. Soc.* 77, 418-426.
- Cahill, T. A., Annegarn, H., Ewell, D. and Feeney, P. J. (1986) Particulate monitoring for acid deposition research at Sequoia National Park California. Final report to California Air Resources Board, Sacramento, CA.
- Carlier, P., Hannachi, H. and Mouvier, G. (1986) The Chemistry of carbonyl compounds in the atmosphere - A Review. *Atmos. Environ.* 20, 2079-2099.
- Collett, J., Jr., Daube, B., Jr., Munger, J. W. and Hoffmann, M. R. (1989) Cloudwater chemistry in Sequoia National Park. *Atmos. Environ.*, in press.
- Daube, B. C., Jr., Flagan, R. C. and Hoffmann, M. R. (1987) *Active Cloudwater Collector*. United States Patent # 4,697,462, Oct. 6, 1987.
- Dasgupta, P. K., DeCesare, K. and Ullrey, J. C. (1980) Determination of atmospheric sulfur dioxide without tetrachloromercurate (II) and the mechanism of the Schiff reaction. *Anal. Chem.* 52, 1912-1922.
- Dong, S. and Dasgupta, P. K. (1987) Fast fluorimetric flow injection analysis of formaldehyde in atmospheric water. *Environ. Sci. Technol.* 21, 581-588.
- Finlayson-Pitts, B. J. and Pitts, J. N., Jr. (1986) *Atmospheric Chemistry: Fundamentals and Experimental Techniques*. John Wiley, New York, 1098 p.
- Graedel, T. E., Hawkins, D. T. and Claxton, L. D. (1986) *Atmospheric chemical compounds: Sources, occurrence, and bioassay*. Academic Press, New York.
- Grosjean, D. 1982. Formaldehyde and other carbonyls in Los Angeles ambient air. *Environ. Sci. Technol.* 16, 254-262.

Grosjean, D. and Wright, B. 1983. Carbonyls in urban fog, ice fog, and cloudwater and rainwater. *Atmos. Environ.* 17,2093-2096.

Jacob, D. J. and Hoffmann, M. R. (1983) A dynamic model for the production of  $H^+$ ,  $NO_3^-$ , and  $SO_4^{2-}$  in urban fog. *J. Geophys. Res.*, 88, 6611-6621.

Jacob, D. J., Waldman, J. M., Munger, J. W. and Hoffmann, M. R. (1985) Chemical composition of fogwater collected along the California coast. *Envir. Sci. Technol.* 19, 730-736.

Jacob, D. J., Munger, J. W., Waldman, J. M. and Hoffmann, M. R. (1986a) The  $H_2SO_4$ - $HNO_3$ - $NH_3$  system at high humidities and in fogs: I. Spatial and temporal patterns in the San Joaquin Valley of California. *J. Geophys. Res.* 91, 1073-1088.

Jacob, D. J., Waldman, J. M., Munger, J. W. and Hoffmann, M. R. (1986a) The  $H_2SO_4$ - $HNO_3$ - $NH_3$  system at high humidities and in fogs: II. Comparison of field data with thermodynamic calculations. *J. Geophys. Res.* 91, 1089-1096.

Jacob, D. J., Shair, F. H., Waldman, J. M., Munger, J. W. and Hoffmann, M. R. (1987) Transport and oxidation of  $SO_2$  in a stagnant foggy valley. *Atmos. Environ.* 21, 1305-1314.

Jacob, D. J. and Wofsy, S. C. (1988) Photochemical production of carboxylic acids in a clean continental atmosphere, in *Acid Deposition Processes at High Elevation Sites*, edited by H. M. Dunsworth, D. Reidel, Hingham, Mass. (in press).

Kawamura, K., Ng, L. L. and Kaplan, I. R. (1985) Determination of organic acids ( $C_1$ - $C_{10}$ ) in the atmosphere, motor exhausts, and engine oils, *Environ. Sci. Technol.* 19, 1082-1086.

Kawamura, K. and Kaplan, I. R. (1984) Capillary gas chromatography determination of volatile organic acids in rain and fog samples. *Anal. Chem.* 56, 1616-1620.

Keene, W. C. and Galloway, J. N. (1984) Organic acidity in precipitation of North America. *Atmos. Environ.* 18, 2491-2497.

Keene, W. C. and Galloway, J. N. (1986) Considerations regarding sources for formic and acetic acids in the troposphere. *J. Geophys. Res.* 91, 14466-14474.

Keene, W. C., Galloway, J. N. and Holden, J. D. (1983) Measurement of weak organic acidity in precipitation from remote areas of the world. *J. Geophys. Res.* 88, 5122-5130.

Lazrus, A., Kok, G. L., Gitlin, S. N., Lind, J. A. and McLaren, S. E. (1985) Automated fluorometric method for hydrogen peroxide in atmospheric precipitation. *Anal. Chem.* 57, 917-922.

Mason, B. J. (1971) *The Physics of Clouds*, 2<sup>nd</sup> Ed., Oxford University Press, London.

McElroy, W. J. (1986) Sources of hydrogen peroxide in cloud water. *Atmos. Environ.* 20, 427-438.

Munger, J. W., Collett, J., Jr., Daube, B. D., Jr. and Hoffmann, M. R. (1989) Carboxylic acids and carbonyl compounds in southern California clouds and fogs. *Tellus*, in press.

Nash, T. (1953) The colorimetric estimation of formaldehyde by means of the Hantzsch reaction. *Biochem. J.* 55, 416-421.

National Oceanic and Atmospheric Administration (1988a) California climatological data, April 1988, 92, No. 4, 52 p.

National Oceanic and Atmospheric Administration (1988b) Local climatological data - Bakersfield, CA, April 1988, available from the National Climatic Data Center, Asheville, NC, 4 p.

National Oceanic and Atmospheric Administration (1988c) Local climatological data – Fresno, CA, April 1988, available from the National Climatic Data Center, Asheville, NC, 4 p.

Pilinis, C. and Seinfeld, J. H. (1987) Continued development of a general equilibrium model for inorganic multicomponent atmospheric aerosols. *Atmos. Environ.* 21, 2453–2466.

Reitz, E. B. (1980) The stabilization of small concentrations of formaldehyde in aqueous solutions. *Analyt. Lett.* 13, 1073–1084.

Seinfeld, J. H. (1986) *Atmospheric Chemistry and Physics of Air Pollution*, John Wiley. New York, 738 pp.

Smith, R. V. and Erhardt, P. W. (1975) Nash determination for formaldehyde in the presence of bisulfite. *Anal. Chem.* 47, 2462–2454.

Smith, T. B., Lehrman, D. E., Reible, D. D. and Shair, F. H. (1981) The origin and fate of airborne pollutants within the San Joaquin Valley. Final Report to California Air Resources Board, Sacramento, CA.

Solorzano, L. (1967) Determination of ammonia in natural waters by the phenol–hypochlorite method. *Limnol. Oceanogr.* 14, 799–801.

Steinberg, S. and Kaplan, I. R. (1984) The determination of low molecular weight aldehydes in rain, fog, and mist by reversed phase liquid chromatography of the 2,4–dinitrophenyl hydrazone derivatives. *Intern. J. Environ. Anal. Chem.* 18, 253–266.

Stockwell, W. R. (1986) A homogeneous gas phase mechanism for use in a regional acid deposition model. *Atmos. Environ.* 20, 1615–1632.

Talbot, R. W., Beecher, K. M., Harriss, R. C. and Cofer, W. R., III. (1988) Atmospheric geochemistry of formic and acetic acids at a mid–latitude temperate site. *J. Geophys. Res.* 93, 1638–1652.

Yoshizumi, K., Aoki, K., Nouchi, I., Okita, T., Kobayashi, T., Kamakura, S. and Tajima, M. (1984) Measurements of the concentration in rainwater and of the Henry's law constant of hydrogen peroxide. *Atmos. Environ.* 18, 395-401.

Table 1. Aerosol and Gas Composition: 1988

Date	Time	Na <sup>+</sup>	NH <sub>4</sub> <sup>+</sup>	Ca <sup>2+</sup>	Mg <sup>2+</sup>	Cl <sup>-</sup>	NO <sub>3</sub> <sup>-</sup>	SO <sub>4</sub> <sup>2-</sup>	NH <sub>3</sub>	HNO <sub>3</sub>
		← neq · m <sup>-3</sup> →						← nmole · m <sup>-3</sup> →		
LOWER KAWEAH										
4/26	0100-0700	0.0	18.0	9.8	3.0	0.8	5.1	13.4	42.8	4.1
4/26	0700-1300	0.0	12.7	7.1	4.5	0.0	5.4	10.3	22.2	0.0
4/26	1300-1900	0.0	35.3	8.5	3.0	0.0	11.2	30.6	66.5	17.1
4/27	0100-0700	0.0	30.7	16.1	4.5	0.5	9.1	26.2	10.7	2.2
4/27	0700-1300	0.0	24.4	6.9	3.0	0.0	8.6	12.3	43.3	9.1
4/27	1300-1900	0.0	73.7	6.4	3.6	0.0	32.0	35.8	61.1	17.0
4/27	1900-0100	0.0	66.5	7.8	4.5	0.5	16.8	47.8	18.9	4.6
4/28	0100-0700	0.0	70.5	6.4	2.1	0.0	21.2	50.4	8.6	2.1
4/28	0700-1130	1.5	98.1	8.6	3.9	0.3	54.4	40.5	37.9	3.4
4/28	1530-1900	0.0	166.3	6.2	3.5	3.3	88.4	78.9	15.7	1.1
4/28	1900-0100	0.0	93.8	9.1	4.1	0.0	36.3	44.2	12.2	1.0
4/29	0100-0700	0.0	39.3	7.8	3.0	0.0	9.0	32.9	6.3	0.3
4/29	0700-1300	0.3	101.6	7.7	4.5	0.0	38.8	64.0	21.2	3.5
ASH MOUNTAIN										
4/26	0100-0700	0.0	51.6	4.2	4.5	0.0	6.6	18.8	67.3	1.7
4/26	0700-1300	0.0	47.2	13.2	4.0	0.8	12.2	38.6	159.3	23.7
4/26	1300-1900	0.0	103.5	11.8	5.5	0.0	30.3	72.0	320.9	37.2
4/26	1900-0100	0.0	63.3	8.5	2.4	0.0	9.5	52.2	115.9	13.2
4/27	0100-0700	0.0	40.1	12.6	3.5	0.0	8.6	30.3	48.5	6.0
4/27	0700-1300	0.0	37.2	11.2	2.1	0.0	9.3	23.7	95.3	22.5
4/27	1300-1900	0.0	88.7	13.2	5.5	8.2	21.3	61.2	266.1	67.9
4/27	1900-0100	0.0	64.6	12.0	5.5	8.4	20.3	47.8	132.1	12.5
4/28	0100-0700	0.0	64.6	9.9	5.5	1.0	17.5	49.9	59.8	5.4
4/28	0700-1300	10.7	126.1	12.6	9.1	12.0	76.8	69.2	112.3	14.4
4/28	1300-1900	20.0	194.5	16.7	9.1	0.0	109.6	108.8	76.5	37.3
4/28	1900-0100	6.6	141.5	5.7	5.5	0.0	41.8	101.6	45.9	9.4
4/29	0100-0700	0.0	98.1	5.0	4.5	14.0	21.6	83.3	39.0	6.2
4/29	0700-1300	1.9	100.8	6.8	4.5	0.0	28.4	88.7	109.4	39.1
VISALIA										
4/26	0100-0700	0.0	293.0	28.5	8.1	4.8	124.9	100.1	685.6	7.8
4/26	0700-1300	2.8	335.3	34.9	9.6	2.4	246.3	101.1	934.8	47.6
4/26	1300-1900	0.0	163.1	24.4	6.6	0.0	80.9	76.4	940.2	135.2
4/26	1900-0100	0.0	229.2	56.8	12.1	3.2	125.0	91.3	1200.5	19.9
4/27	0100-0700	0.0	181.3	46.4	7.6	0.6	69.2	86.4	527.4	12.9
4/27	0700-1300	0.0	318.4	59.5	11.6	0.0	212.2	121.7	863.8	101.5
4/27	1300-1900	1.2	152.5	33.3	9.1	0.5	63.9	87.2	840.4	157.4
4/27	1900-0100	22.2	96.1	38.1	13.1	4.8	58.1	72.3	916.8	13.5
4/28	0100-0700	19.9	186.0	25.7	15.0	6.7	85.0	87.7	839.9	5.9
4/28	0700-1300	21.2	233.0	43.6	12.6	10.7	178.1	79.0	549.0	26.5
4/28	1300-1900	15.8	175.0	33.3	11.1	0.1	98.5	97.7	398.8	106.9
4/28	1900-0100	15.2	294.2	34.7	13.1	5.0	192.5	116.3	500.4	27.6
4/29	0100-0700	9.3	256.8	22.4	10.0	3.3	131.9	89.2	605.1	8.1
4/29	0700-1300	7.1	183.3	65.1	12.6	2.1	149.8	78.4	670.4	86.0

Table 2. Chemical Composition of  
Sequoia Cloudwater: April 28, 1988

Time	pH	Na <sup>+</sup>	K <sup>+</sup>	NH <sub>4</sub> <sup>+</sup>	Ca <sup>2+</sup>	Mg <sup>2+</sup>	Cl <sup>-</sup>	NO <sub>3</sub> <sup>-</sup>	SO <sub>4</sub> <sup>2-</sup>	LWC
		←————— μN —————→								ml · m <sup>-3</sup>
LOWER KAWEAH										
1230-1300	4.62	27	3	411	18	9	16	216	184	0.25
1300-1330	4.64	20	2	399	14	7	17	199	175	0.20
1330-1400	4.54	15	2	398	9	6	30	200	175	0.19
1400-1430	4.48	14	1	425	9	5	16	211	177	0.19
1430-1500	4.36	16	3	523	11	7	20	273	231	0.08
MORO ROCK										
1145-1200	4.75	29	NA	345	18	9	NA	175	144	0.23
1200-1230	4.70	22	12	345	11	7	23	164	144	0.26
1230-1300	4.69	17	3	303	8	5	13	154	135	0.37
1300-1330	4.64	19	2	346	9	6	14	183	150	0.28
1330-1400	4.61	21	2	386	10	7	15	211	164	0.27
1400-1430	4.48	19	1	358	9	6	13	207	156	0.28
1430-1500	4.44	20	2	385	12	7	5	191	142	0.31
1500-1530	4.38	18	2	389	10	7	5	209	157	0.21
1530-1600	4.34	35	3	584	18	12	14	336	236	0.15
BLANK		1	1	4	2	1	1	2	2	

NA denotes not available.

The blank concentration has been subtracted from the sample concentration for each species.

Table 3. H<sub>2</sub>O<sub>2</sub> and S(IV) in  
Sequoia Cloudwater: April 28, 1988

Site	Time	pH	←— μM —→	
			H <sub>2</sub> O <sub>2</sub>	S(IV)
LK	1230-1300	4.62	26	6
LK	1300-1330	4.64	36	6
LK	1330-1400	4.54	35	6
LK	1400-1430	4.48	37	<4
LK	1430-1500	4.36	47	<4
MR	1145-1200	4.75	16	<4
MR	1200-1230	4.70	15	6
MR	1230-1300	4.69	16	<4
MR	1300-1330	4.64	22	<4
MR	1330-1400	4.61	22	<4
MR	1400-1430	4.48	23	6
MR	1430-1500	4.44	23	<4
MR	1500-1530	4.38	27	<4
MR	1530-1600	4.34	30	<4
BLANK			0	<4

LK denotes Lower Kaweah. MR denotes Moro Rock.  
S(IV) concentrations <4 μM were not detected.

Table 4. Carboxylic Acids in  
Sequoia Cloudwater: April 28, 1988

Site	Time	pH	Formate	Acetate	Pyruvate*	% H <sup>+</sup>	-/+
			←————— μN —————→				
LK	1230-1300	4.62	30.1	3.8	3.9	157.5	0.92
LK	1300-1330	4.64	30.2	4.0	3.0	162.5	0.91
LK	1330-1400	4.54	25.8	3.0	3.7	112.6	0.95
LK	1400-1430	4.48	24.4	2.7	4.0	93.9	0.89
LK	1430-1500	4.36	23.5	2.0	4.7	69.3	0.91
MR	1145-1200	4.75	28.6	3.9	2.8	198.1	NA
MR	1200-1230	4.70	26.5	3.4	2.6	162.9	0.87
MR	1230-1300	4.69	24.2	3.5	1.2	141.7	0.92
MR	1300-1330	4.64	24.6	3.1	2.1	129.9	0.92
MR	1330-1400	4.61	25.5	3.0	2.1	124.4	0.93
MR	1400-1430	4.48	20.4	2.2	1.8	73.6	0.93
MR	1430-1500	4.44	18.2	1.9	1.7	60.0	0.78
MR	1500-1530	4.38	19.8	1.9	1.8	56.2	0.84
MR	1530-1600	4.34	23.9	1.9	2.1	60.8	0.87
BLANK			0	0	0		

LK denotes Lower Kaweah; MR denotes Moro Rock.

\* Identification of this species is tentative.

% H<sup>+</sup> denotes the maximum contribution of the carboxylate anions to free acidity.

-/+ denotes the total ion balance including all measured species, organic and inorganic.

NA denotes not available.

Table 5. Carbonyls in Sequoia  
Cloudwater: April 28, 1988

Site	Time	Form	Acet	Glyox	Mglyox	Benz	
		←————— $\mu\text{M}$ —————→					
LK	1230-1300	14.1	2.8	9.7	2.2	0.0	
LK	1300-1330	12.2	2.2	10.6	2.2	0.0	
LK	1330-1400	10.5	1.9	7.2	1.6	0.0	
LK	1400-1430	11.5	2.1	9.8	1.9	0.8	
LK	1430-1500	10.3	2.8	13.1	2.5	0.6	
MR	1145-1200	10.6	1.1	5.9	1.4	0.0	
MR	1200-1230	10.2	1.0	5.5	1.3	0.0	
MR	1230-1300	11.2	1.1	7.7	1.5	0.0	
MR	1300-1330	10.6	0.5	4.7	1.2	0.0	
MR	1330-1400	9.0	0.2	6.5	1.3	0.0	
MR	1400-1430	7.9	0.5	4.4	0.9	0.0	
MR	1430-1500	8.7	0.9	5.4	1.1	0.0	
MR	1500-1530	7.8	0.9	5.8	1.3	0.1	
MR	1530-1600	11.6	1.9	9.6	1.9	0.4	
	BLANK	2.7	1.0	1.2	0.0	0.0	

LK denotes Lower Kaweah; MR denotes Moro Rock.

Form denotes formaldehyde; Acet denotes acetaldehyde; Glyox denotes glyoxal; Mglyox denotes methylglyoxal; Benz denotes benzaldehyde.

The blank concentration has been subtracted from the sample concentration for each species.

## Figure Captions

- Figure 1. Map of central California indicating the location of Sequoia National Park relative to the major population centers. Also indicated are major highways in the region. Contours are included for the 1000 and 3000 foot levels to illustrate the general topography of the region.
- Figure 2. The automated aerosol and gas sampler used in the study. Air is sampled using a filter pack method described in the text.
- Figure 3. Balance of ammonium with nitrate and sulfate (all in  $\text{neq}\cdot\text{m}^{-3}$ ) in aerosol samples collected at Visalia, Ash Mountain, and Lower Kaweah between April 26 and April 29, 1988.
- Figure 4. Balance of ammonium ( $\text{neq}\cdot\text{m}^{-3}$ ) plus ammonia ( $\text{nmole}\cdot\text{m}^{-3}$ ) with nitrate ( $\text{neq}\cdot\text{m}^{-3}$ ), sulfate ( $\text{neq}\cdot\text{m}^{-3}$ ), and nitric acid ( $\text{nmole}\cdot\text{m}^{-3}$ ) in aerosol and gas samples collected at Visalia, Ash Mountain, and Lower Kaweah between April 26 and April 29, 1988.
- Figure 5. Map of the San Joaquin Valley illustrating some of the major ammonia emissions sources for the region. The black circles represent confined feeding operations.
- Figure 6. Acid-base balance as a function of time in the air masses sampled at Visalia, Ash Mountain, and Lower Kaweah between April 26 and April 29, 1988. Species included are nitrate, nitric acid, sulfate, ammonium, and ammonia. Nitrate, sulfate, and ammonium contributions were calculated as  $\text{neq}\cdot\text{m}^{-3}$ ; ammonia and nitric acid contributions were calculated as  $\text{nmole}\cdot\text{m}^{-3}$ .
- Figure 7. Ratios of N(V) to S(VI) in the air masses sampled at Visalia, Ash Mountain, and Lower Kaweah between April 26 and April 29, 1988. Species included are nitrate, nitric acid, and sulfate. Nitrate and sulfate contributions were calculated as  $\text{neq}\cdot\text{m}^{-3}$  while nitric acid contributions were calculated as  $\text{nmole}\cdot\text{m}^{-3}$ .

- Figure 8. Half-hour averages of wind direction at Visalia between April 24 and April 30, 1988. Breaks in the line indicate missing data.
- Figure 9. Aerosol loading of sulfate at Visalia between April 26 and April 29, 1988.
- Figure 10. (a) Aerosol loading of nitrate at Visalia between April 26 and April 29, 1988. (b) Gas phase loading of nitric acid at Visalia between April 26 and April 29, 1988.
- Figure 11. Comparison of aerosol nitrate loadings at Visalia, Ash Mountain, and Lower Kaweah between April 26 and April 29, 1988.
- Figure 12. Comparison of aerosol sulfate loadings at Visalia, Ash Mountain, and Lower Kaweah between April 26 and April 29, 1988.
- Figure 13. Comparison of aerosol ammonium loadings at Visalia, Ash Mountain, and Lower Kaweah between April 26 and April 29, 1988.
- Figure 14. Vertical temperature profiles measured at Fresno and Bakersfield at 0600 PST on the mornings of April 26, 27, and 28, 1988.
- Figure 15. Comparison of gas phase ammonia loadings at Visalia, Ash Mountain, and Lower Kaweah between April 26 and April 29, 1988.
- Figure 16. Comparison of gas phase nitric acid loadings at Visalia, Ash Mountain, and Lower Kaweah between April 26 and April 29, 1988.
- Figure 17. Comparison of total N(V) loadings in the air masses sampled at Visalia, Ash Mountain, and Lower Kaweah between April 26 and April 29, 1988. N(V) includes aerosol nitrate ( $\text{neq} \cdot \text{m}^{-3}$ ) and gas phase nitric acid ( $\text{nmole} \cdot \text{m}^{-3}$ ).

- Figure 18. Comparison of total N(-III) loadings in the air masses sampled at Visalia, Ash Mountain, and Lower Kaweah between April 26 and April 29, 1988. N(-III) includes aerosol ammonium ( $\text{neq} \cdot \text{m}^{-3}$ ) and gas phase ammonia ( $\text{nmole} \cdot \text{m}^{-3}$ ).
- Figure 19. Wind direction at Lower Kaweah during the study period.
- Figure 20. Vertical profiles of wind measured at Fresno at 0600 PST on the mornings of April 26, 27, and 28, 1988.
- Figure 21. pH of the cloudwater samples collected at Lower Kaweah and Moro Rock on April 28, 1988.
- Figure 22. Concentrations of nitrate, sulfate, and ammonium in cloudwater samples collected at Lower Kaweah on April 28, 1988.
- Figure 23. Concentrations of nitrate, sulfate, and ammonium in cloudwater samples collected at Moro Rock on April 28, 1988.
- Figure 24. Cloudwater loadings of nitrate ( $\text{neq} \cdot \text{m}^{-3}$ ) at Lower Kaweah and Moro Rock on April 28, 1988. The loading for each period is calculated based on the collection rate of the CASCC and the sample nitrate concentration. Total N(V) loadings observed in the air mass at Lower Kaweah prior to and following the cloud interception event are included for reference.
- Figure 25. Cloudwater loadings of sulfate ( $\text{neq} \cdot \text{m}^{-3}$ ) at Lower Kaweah and Moro Rock on April 28, 1988. The loading for each period is calculated based on the collection rate of the CASCC and the sample sulfate concentration. Aerosol sulfate loadings observed in the air mass at Lower Kaweah prior to and following the cloud interception event are included for reference.

- Figure 26. Cloudwater loadings of ammonium ( $\text{neq} \cdot \text{m}^{-3}$ ) at Lower Kaweah and Moro Rock on April 28, 1988. The loading for each period is calculated based on the collection rate of the CASCC and the sample ammonium concentration. Total N(-III) loadings observed in the air mass at Lower Kaweah prior to and following the cloud interception event are included for reference.
- Figure 27.  $\text{H}_2\text{O}_2$  loadings in cloudwater collected at Lower Kaweah and Moro Rock on April 28, 1988. The loading for each period is calculated based on the collection rate of the CASCC and the sample  $\text{H}_2\text{O}_2$  concentration.

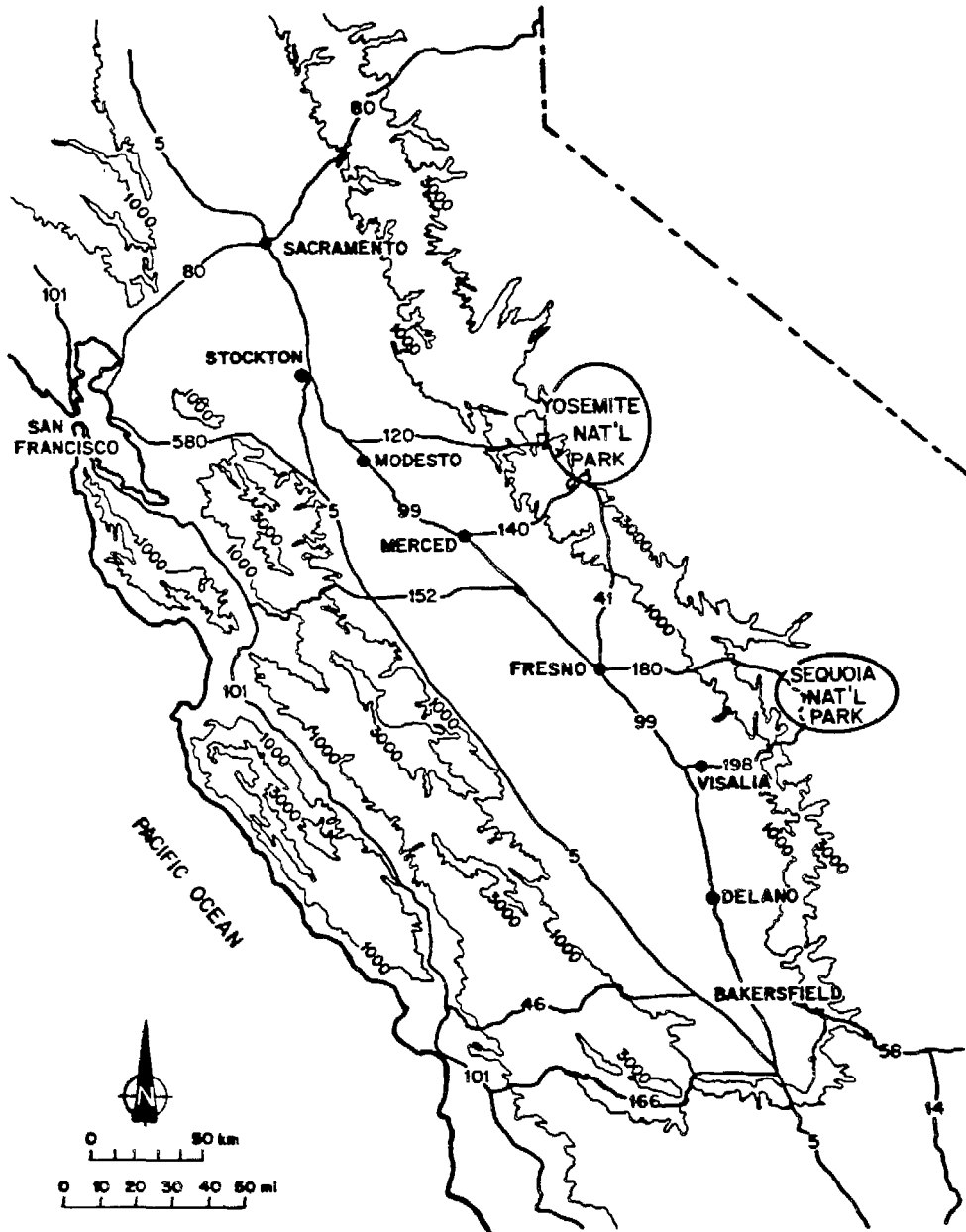


Figure 1. Map of central California indicating the location of Sequoia National Park relative to the major population centers. Also indicated are major highways in the region. Contours are included for the 1000 and 3000 foot levels to illustrate the general topography of the region.

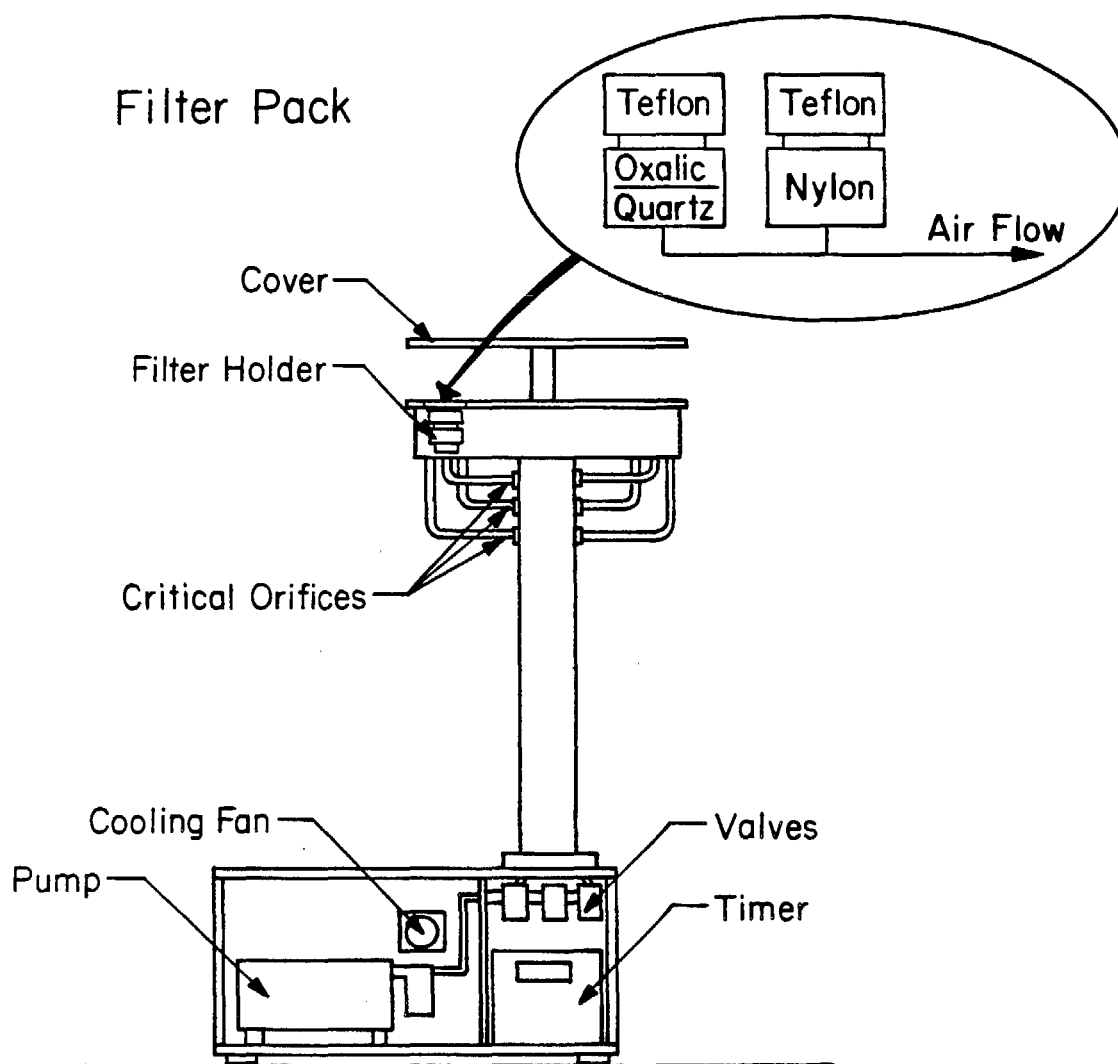


Figure 2. The automated aerosol and gas sampler used in the study. Air is sampled using a filter pack method described in the text.

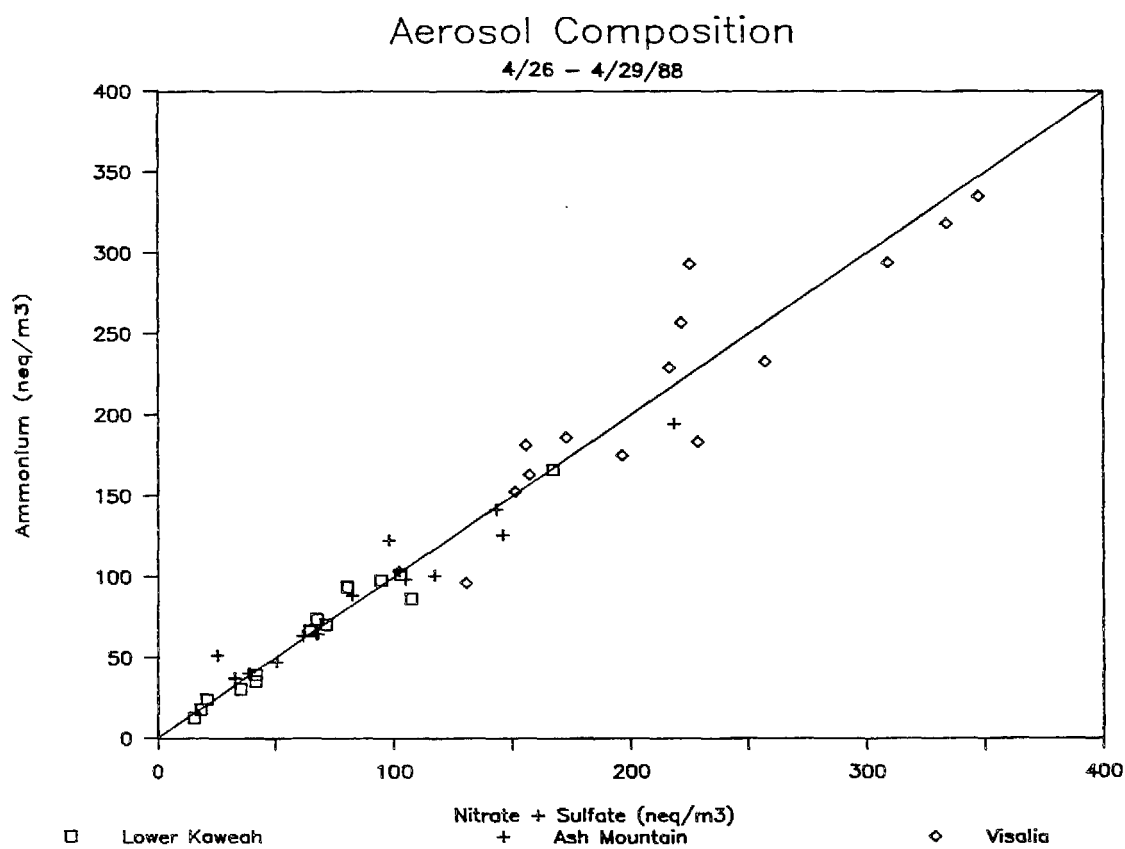


Figure 3. Balance of ammonium with nitrate and sulfate (all in  $\text{neq}\cdot\text{m}^{-3}$ ) in aerosol samples collected at Visalia, Ash Mountain, and Lower Kaweah between April 26 and April 29, 1988.

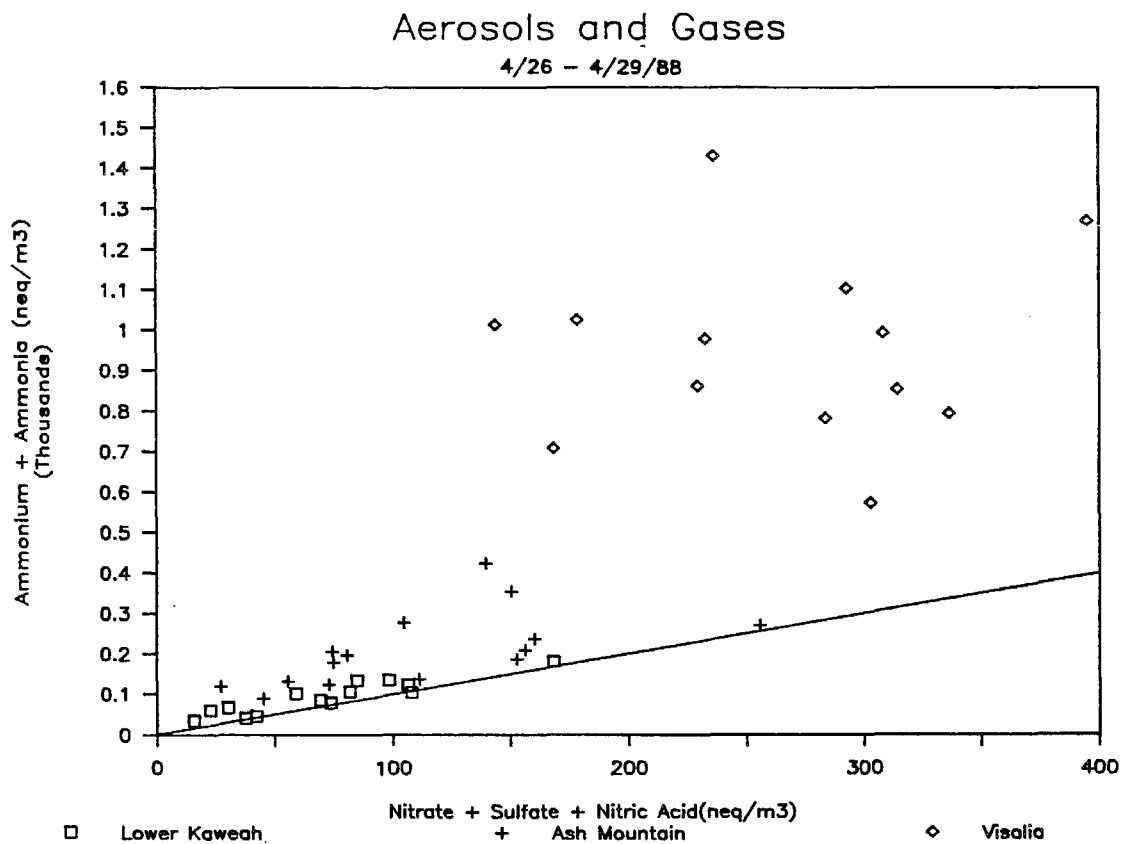


Figure 4. Balance of ammonium ( $\text{neq}\cdot\text{m}^{-3}$ ) plus ammonia ( $\text{nmole}\cdot\text{m}^{-3}$ ) with nitrate ( $\text{neq}\cdot\text{m}^{-3}$ ), sulfate ( $\text{neq}\cdot\text{m}^{-3}$ ), and nitric acid ( $\text{nmole}\cdot\text{m}^{-3}$ ) in aerosol and gas samples collected at Visalia, Ash Mountain, and Lower Kaweah between April 26 and April 29, 1988.

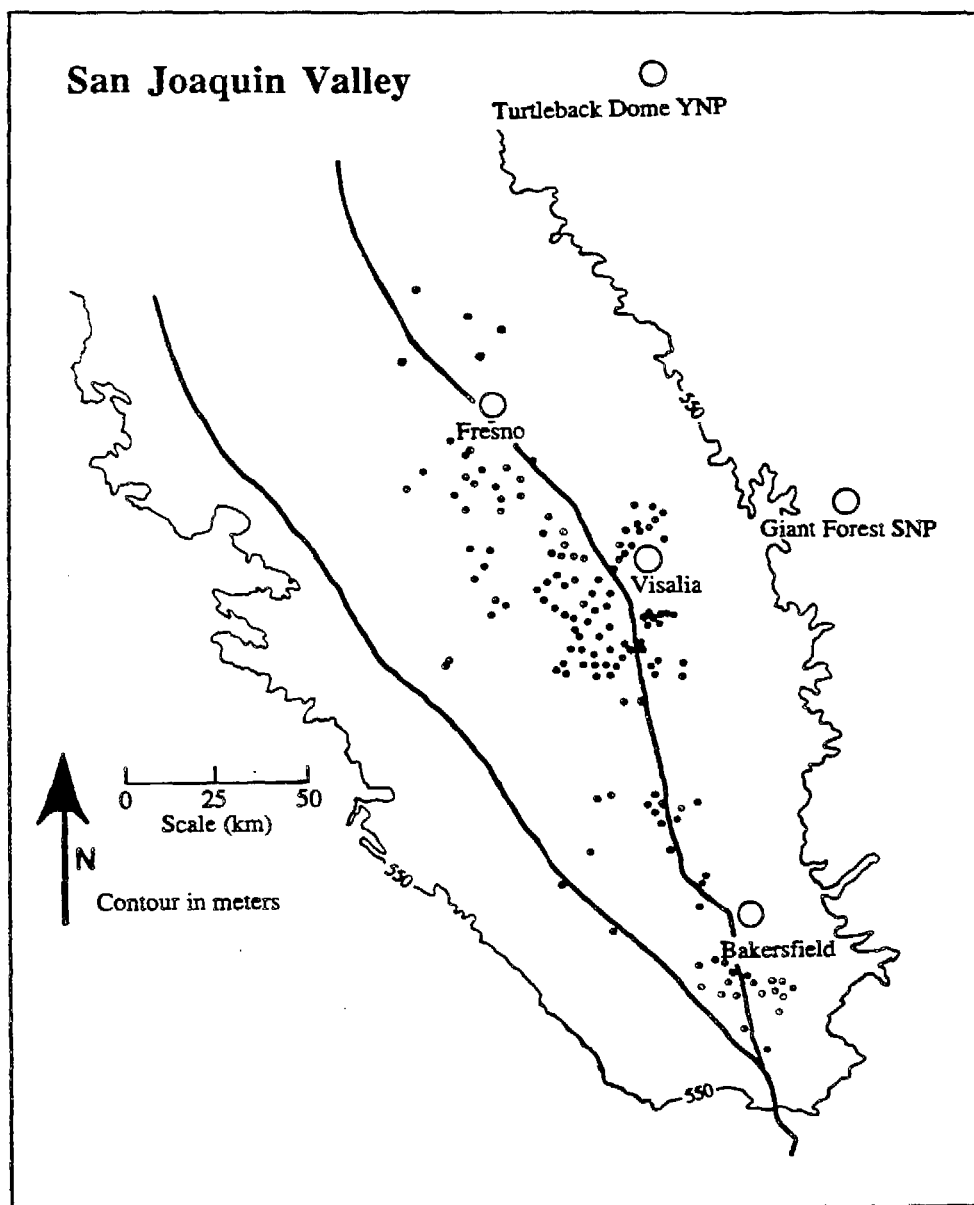


Figure 5. Map of the San Joaquin Valley illustrating some of the major ammonia emissions sources for the region. The black circles represent confined feeding operations.

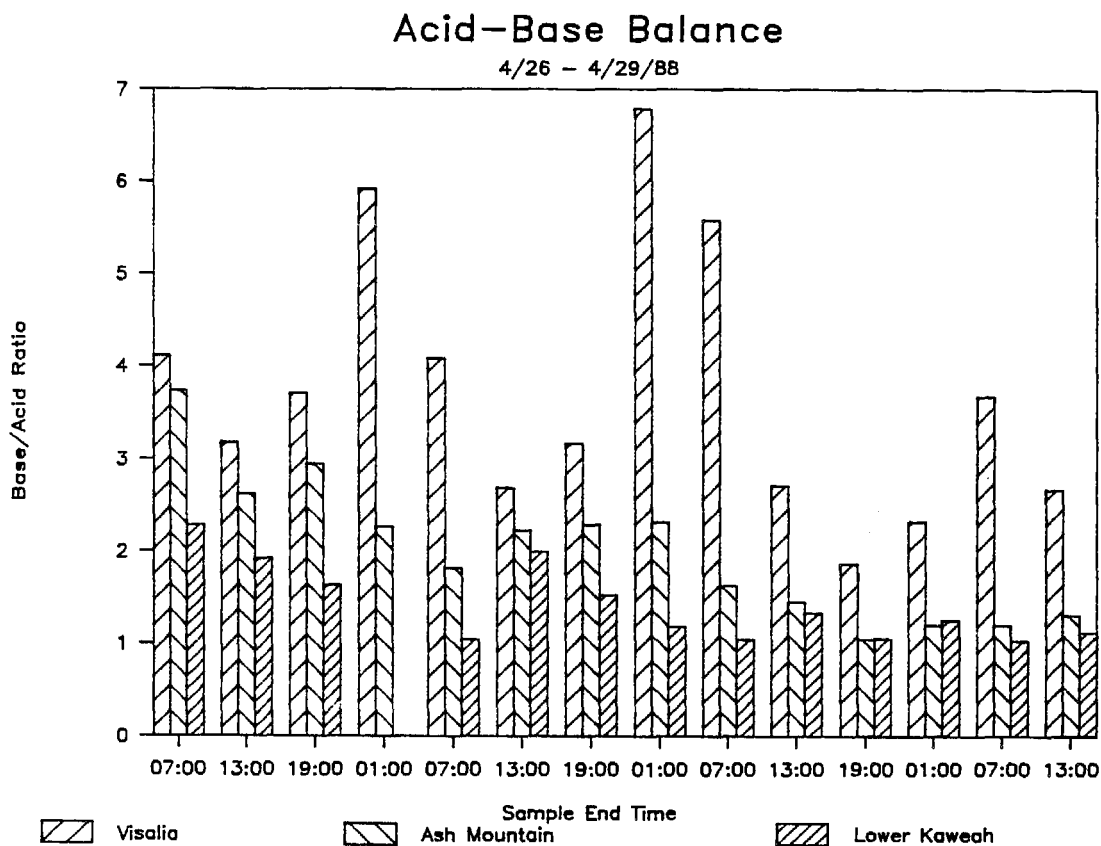


Figure 6. Acid-base balance as a function of time in the air masses sampled at Visalia, Ash Mountain, and Lower Kaweah between April 26 and April 29, 1988. Species included are nitrate, nitric acid, sulfate, ammonium, and ammonia. Nitrate, sulfate, and ammonium contributions were calculated as  $\text{neq}\cdot\text{m}^{-3}$ ; ammonia and nitric acid contributions were calculated as  $\text{nmole}\cdot\text{m}^{-3}$ .

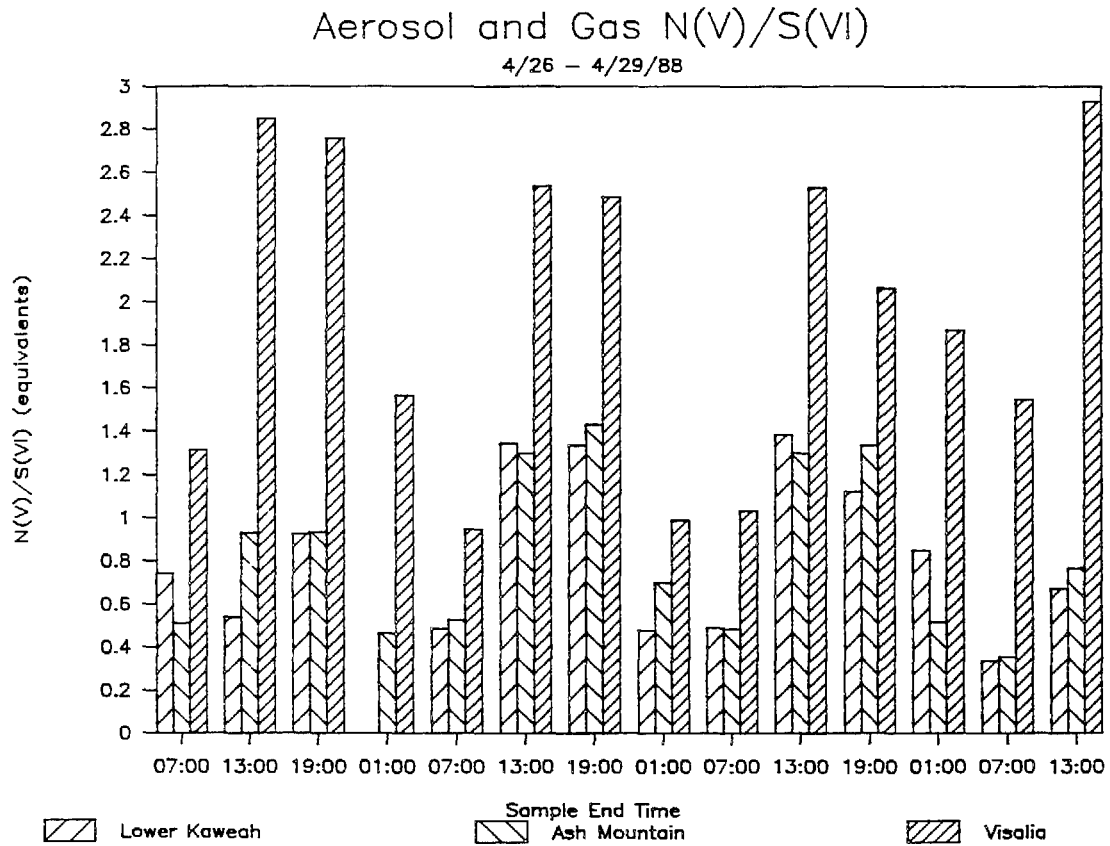
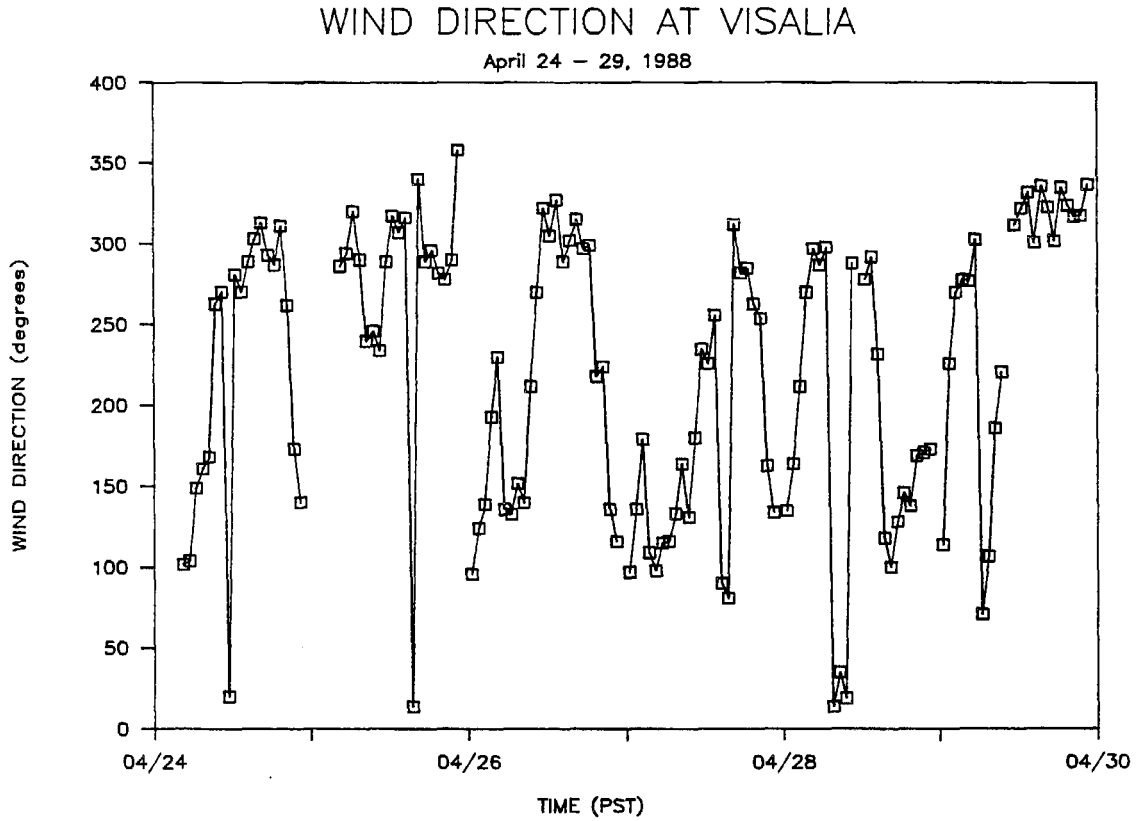


Figure 7. Ratios of N(V) to S(VI) in the air masses sampled at Visalia, Ash Mountain, and Lower Kaweah between April 26 and April 29, 1988. Species included are nitrate, nitric acid, and sulfate. Nitrate and sulfate contributions were calculated as  $\text{neq}\cdot\text{m}^{-3}$  while nitric acid contributions were calculated as  $\text{nmole}\cdot\text{m}^{-3}$ .



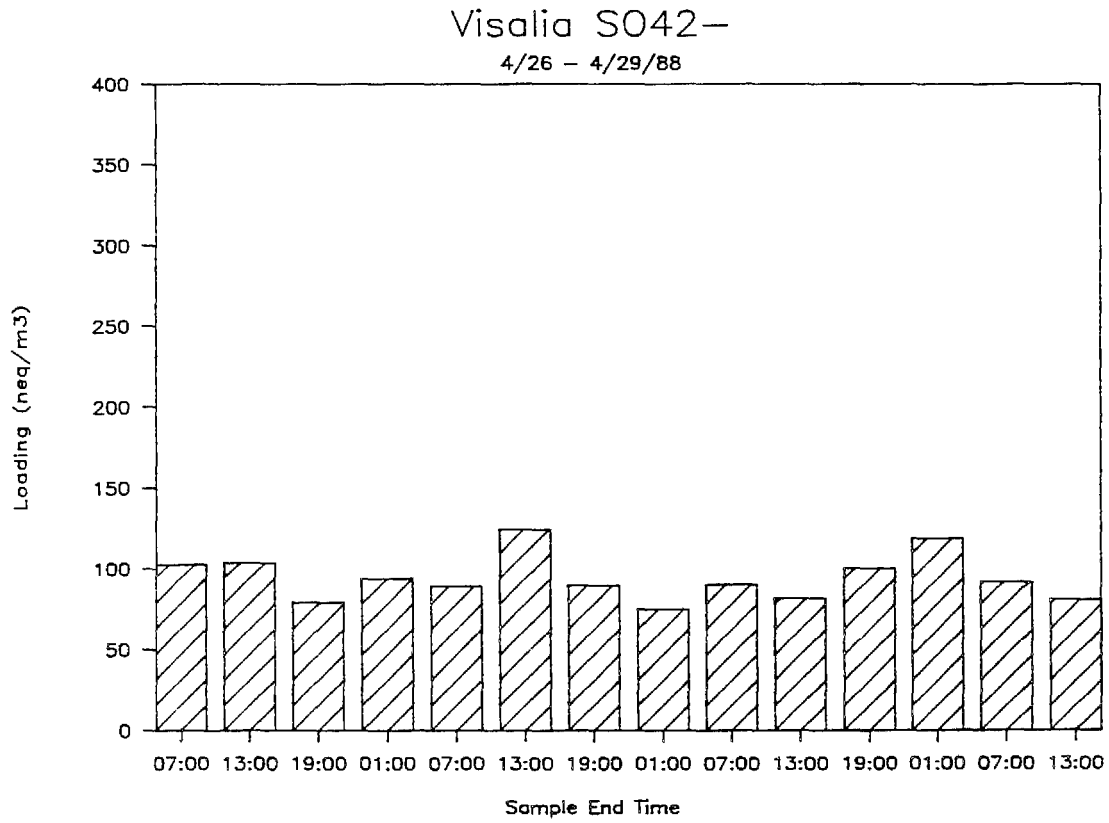


Figure 9. Aerosol loading of sulfate at Visalia between April 26 and April 29, 1988.

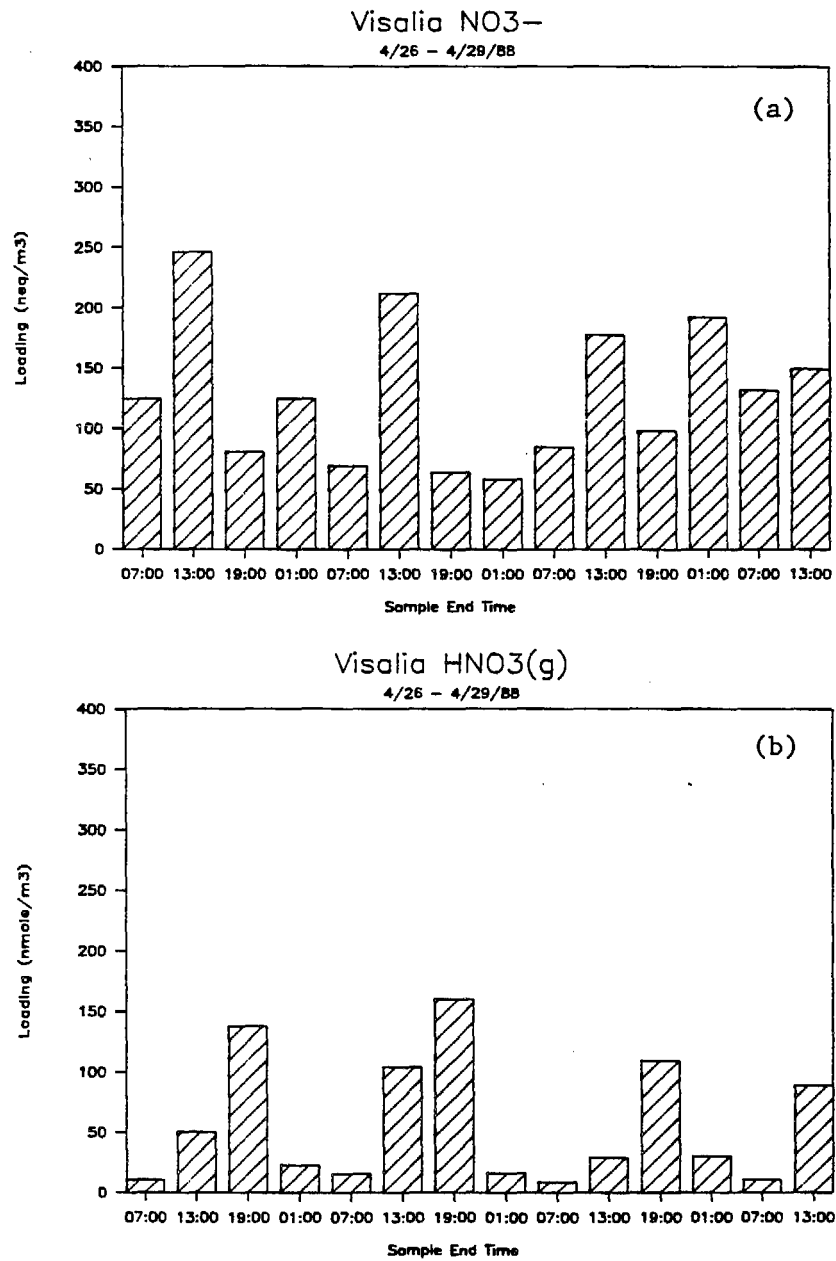


Figure 10. (a) Aerosol loading of nitrate at Visalia between April 26 and April 29, 1988. (b) Gas phase loading of nitric acid at Visalia between April 26 and April 29, 1988.

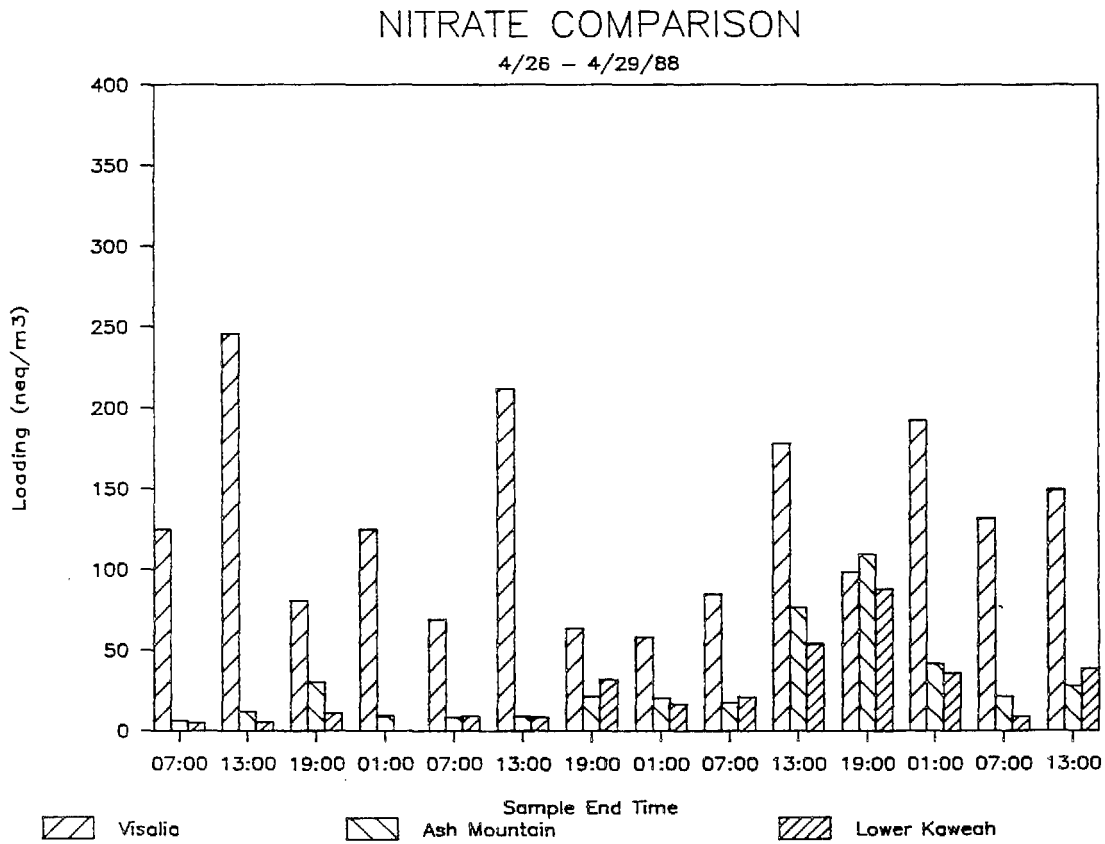


Figure 11. Comparison of aerosol nitrate loadings at Visalia, Ash Mountain, and Lower Kaweah between April 26 and April 29, 1988.

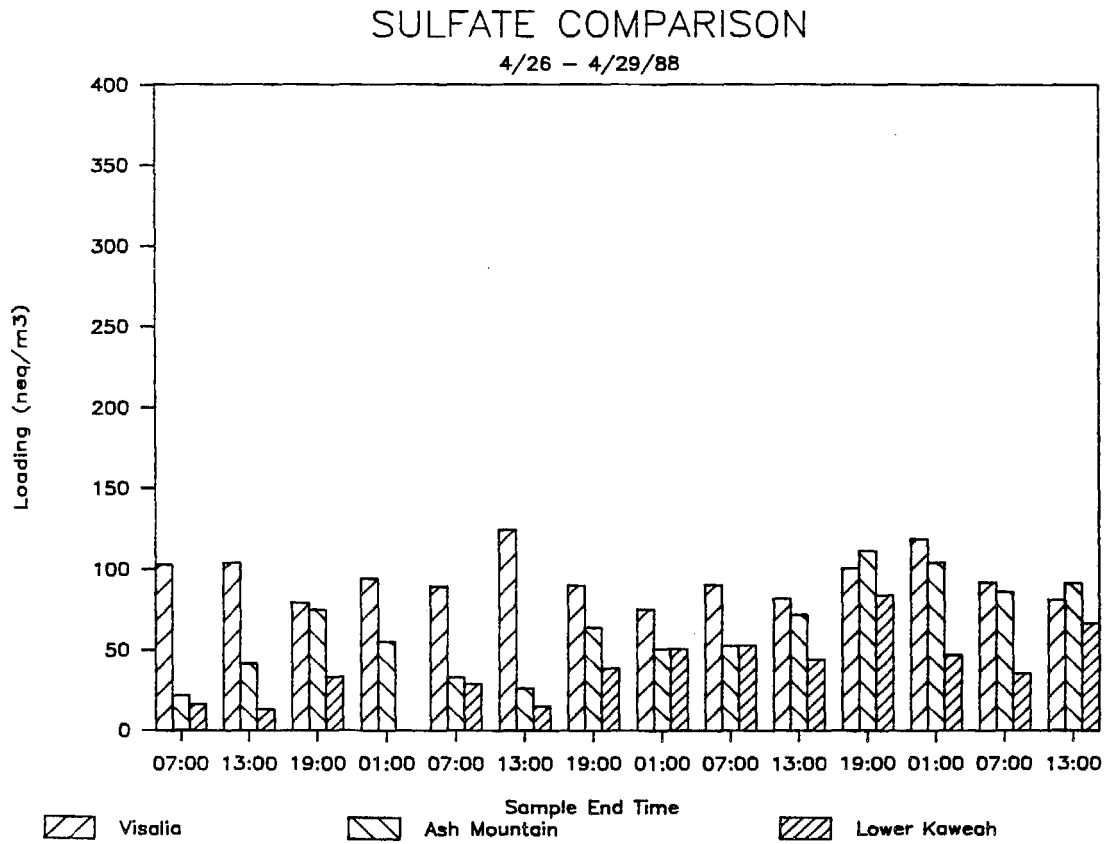


Figure 12. Comparison of aerosol sulfate loadings at Visalia, Ash Mountain, and Lower Kaweah between April 26 and April 29, 1988.

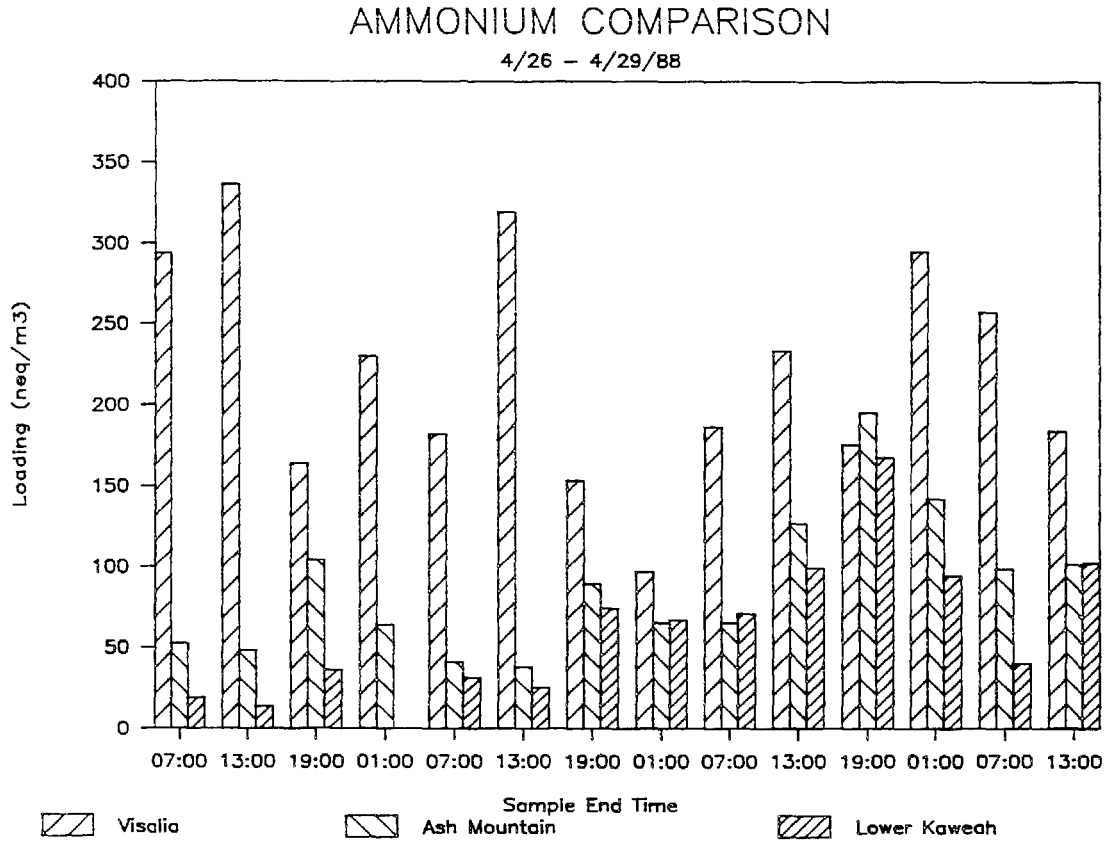


Figure 13. Comparison of aerosol ammonium loadings at Visalia, Ash Mountain, and Lower Kaweah between April 26 and April 29, 1988.

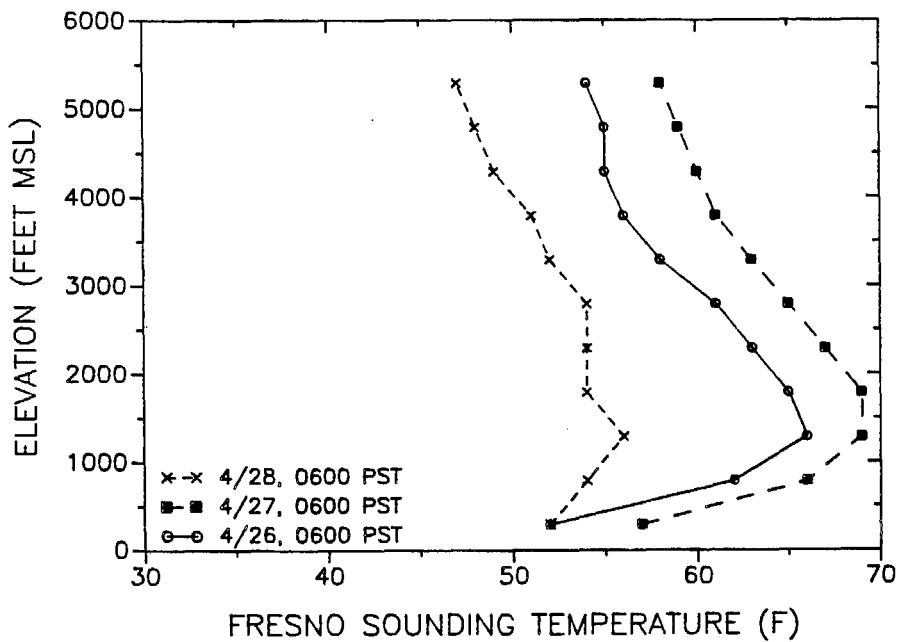
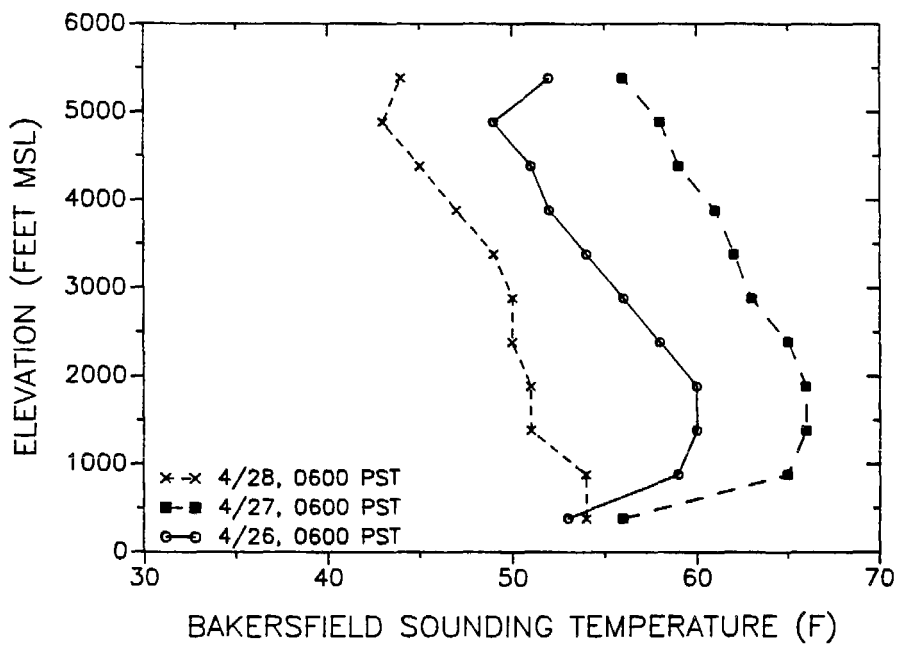


Figure 14. Vertical temperature profiles measured at Fresno and Bakersfield at 0600 PST on the mornings of April 26, 27, and 28, 1988.

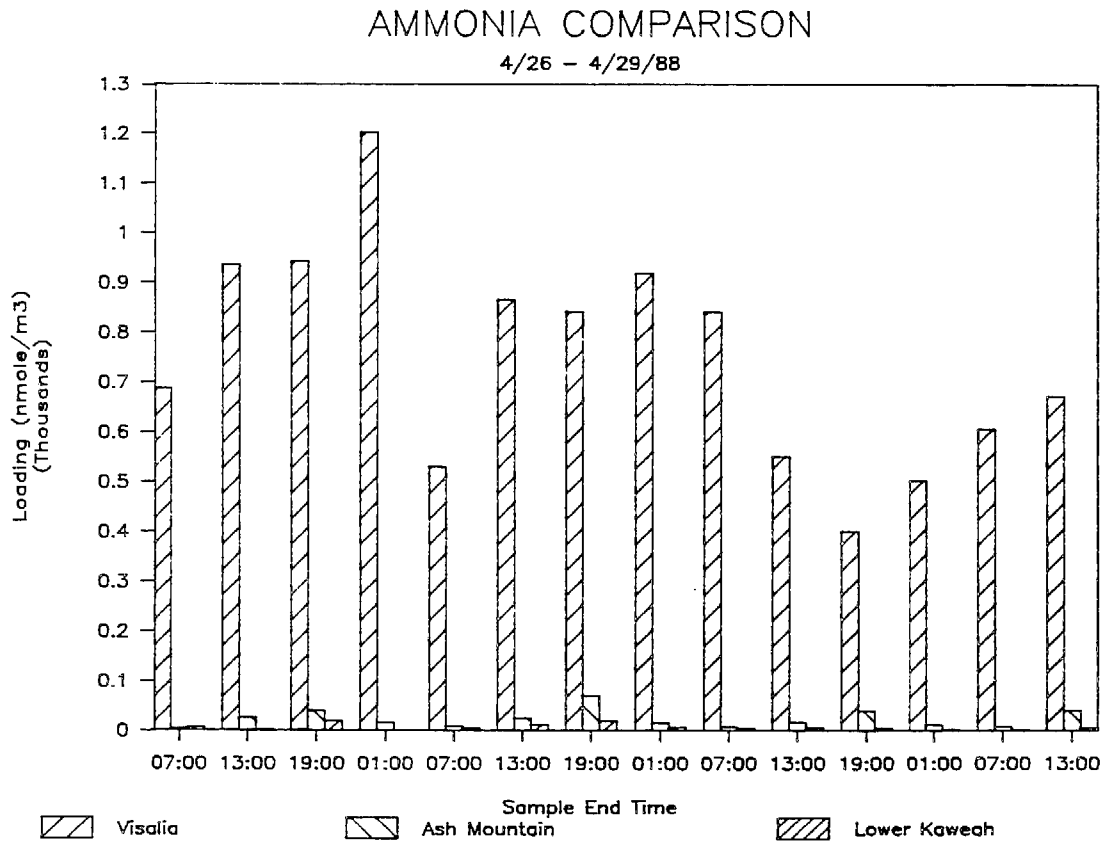


Figure 15. Comparison of gas phase ammonia loadings at Visalia, Ash Mountain, and Lower Kaweah between April 26 and April 29, 1988.

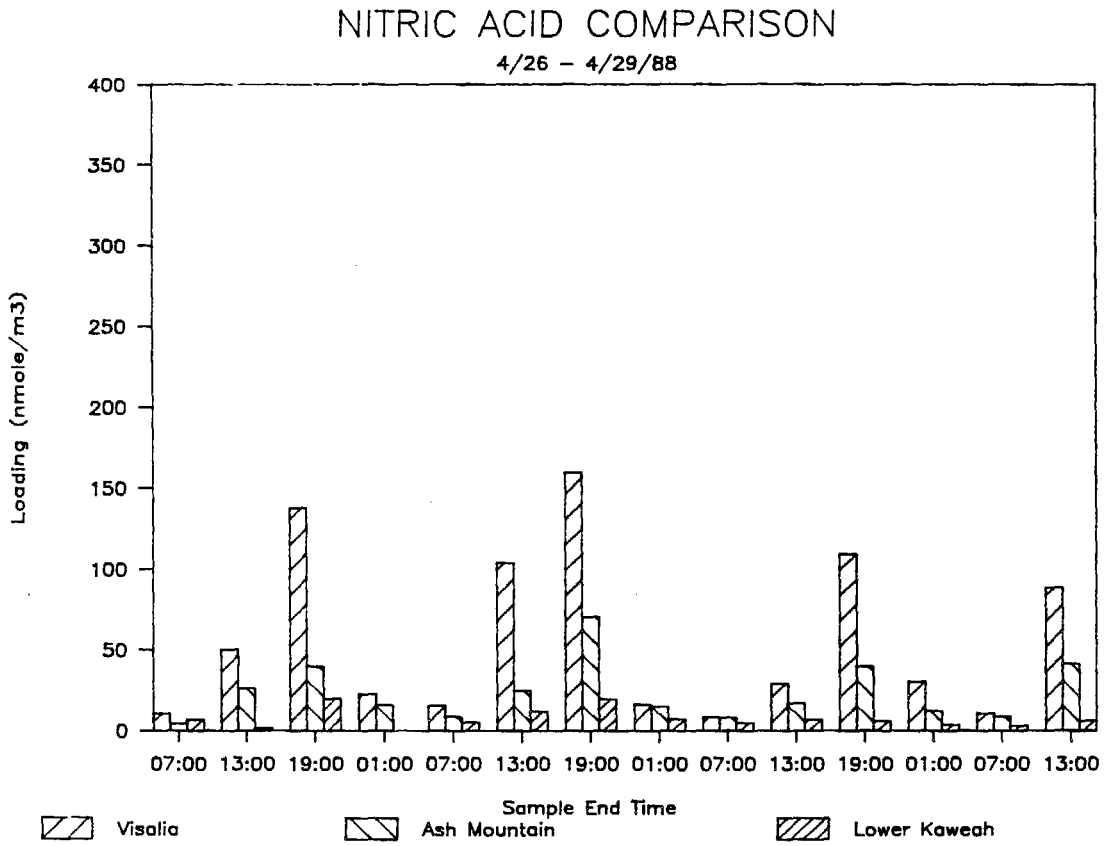


Figure 16. Comparison of gas phase nitric acid loadings at Visalia, Ash Mountain, and Lower Kaweah between April 26 and April 29, 1988.

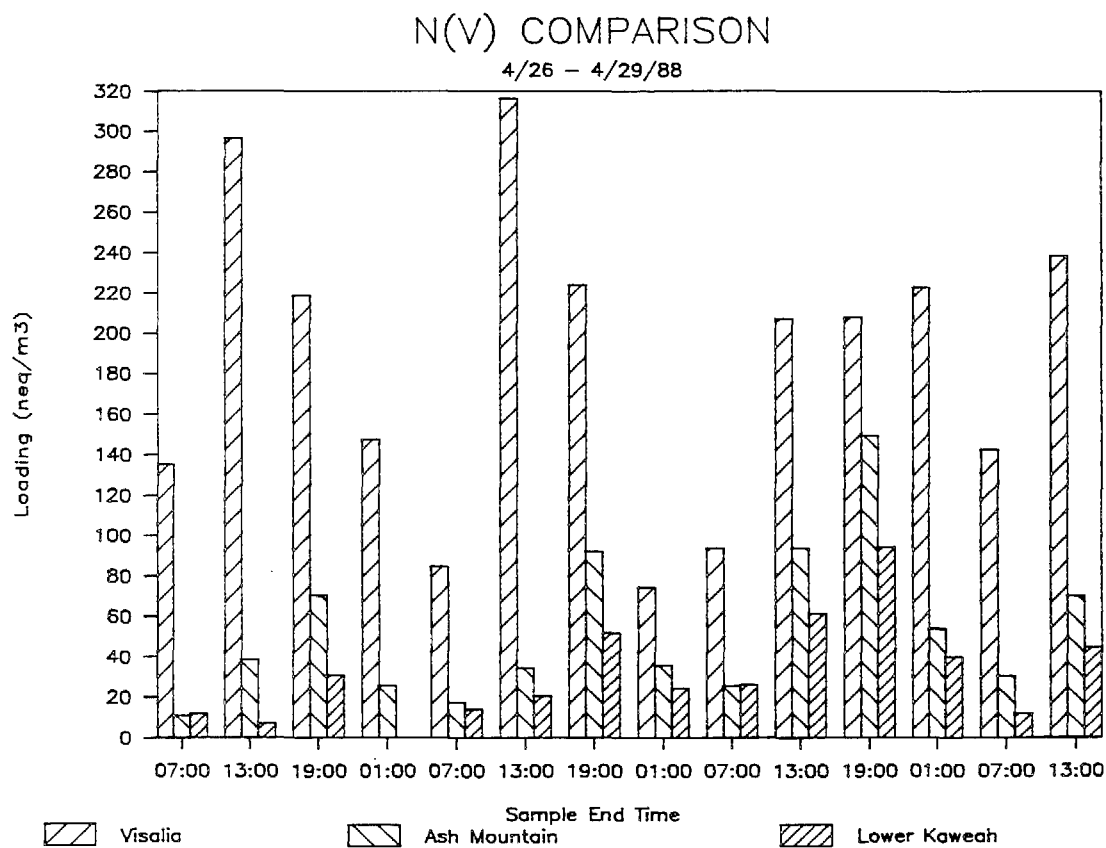


Figure 17. Comparison of total N(V) loadings in the air masses sampled at Visalia, Ash Mountain, and Lower Kaweah between April 26 and April 29, 1988. N(V) includes aerosol nitrate ( $\text{neq} \cdot \text{m}^{-3}$ ) and gas phase nitric acid ( $\text{nmole} \cdot \text{m}^{-3}$ ).

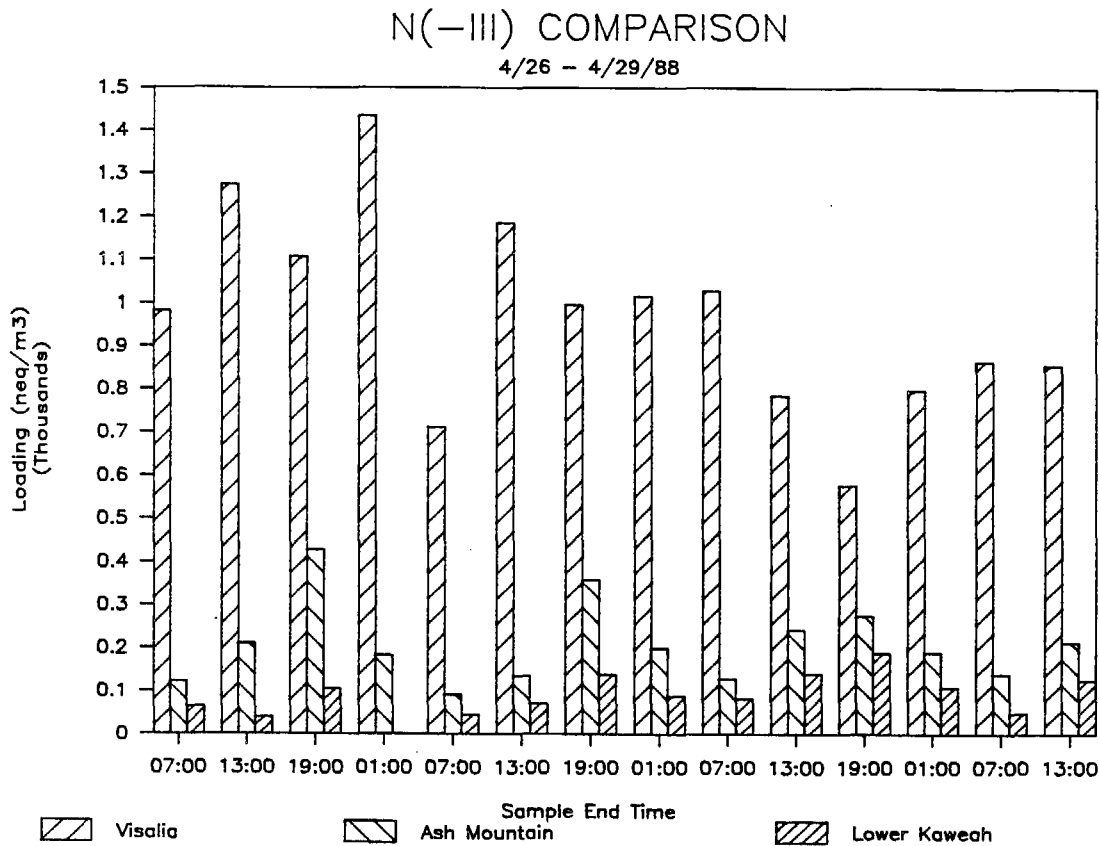


Figure 18. Comparison of total N(-III) loadings in the air masses sampled at Visalia, Ash Mountain, and Lower Kaweah between April 26 and April 29, 1988. N(-III) includes aerosol ammonium ( $\text{neq} \cdot \text{m}^{-3}$ ) and gas phase ammonia ( $\text{nmole} \cdot \text{m}^{-3}$ ).

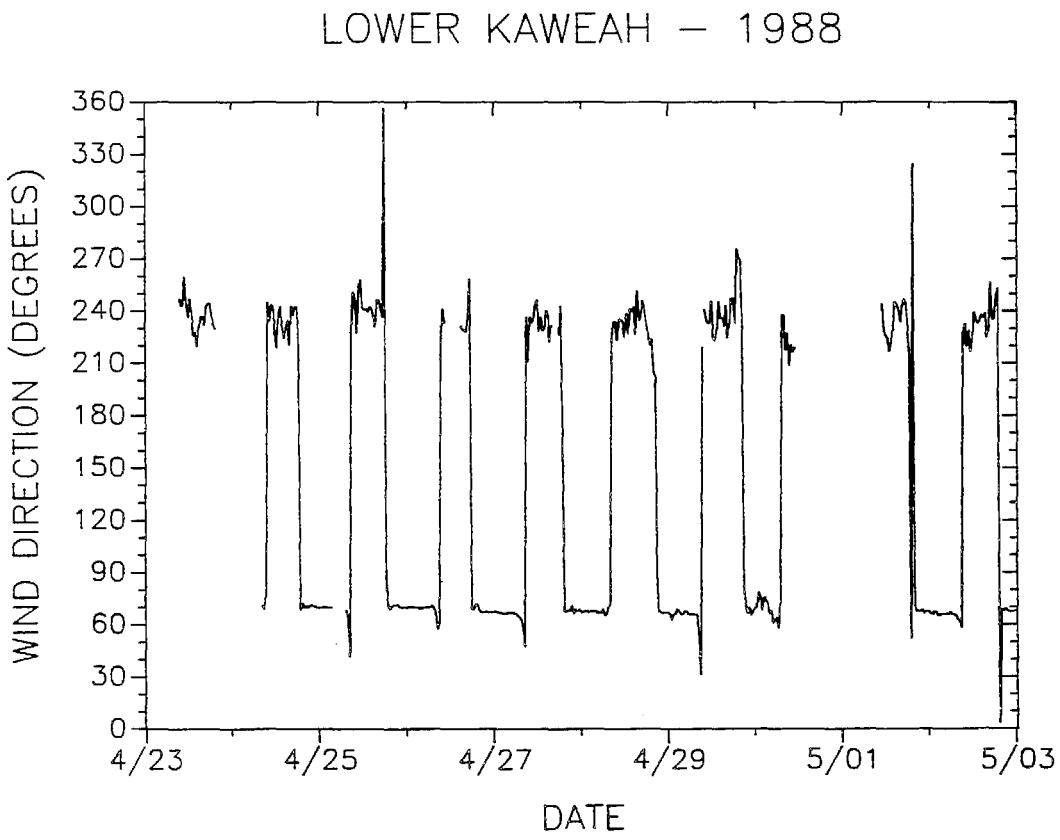


Figure 19. Wind direction at Lower Kaweah during the study period.

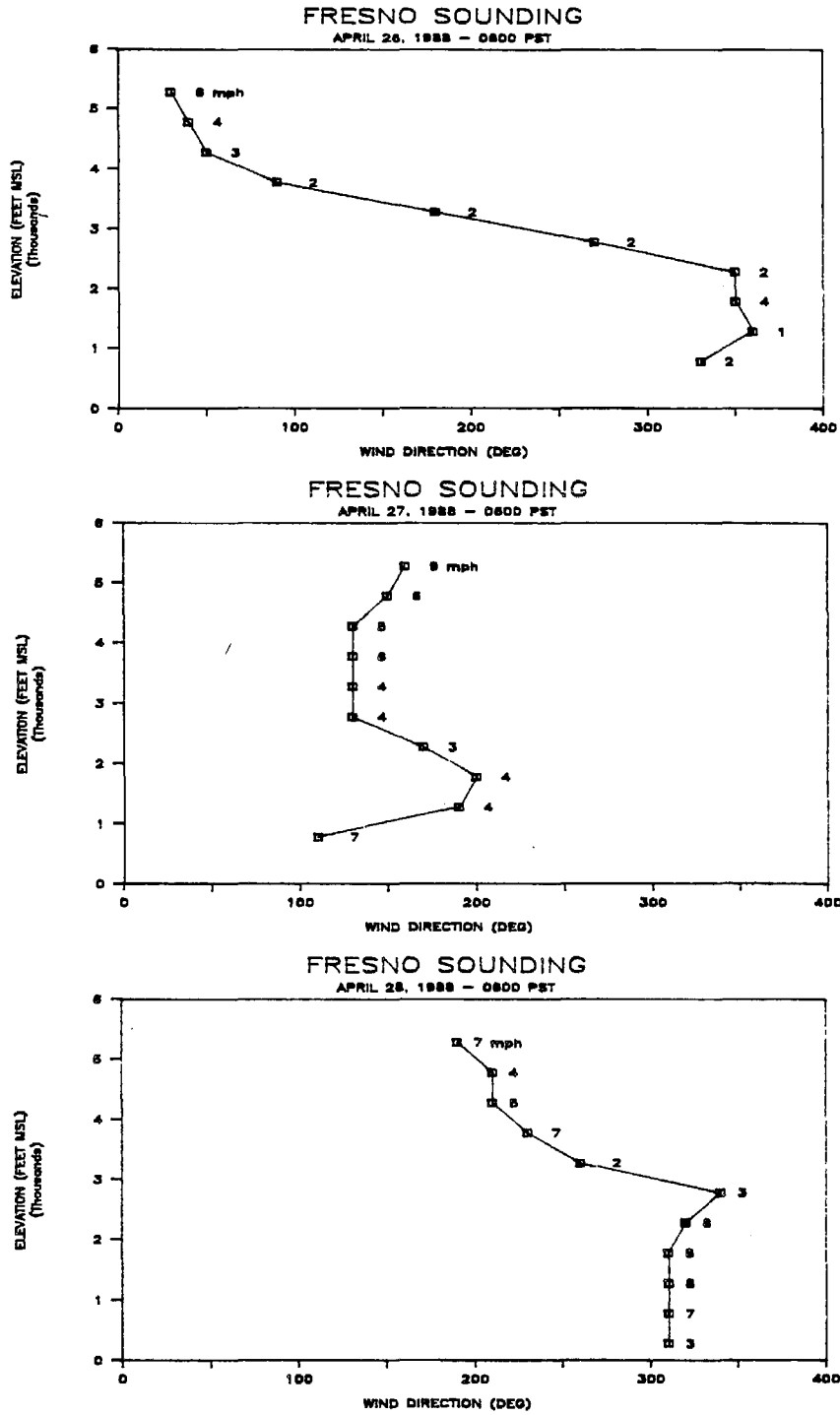


Figure 20. Vertical profiles of wind measured at Fresno at 0600 PST on the mornings of April 26, 27, and 28, 1988.

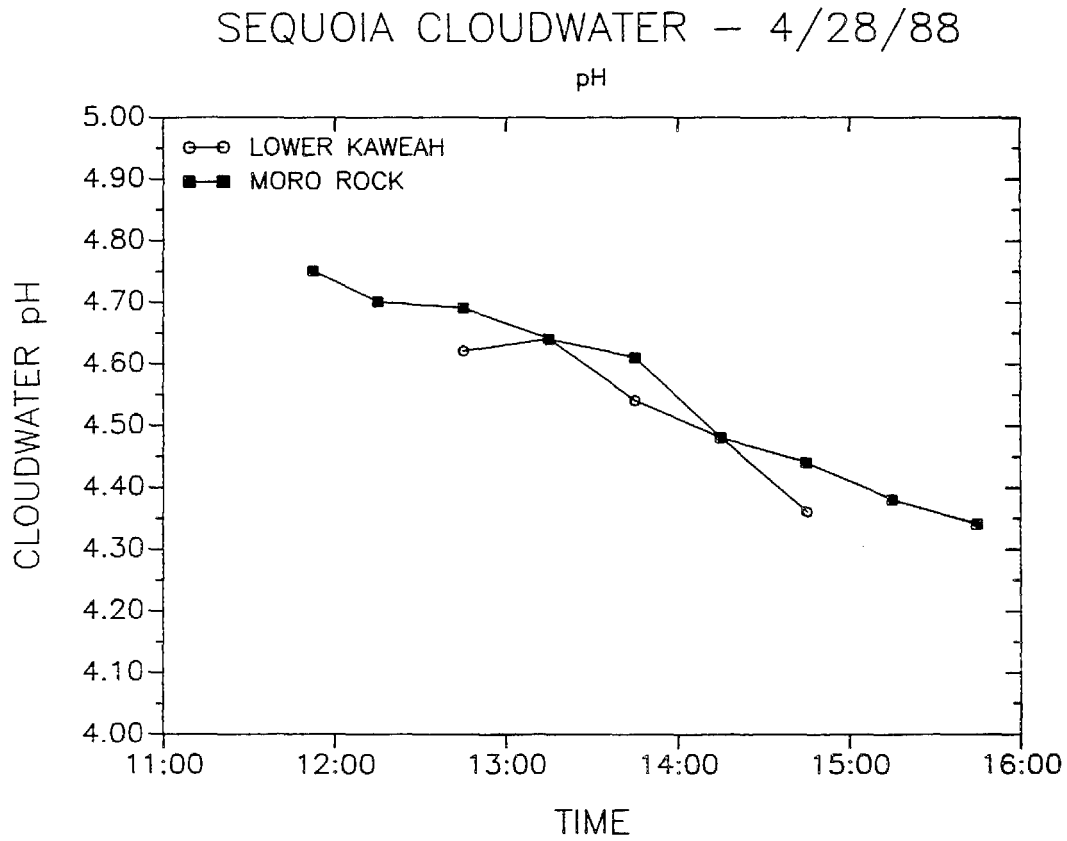


Figure 21. pH of the cloudwater samples collected at Lower Kaweah and Moro Rock on April 28, 1988.

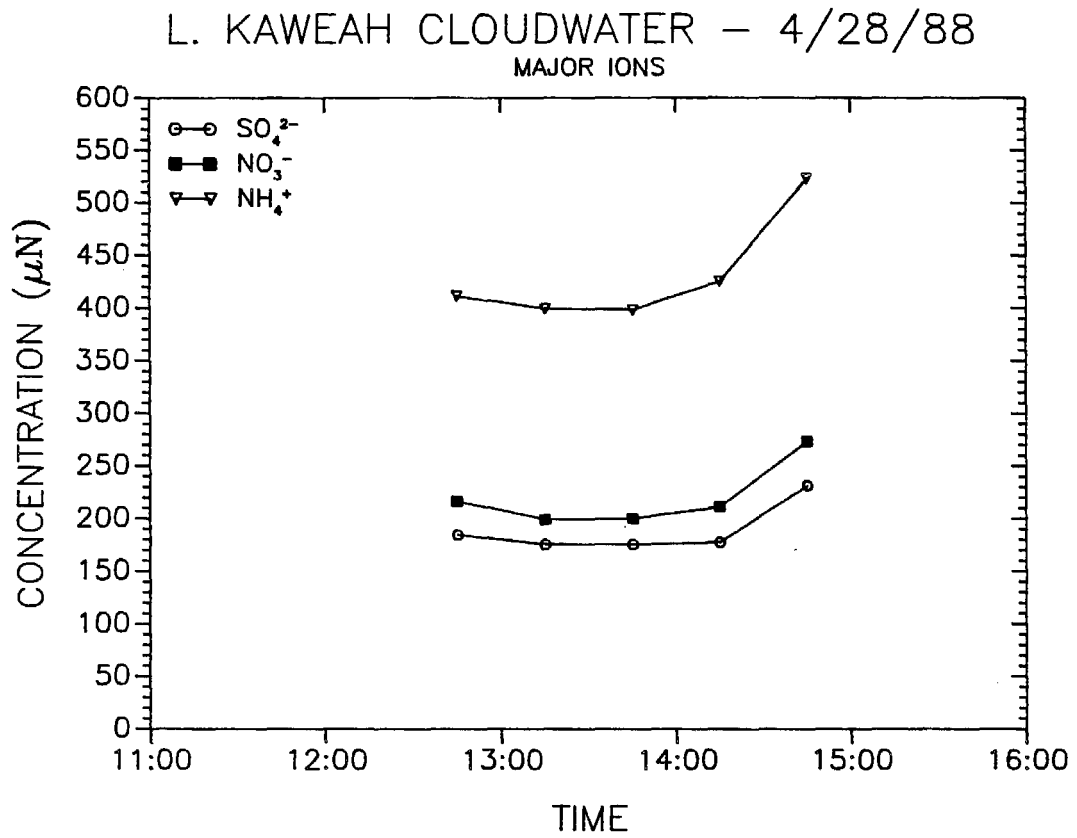


Figure 22. Concentrations of nitrate, sulfate, and ammonium in cloudwater samples collected at Lower Kaweah on April 28, 1988.

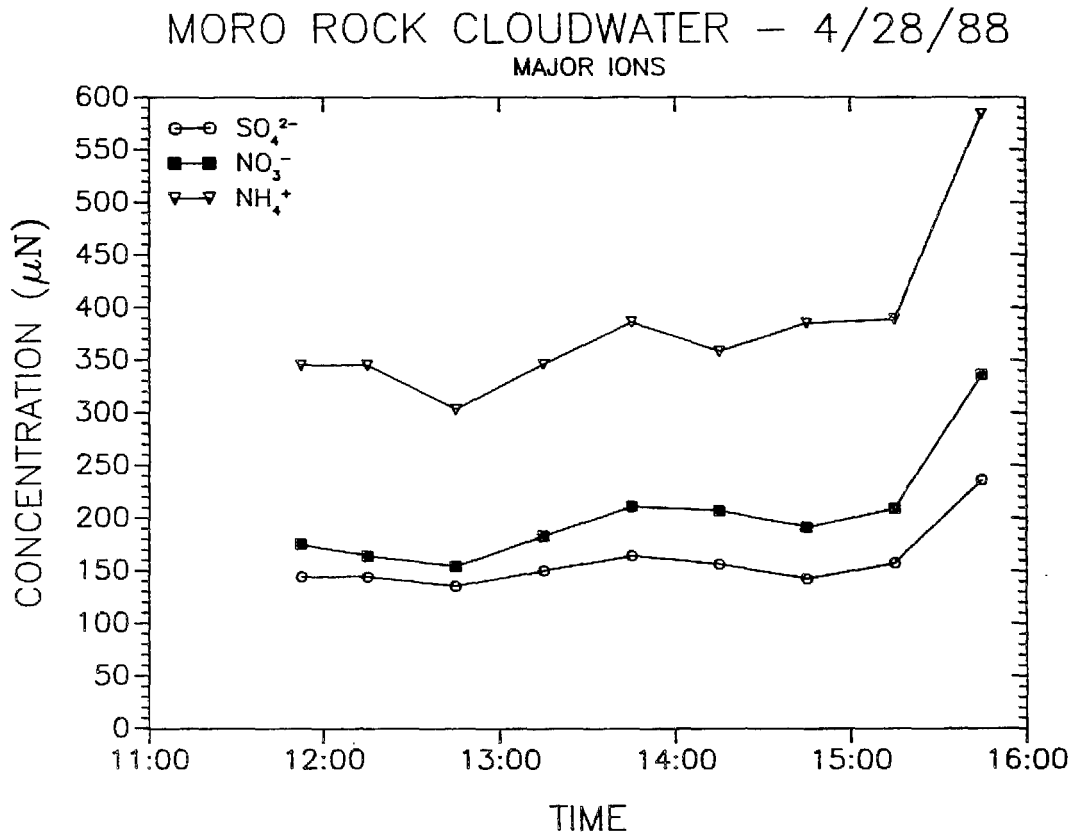


Figure 23. Concentrations of nitrate, sulfate, and ammonium in cloudwater samples collected at Moro Rock on April 28, 1988.

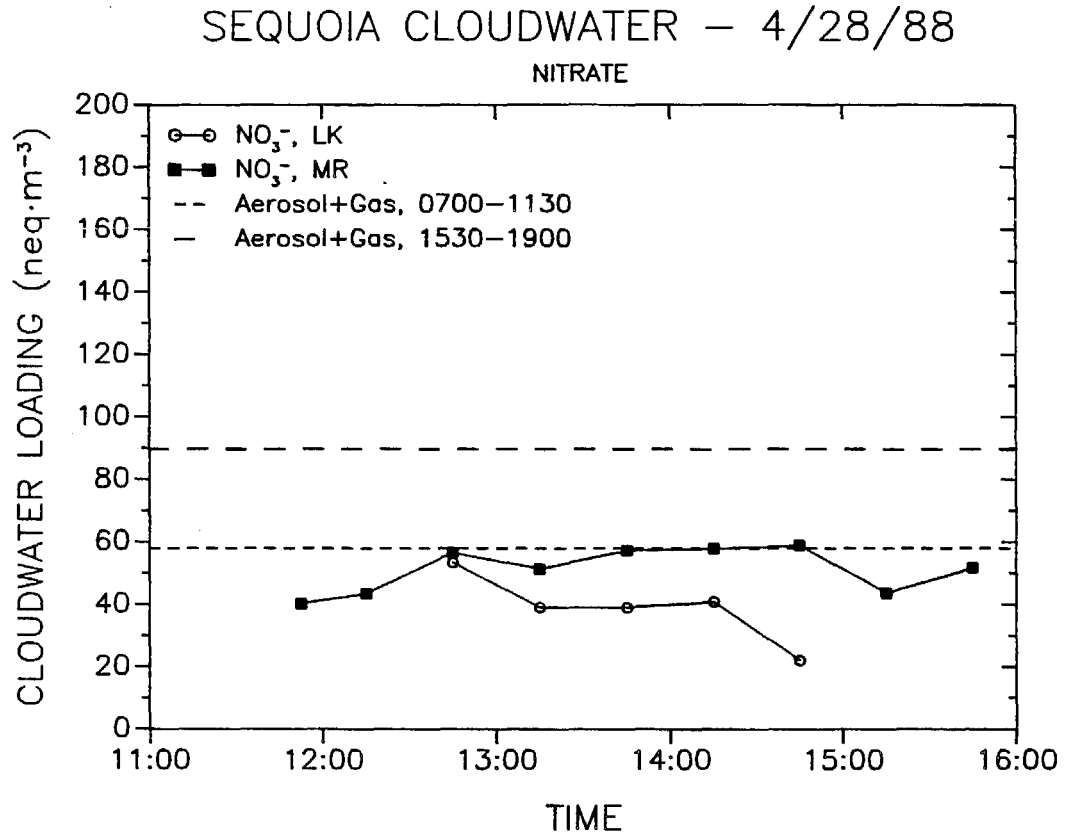


Figure 24. Cloudwater loadings of nitrate ( $\text{neq}\cdot\text{m}^{-3}$ ) at Lower Kaweah and Moro Rock on April 28, 1988. The loading for each period is calculated based on the collection rate of the CASCC and the sample nitrate concentration. Total N(V) loadings observed in the air mass at Lower Kaweah prior to and following the cloud interception event are included for reference.

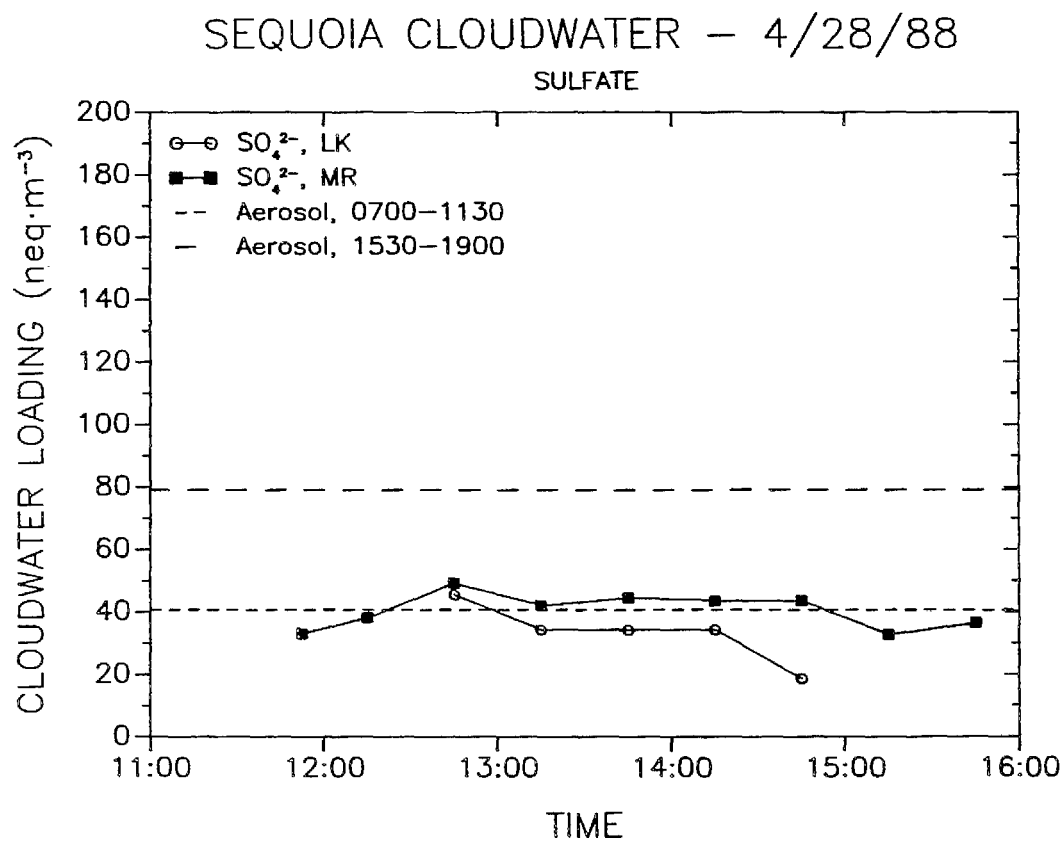


Figure 25. Cloudwater loadings of sulfate ( $\text{neq}\cdot\text{m}^{-3}$ ) at Lower Kaweah and Moro Rock on April 28, 1988. The loading for each period is calculated based on the collection rate of the CASC and the sample sulfate concentration. Aerosol sulfate loadings observed in the air mass at Lower Kaweah prior to and following the cloud interception event are included for reference.

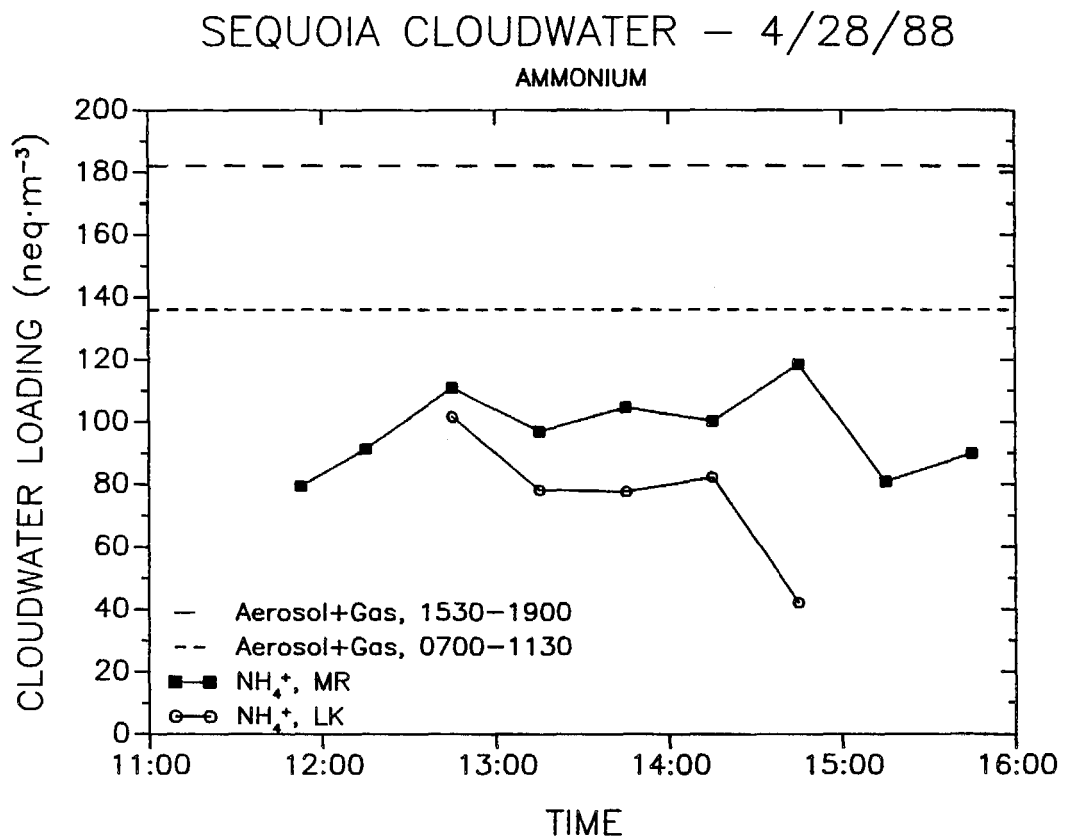


Figure 26. Cloudwater loadings of ammonium ( $\text{neq}\cdot\text{m}^{-3}$ ) at Lower Kaweah and Moro Rock on April 28, 1988. The loading for each period is calculated based on the collection rate of the CASC and the sample ammonium concentration. Total N(-III) loadings observed in the air mass at Lower Kaweah prior to and following the cloud interception event are included for reference.

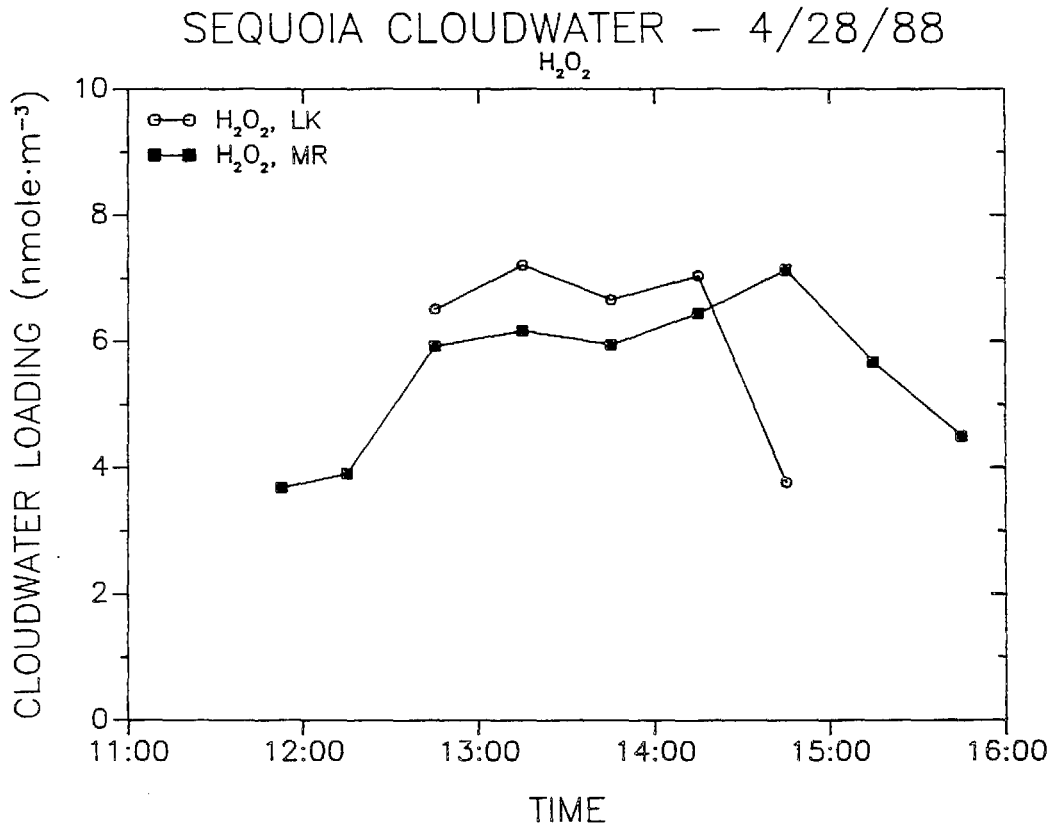


Figure 27.  $H_2O_2$  loadings in cloudwater collected at Lower Kaweah and Moro Rock on April 28, 1988. The loading for each period is calculated based on the collection rate of the CASC and the sample  $H_2O_2$  concentration.

CHAPTER 4

SPATIAL AND TEMPORAL VARIATIONS IN  
PRECIPITATION AND CLOUD INTERCEPTION IN  
THE SIERRA NEVADA OF CENTRAL CALIFORNIA

## Introduction

Interception of fog and clouds by forests has been shown to remove significant quantities of water, nutrients, and pollutants from the atmosphere. This is particularly true for forests growing near the ocean, or on mountain slopes, which are frequently immersed in fog or clouds. Kerfoot (1968) and Schemenauer (1986) have reviewed several studies undertaken to examine this phenomenon. In some cases, intercepted cloudwater has been estimated to deposit as much water as rainfall deposits. Kerfoot (1968) cites several instances where interception of cloudwater is believed to supply the water necessary for the survival of certain plant varieties in otherwise inhospitable habitats.

The rate of cloudwater deposition depends strongly on four factors: (1) the liquid water content (LWC) of the fog or cloud, (2) the droplet size distribution, (3) the structure of the forest canopy, and (4) the ambient wind speed (Lovett and Reiners, 1986). Cumulative deposition over a specified period of time also depends on the frequency and duration of fog or cloud interception in that interval.

The quantity of cloudwater deposited to the forest on a mountain slope may vary significantly with elevation, due to variations in the parameters governing the deposition process. Cloudwater deposition may increase with elevation, due to increases in average wind speeds and higher liquid water contents. The most important factor determining the elevational dependence of cloudwater deposition, however, is the elevational pattern of cloud interception. Different meteorological conditions may tend to favor cloud interception at different elevations. The upper boundary of coastal stratus clouds, for example, may be limited to 500 to 1000 m elevation by the presence of a strong temperature inversion. Cloud interception in

this environment will occur primarily at elevations at or below the predominant inversion height. Alternatively, convective clouds associated with frontal systems often have base elevations exceeding 1500 m; thus, these clouds will be intercepted most frequently at higher elevations. Schemenauer et al. (1987) found that deposition rates of cloudwater to passive cloudwater collectors located on a coastal mountain in Chile were maximal at 700 m and decreased at higher elevations. While this pattern presumably reflects a prevalence of cloud interception at 700 m elevation, their monitoring system did not actually collect information regarding the frequency or duration of interception, which could support or refute this hypothesis.

In the southern and central Sierra Nevada of California, interception of cloudwater by the forest canopy is believed to contribute significantly to regional deposition budgets for water, nutrients, and pollutants (Chapters 1, 2; Collett et al., 1989). Three mechanisms are thought to lead to the interception of fog and clouds in the region: (1) the passage of frontal systems, which often leads to interception of convective clouds by the mountain slopes; (2) local formation of fog due to the rapid cooling of moist air produced during snow melt on sunny days; and (3) the lifting of dense "Tule" fogs previously trapped near the floor of the San Joaquin Valley (Jacob et al., 1986), due to a reduction in atmospheric stability over the valley. In conjunction with a study of the chemical composition of intercepted cloudwater in the Sierra (Chapter 2), a field program was initiated to evaluate the frequency and duration of cloudwater interception, as a function of elevation, in Sequoia and Yosemite National Parks. The results of this investigation, which are essential for determining which elevations in the Sierra are likely to be affected by the deposition of cloudwater, are described in this chapter.

## Experimental Procedure

### *Monitoring Sites*

Fourteen Sierra sites were selected to serve as cloudwater monitoring stations throughout the course of the study, which lasted from September, 1987 until November, 1988. Eight of the sites, referred to as SQ1 through SQ8, were located in Sequoia National Park (Figure 1); six, YO1 through YO6, were located in Yosemite National Park (Figure 2). The chemical composition of intercepted cloudwater was monitored at sites YO3 and SQ5 (see Chapter 2). Sites were generally located in open areas where ambient clouds could intercept the site directly, although two stations (SQ4 and YO1) were situated in sparse woodland. Sites were selected so that an elevational gradient was represented in each Park; sites also were chosen to represent roughly the same range of elevations in the two Parks, in order to facilitate regional comparisons. Several factors prevented the selection of entirely comparable sites. Sites generally could not be highly visible to Park visitors, could not be located in designated wilderness areas, and had to be accessible by foot. Figures 3 and 4 illustrate the elevations of the chosen sites in Sequoia and Yosemite National Parks, respectively. The elevational gradient represented in Sequoia National Park stretched from 820 to 2360 m; site elevations in Yosemite National Park ranged from 1220 to 2300 m.

### *Equipment*

Intercepted cloudwater was collected at each site using a passive cloudwater monitoring system, described in detail in Chapter 5. This system included a passive cloudwater collector, which utilized ambient winds to collect cloudwater droplets by

inertial impaction on Teflon strands. Use of a passive collector, rather than an active collector, served to minimize power requirements (all power had to be supplied from batteries carried in to each site), and to provide a good record of only those interception periods when ambient winds were high enough to produce significant rates of cloudwater deposition to the forest canopy. The monitoring system also includes a tipping cup gauge which measures the volume of cloudwater collected, an anemometer which measures ambient wind speeds during interception, a tipping cup rain gauge which measures rainfall at the site, a data-logging system, and two 6 V batteries which supply all power used at the site.

Sites were serviced monthly. Data was transferred from the data-logger to an NEC Multispeed portable computer carried to each site. After transferring the data, the monitoring system was checked to make sure that the equipment was functioning properly, and the batteries were replaced. In the event of damage to the equipment or equipment malfunction, an attempt was made to remedy the problem at the site. When this was not possible, due to extensive damage or an unanticipated malfunction, site operations had to be discontinued, or at least curtailed, until the next visit. The most common problems encountered were failure of components in the data-logging system, errors in the data-logging software, and equipment damage by curious black bears.

The tipping cup gauges used to measure collected volumes of rainfall and intercepted cloudwater were identical. The gauges tip every time 8.7 ml of water is collected, corresponding to 0.26 mm of rainfall for the rain gauge and 0.46 mm of intercepted cloudwater for the passive cloudwater collector. Predicting actual rates of cloudwater deposition to the nearby forest canopy, based on observed rates of deposition to the passive cloudwater collector, is difficult because the structure of

the canopy is largely unknown. Furthermore, the structure varies considerably from one location to another. Dasch (1988) and Lovett (1984) modeled cloudwater deposition to two eastern U.S. fir stands with total surface area indexes (SAI) of 6 and 7, respectively (SAI is defined as the ratio of the total surface area of a canopy component to the corresponding plan area). Trees studied in both areas were approximately 10 m high. Taller trees in the Sierra probably have greater values of SAI. The SAI of the passive cloudwater collector is 11.8, suggesting that deposition rates to this instrument are probably roughly comparable to cloudwater deposition rates experienced by the larger exposed conifers in the Sierra. Deposition rates to trees within a closed canopy will be considerably lower because of reduced wind speeds within the canopy and removal of droplets by trees located upwind.

#### *Data Processing*

The data record from each site includes a log of the number of tips recorded by each tipping cup counter (rain and cloudwater) during the monitoring period, and the time at which each tip occurred. Five minute averages of the wind speeds were also recorded during all periods of precipitation or cloud interception. The design of the data-logging system limited observations to a single output at a time (tipping cup gauges or anemometer). In order to accommodate this restriction, the data-logger program contained a loop which alternately monitored the status of each input. The time required to execute this loop depends on the wind speed, since a wind speed measurement subroutine in the loop monitors one full period of the sinusoidal output of the anemometer, the length of which is inversely proportional to the anemometer's rotational velocity. If the length of the period exceeds a predetermined time, corresponding to a wind speed of approximately  $0.5 \text{ m}\cdot\text{s}^{-1}$ , execution of the subroutine is terminated. In order not to miss any pulses generated

by tips of the rain or cloudwater gauges, which might occur while the wind speed subroutine is executed, the data logging circuitry lengthens the duration of the incoming tipping cup pulses. Initially, the pulses were lengthened to approximately one second. Longer pulses were not used, so that the chance of obtaining overlapping responses from the two gauges would be reduced. At low wind speeds ( $\leq 1 \text{ m}\cdot\text{s}^{-1}$ ), however, execution of the wind speed subroutine requires slightly longer than one second; consequently, rain or cloudwater tips occurring right at the beginning of the subroutine go undetected under these conditions. We estimate, based on field experiments, that the percentage of tips missed during low wind speeds is approximately 10% using this system. Because of the prevalence of low wind speeds observed during cloud interception and rainfall during the fall of 1987, the system was modified for the spring sampling period by lengthening the pulse duration. While this modification resulted in a few cases of overlapping responses from the two gauges, it eliminated the problem of underestimating rainfall and cloud interception at low wind speeds.

As indicated in Chapter 5, data collected by the data-logger was stored as compactly as possible to reduce the memory requirements. Data collected from the data-loggers was first processed by a BASIC program which converted the compact data to a form which was more readily analyzed. The transformed data was then imported into a spreadsheet file for further processing. Since the passive cloudwater collector is an efficient collector of rain as well as intercepted cloudwater, the tips of the cloudwater gauge had to be partitioned into two groups: those due to rainfall and those due to cloudwater. Partitioning was possible only because of the simultaneous collection of rainfall data at each site. Experiments designed to compare the relative responses to rainfall exhibited by the cloudwater collector and the rain gauge indicated essentially equivalent responses at wind speeds between 1.5

and  $3 \text{ m}\cdot\text{s}^{-1}$ ; however, preferential collection of rainfall by the rain gauge was observed at lower wind speeds (see Chapter 5). Similar patterns were observed in Sierra field data during periods of rainfall without simultaneous cloud interception; consequently, tips of the cloudwater gauge, observed during rainfall, were removed from the Sierra site records, on a one-to-one correspondence with observed tips of the rain gauge. This method of eliminating the rain response of the cloudwater gauge is believed to provide a slightly conservative estimate of the overall quantity of intercepted cloudwater.

## Results and Discussion

Cloudwater interception was monitored at the fourteen Sierra monitoring stations from September, 1987 through October, 1988, although some of the sites were not in use during the entire period. Approximately half of the sites were removed during the winter months because freezing of the intercepted cloudwater on the collection strands of the passive cloudwater collector would prevent measurement of the volume collected, and could lead to strand breakage. Snowfall collected by both the rain gauge and the cloudwater collector also creates data interpretation difficulties. Some of the lower elevation sites were left in place through the winter, however, to test winter operation of the system and to obtain a record of cloud interception at lower elevations during this period. One of the sites in Yosemite, YO1, was accidentally damaged when it was removed by untrained personnel in November of 1987. In addition to the equipment damage, data collected by this station during late October and early November was lost as well. This station was not used following this incident.

Figures 5 through 9 illustrate the record of rainfall and cloudwater deposition

for sites SQ1, SQ2, SQ3, SQ6, and SQ8, respectively, from September through mid-November of 1987 (records for some of the sites extend through December). The ordinate in each plot depicts the number of tips by each gauge at the given site; the abscissa represents time. Precipitation contributions to the cloudwater collector record have already been subtracted. Little activity in the way of precipitation or cloud interception was observed before late October, but late October and early November comprised the most active period of cloud interception observed during the study. Rainfall collected at all five sites exceeded the amount of deposited cloudwater, on an absolute basis. Typically, the ratio of rainfall collected to cloudwater collected was on the order of three or four during this period, although at SQ6 the ratio was only slightly higher than one. SQ6 (elev. 2010 m) is located on a fairly open ridge-top and at least part of the increased cloudwater deposition at this site is attributable to higher wind speeds observed during cloud interception. We also can compare the hydrological inputs of rainfall and cloud interception per square meter of surface area covered by each collector. Recalling that each tip of the rain gauge corresponds to 0.26 mm of rainfall, while each tip of the cloudwater gauge corresponds to nearly twice as much deposited cloudwater (0.46 mm), it is clear that cloudwater interception is an important phenomenon at these sites. On the basis of deposition per unit area, it seems likely that the input of cloudwater to exposed conifers near SQ6 exceeded the input from rainfall during this period. Since the roots of each tree have access to rainfall deposited in some undefined region beyond this area, however, exact apportionment of the hydrological deposition to the tree is not possible.

It is instructive to examine rates of cloudwater deposition to the passive collectors during individual events, to assess the magnitude of deposition rates observed. Deposition rates during the fall of 1987 typically were observed to be the

largest at SQ6. During a 2.5 hour period on the evening of October 28, 1987, cloudwater was deposited to the collector at SQ6 at an average rate of  $4.0 \text{ mm}\cdot\text{hr}^{-1}$ ; a rate of  $1.2 \text{ mm}\cdot\text{hr}^{-1}$  was observed during a four hour period the following day. Cloudwater deposition rates at SQ6, during an extended interception event on November 1, averaged  $4.3 \text{ mm}\cdot\text{hr}^{-1}$  over an 11 hour period. Wind speeds ranged from 1 to  $3 \text{ m}\cdot\text{s}^{-1}$  during this period. High deposition rates also were observed at other monitoring stations. During an overlapping 7 hour period on November 1, cloudwater deposition to the collector at SQ3 (1510 m) averaged  $3.1 \text{ mm}\cdot\text{hr}^{-1}$ . These deposition rates are somewhat greater than reported for deposition to an exposed redwood in northern California ( $1.6 \text{ mm}\cdot\text{hr}^{-1}$ ; Azevedo and Morgan, 1974), and much higher than reported values for cloudwater deposition to a single exposed 10 m fir tree on the summit of Clingmans Peak in North Carolina ( $0.3 \text{ mm}\cdot\text{hr}^{-1}$ ; Dasch, 1988). The surface area index of the tree studied by Dasch (1988) was estimated to be approximately half that of our collector, suggesting that larger cloudwater deposition rates experienced by the collector in this study probably are indicative of substantially higher deposition rates to exposed conifers near the sites as well.

Cloudwater concentrations of  $\text{NO}_3^-$  and  $\text{NH}_4^+$  are typically an order of magnitude or more higher in Sequoia National Park (SNP) than SNP precipitation concentrations of these same species (see Chapter 2). Therefore, it is likely that the deposition of these species to exposed conifers near SQ3, SQ6, and SQ8, via cloud interception, exceeded that due to precipitation during the fall of 1987; deposition of  $\text{SO}_4^{2-}$  probably also was dominated by cloudwater interception, at least at SQ6, since  $\text{SO}_4^{2-}$  concentrations average more than three times higher in SNP cloudwater than in SNP precipitation (Chapter 2). Cloudwater deposition rates to trees located in closed canopies in the region are probably significantly lower than the rates

hypothesized here for exposed trees (Lovett and Reiners, 1986; Dasch, 1988); consequently, pollutant deposition to closed canopies may be dominated by rainfall or dry deposition.

Rainfall amounts at SQ2, SQ3, SQ6, and SQ8, from September through mid-November of 1987, were quite comparable (130 – 160 mm), while the lowest elevation site, SQ1, experienced considerably less rainfall (80 mm). Rainfall was generally observed simultaneously at most of the sites; amounts were just smaller at lower elevation (see Figures 5 through 9). A comparison of the cloudwater interception records illustrated in these figures reveals that cloud interception events, in contrast to rainfall, often occurred only at the higher elevation sites. This is a reflection of the fact that most of the intercepted clouds were associated with frontal systems approaching from the north or northwest, with cloud bases often located above 1500 m.

Rainfall and cloudwater interception data for the fall of 1987 are presented for Yosemite National Park (YNP) sites YO2, YO3, YO4, and YO6 in Figures 10 through 13, respectively. Rainfall at YO2, YO4, and YO6 was comparable to that observed at the higher elevation SNP sites during the period ending in mid-November. Data for YO3 is missing for much of this period because of data-logger failure. Cloudwater deposition at YO2 (1490 m) and YO4 (1220 m) was fairly low during this period, somewhat less than was observed at the lowest elevation SNP site (SQ1, el. 820 m). YO2 and YO4 are situated on the slopes of the Merced River canyon. The canyon, which has a north-south orientation in this region, is relatively narrow, preventing most frontal system clouds, advancing from the west or northwest, from dropping into the canyon interior where these two sites are located. Cloudwater deposition at YO6 (2020 m) was greater than that

observed at all but one of the Sequoia sites (SQ6). The timing of the interception events at YO6 also agreed quite well with that at both SQ6 and SQ8, which are located at 2010 m and 2180 m, respectively. YO6 is situated just below the summit on a fairly open hillside, and, like SQ6 and SQ8, has good exposure to the west.

Several cold fronts crossed the Sierra Nevada during the month of December, depositing a substantial amount of snow. Nevertheless, there were several cloud interception events at lower elevations that we were able to successfully monitor during this period. Data collected at sites SQ1 and SQ3, from late November through the end of 1987, are depicted in Figures 5 and 7. Rainfall during this period represents the sum of actual rainfall and snowmelt in the rain gauge. While cloudwater interception events during this period generally were witnessed simultaneously at both sites, the volume of cloudwater collected differed significantly between the two sites for a given event. Cloudwater interception during the late morning of December 22, for example, was much greater at SQ1 (820 m) than at SQ3 (1510 m). This interception event followed a period of dense fog in the southern San Joaquin Valley, which had persisted through most of December 21 and into the morning of December 22 (NOAA, 1987). Since much greater interception activity was observed at the lower site (SQ1) on December 22, it seems likely that the cloud interception was the result of lifting of the fog layer previously trapped near the valley floor. This observation indicates a need to monitor the chemical composition of cloudwater during the winter at lower elevation sites (500 to 1000 m) in SNP, since southern San Joaquin Valley fogs have been shown to be heavily polluted (Jacob et al., 1986).

Figures 10 through 12 display the observations made at sites YO2, YO3, and YO4, from late November through the end of December, 1987. The measured

rainfall and cloudwater deposition patterns at YO2 and YO4 were quite similar. Approximately 80 mm of rain and melted snow was measured at both sites during this period. Fifty percent more rain was measured at YO3; cloudwater deposition at YO3 was three times the levels observed at YO2 and YO4, despite the close proximity of these three sites (see Figure 2). Wind speeds at YO3 typically were observed to be much higher than at YO2 and YO4, providing a more conducive environment for high rates of cloudwater deposition. In addition, YO3 is situated on top of a granite dome, and is completely exposed to convective clouds approaching from almost any direction, whereas YO2 and YO4 are shielded somewhat by the walls of the Merced River canyon.

Major events involving both rainfall and cloudwater impaction were observed in both Parks on December 6 and December 22, 1987. In fact, there generally seems to be a high degree of correlation between periods of cloud interception and precipitation in the two Parks. In several cases, correlations between deposition rates at a given elevation in SNP and those at a similar elevation in YNP are much stronger than those between sites at different elevations in a single Park. This is not too surprising, given that much of the cloudwater deposition is due to interception of convective clouds associated with the passage of frontal systems across the Sierra. Often the cloud base in such systems lies above the elevations of several of the lower sampling sites, as observed previously, but the horizontal extent of the system may reach for several hundred kilometers, easily covering the 150 km between the two Parks. Nevertheless, there are many occasions when clouds are observed at one Park, but not at the other, particularly when the frontal system is centered in extreme northern or extreme southern California.

Data collection during the winter was greatly complicated by the presence of

snow and rime ice. Since no temperature record was available at the sites, it is difficult to ascertain whether tips of the two gauges during this period were due to cloud interception, rain, hail, or melting snow. In addition, several problems were experienced with the data-loggers during this period. For this reason, only those data collected in December have been presented from the winter sampling period; however, as indicated in Chapter 2, relatively little cloud interception activity was observed during January, February, or March.

Data collected at the thirteen Sierra cloudwater monitoring sites (SQ1 through SQ8 and YO2 through YO6) between early May and late August, 1988 are presented in Figures 14 through 26 (little activity was recorded between the end of August and early November, when the stations were removed). While several rain events were observed over the course of the spring and summer, only two major cloud interception events were observed during this period. These occurred on May 17 and May 28, and were observed at almost all of the monitoring stations.

Amounts of cloudwater deposited in these two events generally were larger at the higher elevation sites, as was observed to be the case in most of the previous interception events. Total cloudwater deposition at SNP, in the two events, was dominated by contributions on May 17, while cloudwater deposition at YNP was generally greater in the May 28 event. Volumes of cloudwater collected at several of the sites in these two events were relatively large compared to the seasonal total precipitation. At YO3, in fact, the volume of cloudwater collected on May 28 exceeded the total volume of precipitation collected between early May and the end of October, underscoring the importance of cloudwater deposition in the Sierra. Rates of cloudwater deposition to the collector, during a 5 hour period on the evening of May 28, averaged more than  $24 \text{ mm}\cdot\text{hr}^{-1}$ . Wind speeds observed at the

site during this period averaged approximately  $10 \text{ m}\cdot\text{s}^{-1}$ . A remarkably high cloudwater deposition rate of  $13.4 \text{ mm}\cdot\text{hr}^{-1}$  also was observed at YO6 during an overlapping 3 hour period on the same evening. Wind speeds at YO6 averaged  $4 - 5 \text{ m}\cdot\text{s}^{-1}$  during the period. These cloudwater deposition rates are much higher than have been reported previously.

Data from the cloudwater monitoring stations can also be used to track the progress of an advancing cloud mass. On May 28, for example, a strong Pacific cold front, approaching from the northwest, reached the Sierra. Cloudwater interception began at YO6, approximately half an hour before interception was observed at YO3. This pattern is consistent with the direction of approach of the storm, since YO6 is located several kilometers northwest of YO3. Cloud interception at YO3 was observed to continue for approximately two hours after it had ceased at YO6.

Volume-weighted average YO3 cloudwater concentrations of  $\text{NO}_3^-$ ,  $\text{SO}_4^{2-}$ ,  $\text{NH}_4^+$ , and  $\text{H}^+$  were observed to be 20, 14, 34, and  $9.4 \mu\text{N}$ , respectively, during the May 28 cloud interception event (see Chapter 2); cloudwater deposition to the passive cloudwater collector at YO3 was approximately 118 mm during this period. Chemical deposition to the collector during this event, therefore, can be estimated as  $150 \text{ mg}\cdot\text{m}^{-2}$  of  $\text{NO}_3^-$ ,  $81 \text{ mg}\cdot\text{m}^{-2}$  of  $\text{SO}_4^{2-}$ ,  $72 \text{ mg}\cdot\text{m}^{-2}$  of  $\text{NH}_4^+$ , and  $1.1 \text{ mg}\cdot\text{m}^{-2}$  of  $\text{H}^+$ . By comparison, the average annual quantities of  $\text{NO}_3^-$ ,  $\text{SO}_4^{2-}$ ,  $\text{NH}_4^+$ , and  $\text{H}^+$  deposited in YNP precipitation in 1983 and 1984 were 550, 495, 145, and  $5.3 \text{ mg}\cdot\text{m}^{-2}$ , respectively (NADP/NTN, 1985, 1986), suggesting that cloudwater deposition of these ions to the passive collector, on May 28, 1988 alone, probably contributed significantly to their total annual deposition at the site. Since rates of cloudwater deposition to exposed conifers may be comparable to those measured by the passive cloudwater collector, as discussed above, a significant portion of the

total annual deposition of  $\text{NO}_3^-$ ,  $\text{SO}_4^{2-}$ ,  $\text{NH}_4^+$ , and  $\text{H}^+$  to the trees at YO6 may have been delivered during this single cloud interception event.

## Conclusions

The spatial and temporal variations exhibited in patterns of precipitation and cloud interception were investigated at fourteen sites in the Sierra Nevada of California. The sites, located in Sequoia and Yosemite National Parks, were selected to represent an elevational gradient in each Park, ranging from approximately 800 to 2400 m in elevation. The study began in September, 1987 and continued through October, 1988. A new monitoring system, which incorporated a passive cloudwater collector, was developed and built specifically for this study. The system also included a rain gauge and an anemometer. A data-logger, designed specifically for this program, maintained a time-resolved record of activity by the cloudwater collector, the rain gauge, and the anemometer.

Data collected during the program illustrates that cloud interception contributes significantly to the total deposition budgets of water and pollutants in the Sierra. The contributions are particularly important for exposed conifers, which are subject to direct impaction of ambient clouds. Rates of deposition to the passive cloudwater collectors, which may be comparable to rates for exposed conifers, were observed to frequently exceed  $1.0 \text{ mm}\cdot\text{hr}^{-1}$  at several sites, and surpassed  $20 \text{ mm}\cdot\text{hr}^{-1}$  at one site in Yosemite National Park during passage of a strong Pacific cold front. Cloudwater deposition of  $\text{NH}_4^+$ ,  $\text{NO}_3^-$ ,  $\text{SO}_4^{2-}$ , and  $\text{H}^+$  to exposed conifers near this site, during this single interception event, is believed to have contributed a significant portion of the total annual atmospheric flux of these species to nearby trees, and the ground beneath them.

Most Sierra cloud interception events are believed to result from the interception of convective clouds, associated with frontal activity; however, there is some evidence to suggest that dense winter "Tule" fogs, formed near the floor of the San Joaquin Valley, may intercept lower elevation sites in Sequoia National Park, when the atmosphere over the valley is destabilized. Interception of convective clouds is observed most frequently at sites above 1500 m elevation. Ridge-top sites, which often experience the highest wind speeds, usually receive the greatest hydrological deposition fluxes from impacting cloudwater. Correlations of cloudwater deposition between sites in Sequoia National Park and similarly elevated sites in Yosemite National Park are often stronger than those between sites with differing elevations in a single Park. The progress of the leading edge of an incoming storm is illustrated by the time-resolved cloud interception records of the spatially distributed sites.

## Acknowledgments

We are grateful to the National Park Service for granting access to the monitoring sites in both Yosemite and Sequoia National Parks. We also would like to acknowledge the assistance of members of the Research staff at Sequoia National Park and the Resource Management staff at Yosemite National Park who helped us to select the sites. John Lee is gratefully acknowledged for development of the data-loggers used in the study. Finally, we would like to thank our colleagues, J. William Munger and Dieter Gunz, who frequently provided field assistance during the project. This work was funded by the California Air Resources Board (CARB contract #A6-185-32).

## References

Azevedo, J. and Morgan, D. L. (1974) Fog precipitation in coastal California forests. *Ecology* **55**, 1135-1141.

Collett, J., Jr., Daube, B., Jr., Munger, J. W. and Hoffmann, M. R. (1989) Cloudwater chemistry in Sequoia National Park. *Atmos. Environ.*, in press.

Dasch, J. M. (1988) Hydrological and chemical inputs to fir trees from rain and clouds during a 1-month study at Clingmans Peak, NC. *Atmos. Environ.* **22**, 2255-2262.

Jacob, D. J., Munger, J. W., Waldman, J. M. and Hoffmann, M. R. (1986) The  $\text{H}_2\text{SO}_4$ - $\text{HNO}_3$ - $\text{NH}_3$  system at high humidities and in fogs: I. Spatial and temporal patterns in the San Joaquin Valley of California. *J. Geophys. Res.* **91**, 1073-1088.

Kerfoot, O. (1968) Mist precipitation on vegetation. *For. Abstr.* **29**, 8-20.

Lovett, G. M. (1984) Rates and mechanisms of cloud water deposition to a subalpine balsam fir forest. *Atmos. Environ.* **18**, 361-371.

Lovett, G. M. and Reiners, W. A. (1986) Canopy structure and cloud water deposition in subalpine coniferous forests. *Tellus* **38B**, 319-327.

National Atmospheric Deposition Program / National Trends Network (1985) 1983 NADP/NTN Annual Data Summary, available from the NADP/NTN Coordinator's Office, Colorado State University, Fort Collins, CO, 209 p.

National Atmospheric Deposition Program / National Trends Network (1986) 1984 NADP/NTN Annual Data Summary, available from the NADP/NTN Coordinator's Office, Colorado State University, Fort Collins, CO, 240 p.

National Oceanic and Atmospheric Administration (1987) Local climatological data Bakersfield, CA, December, 1987, available from the National Climatic Data Center, Asheville, NC, 4 p.

Schemenauer, R. S. (1986) Acidic deposition to forests: the 1985 Chemistry of High Elevation Fog (CHEF) project. *Atmos. Ocean* **24**, 303-328.

Schemenauer, R. S., Cereceda, P. and Carvajal, N. (1987) Measurements of fog water deposition and their relationships to terrain features. *J. Climate Appl. Meteorol.* **26**, 1285-1291.

## Figure Captions

- Figure 1. Map of Sequoia National Park indicating the locations of the cloudwater monitoring sites, labeled as remote and main sites. SQ5, labeled as a main site, also was utilized to collect cloudwater samples for chemical analysis (see Chapter 2). Contours are labeled in feet.
- Figure 2. Map of Yosemite National Park indicating the locations of the cloudwater monitoring sites, labeled as remote and main sites. YO3, labeled as a main site, also was utilized to collect cloudwater samples for chemical analysis (see Chapter 2). Contours are labeled in feet.
- Figure 3. Elevations of the cloudwater monitoring sites in Sequoia National Park.
- Figure 4. Elevations of the cloudwater monitoring sites in Yosemite National Park.
- Figure 5. Precipitation and cloudwater deposition at SQ1 (elev. 820 m) during the fall of 1987. Each tip of the rain gauge corresponds to 0.26 mm of precipitation; each tip of the cloudwater gauge corresponds to 0.46 mm of deposited cloudwater.
- Figure 6. Precipitation and cloudwater deposition at SQ2 (elev. 1070 m) during the fall of 1987. Each tip of the rain gauge corresponds to 0.26 mm of precipitation; each tip of the cloudwater gauge corresponds to 0.46 mm of deposited cloudwater.
- Figure 7. Precipitation and cloudwater deposition at SQ3 (elev. 1510 m) during the fall of 1987. Each tip of the rain gauge corresponds to 0.26 mm of precipitation; each tip of the cloudwater gauge corresponds to 0.46 mm of deposited cloudwater.

- Figure 8. Precipitation and cloudwater deposition at SQ6 (elev. 2010 m) during the fall of 1987. Each tip of the rain gauge corresponds to 0.26 mm of precipitation; each tip of the cloudwater gauge corresponds to 0.46 mm of deposited cloudwater.
- Figure 9. Precipitation and cloudwater deposition at SQ8 (elev. 2180 m) during the fall of 1987. Each tip of the rain gauge corresponds to 0.26 mm of precipitation; each tip of the cloudwater gauge corresponds to 0.46 mm of deposited cloudwater.
- Figure 10. Precipitation and cloudwater deposition at YO2 (elev. 1490 m) during the fall of 1987. Each tip of the rain gauge corresponds to 0.26 mm of precipitation; each tip of the cloudwater gauge corresponds to 0.46 mm of deposited cloudwater.
- Figure 11. Precipitation and cloudwater deposition at YO3 (elev. 1590 m) during the fall of 1987. Each tip of the rain gauge corresponds to 0.26 mm of precipitation; each tip of the cloudwater gauge corresponds to 0.46 mm of deposited cloudwater.
- Figure 12. Precipitation and cloudwater deposition at YO4 (elev. 1220 m) during the fall of 1987. Each tip of the rain gauge corresponds to 0.26 mm of precipitation; each tip of the cloudwater gauge corresponds to 0.46 mm of deposited cloudwater.
- Figure 13. Precipitation and cloudwater deposition at YO6 (elev. 2020 m) during the fall of 1987. Each tip of the rain gauge corresponds to 0.26 mm of precipitation; each tip of the cloudwater gauge corresponds to 0.46 mm of deposited cloudwater.
- Figure 14. Precipitation and cloudwater deposition at SQ1 (elev. 820 m) during the spring and summer of 1988. Each tip of the rain gauge corresponds to 0.26 mm of precipitation; each tip of the cloudwater gauge corresponds to 0.46 mm of deposited cloudwater.

- Figure 15. Precipitation and cloudwater deposition at SQ2 (elev. 1070 m) during the spring and summer of 1988. Each tip of the rain gauge corresponds to 0.26 mm of precipitation; each tip of the cloudwater gauge corresponds to 0.46 mm of deposited cloudwater.
- Figure 16. Precipitation and cloudwater deposition at SQ3 (elev. 1510 m) during the spring and summer of 1988. Each tip of the rain gauge corresponds to 0.26 mm of precipitation; each tip of the cloudwater gauge corresponds to 0.46 mm of deposited cloudwater.
- Figure 17. Precipitation and cloudwater deposition at SQ4 (elev. 1780 m) during the spring and summer of 1988. Each tip of the rain gauge corresponds to 0.26 mm of precipitation; each tip of the cloudwater gauge corresponds to 0.46 mm of deposited cloudwater.
- Figure 18. Precipitation and cloudwater deposition at SQ5 (elev. 1860 m) during the spring and summer of 1988. Each tip of the rain gauge corresponds to 0.26 mm of precipitation; each tip of the cloudwater gauge corresponds to 0.46 mm of deposited cloudwater.
- Figure 19. Precipitation and cloudwater deposition at SQ6 (elev. 2010 m) during the spring and summer of 1988. Each tip of the rain gauge corresponds to 0.26 mm of precipitation; each tip of the cloudwater gauge corresponds to 0.46 mm of deposited cloudwater.
- Figure 20. Precipitation and cloudwater deposition at SQ7 (elev. 2360 m) during the spring and summer of 1988. Each tip of the rain gauge corresponds to 0.26 mm of precipitation; each tip of the cloudwater gauge corresponds to 0.46 mm of deposited cloudwater.
- Figure 21. Precipitation and cloudwater deposition at SQ8 (elev. 2180 m) during the spring and summer of 1988. Each tip of the rain gauge corresponds to 0.26 mm of precipitation; each tip of the cloudwater gauge corresponds to 0.46 mm of deposited cloudwater.

- Figure 22. Precipitation and cloudwater deposition at YO2 (elev. 1490 m) during the spring and summer of 1988. Each tip of the rain gauge corresponds to 0.26 mm of precipitation; each tip of the cloudwater gauge corresponds to 0.46 mm of deposited cloudwater.
- Figure 23. Precipitation and cloudwater deposition at YO3 (elev. 1590 m) during the spring and summer of 1988. Each tip of the rain gauge corresponds to 0.26 mm of precipitation; each tip of the cloudwater gauge corresponds to 0.46 mm of deposited cloudwater.
- Figure 24. Precipitation and cloudwater deposition at YO4 (elev. 1220 m) during the spring and summer of 1988. Each tip of the rain gauge corresponds to 0.26 mm of precipitation; each tip of the cloudwater gauge corresponds to 0.46 mm of deposited cloudwater.
- Figure 25. Precipitation and cloudwater deposition at YO5 (elev. 1370 m) during the spring and summer of 1988. Each tip of the rain gauge corresponds to 0.26 mm of precipitation; each tip of the cloudwater gauge corresponds to 0.46 mm of deposited cloudwater.
- Figure 26. Precipitation and cloudwater deposition at YO6 (elev. 2020 m) during the spring and summer of 1988. Each tip of the rain gauge corresponds to 0.26 mm of precipitation; each tip of the cloudwater gauge corresponds to 0.46 mm of deposited cloudwater.

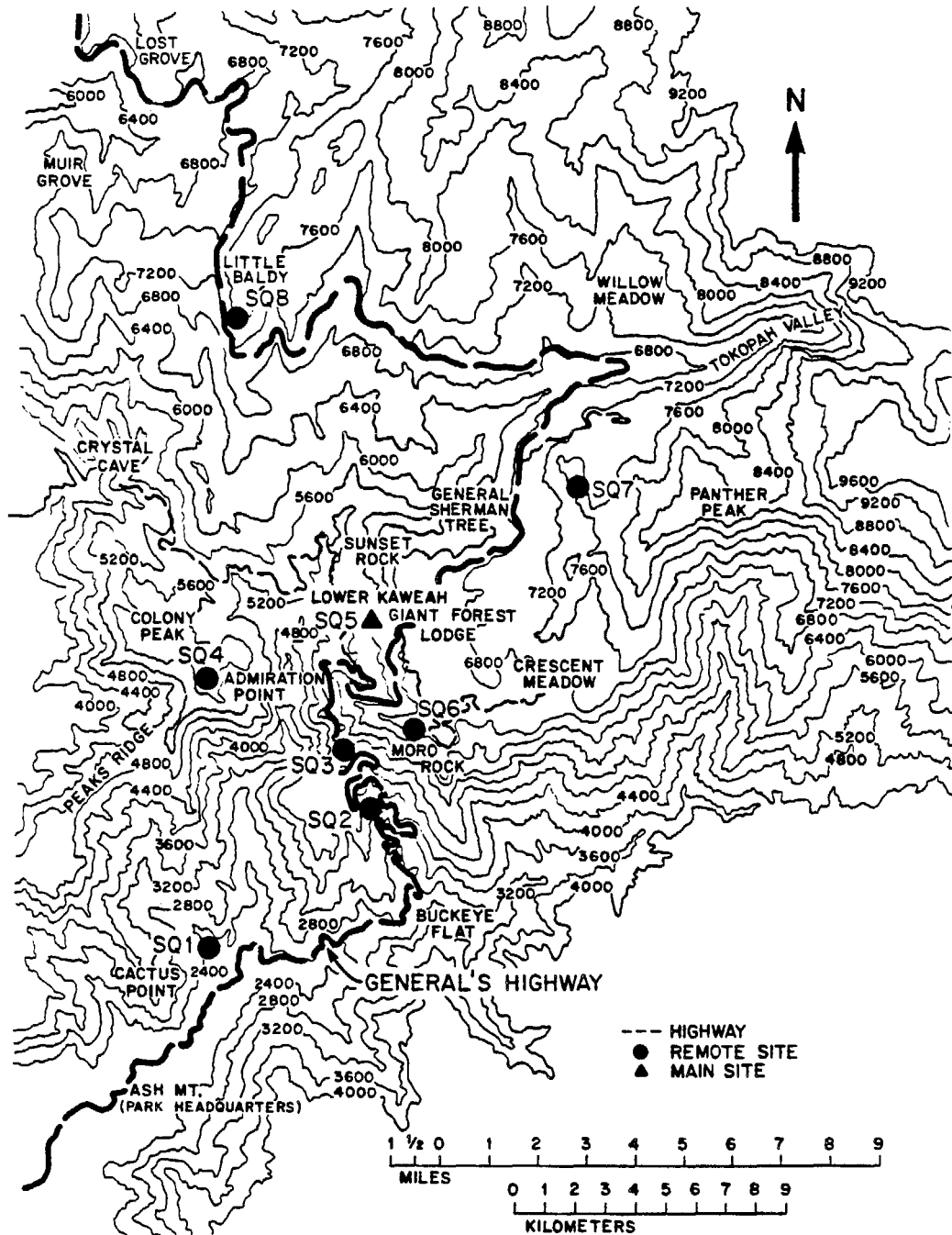


Figure 1. Map of Sequoia National Park indicating the locations of the cloudwater monitoring sites, labeled as remote and main sites. SQ5, labeled as a main site, also was utilized to collect cloudwater samples for chemical analysis (see Chapter 2). Contours are labeled in feet.

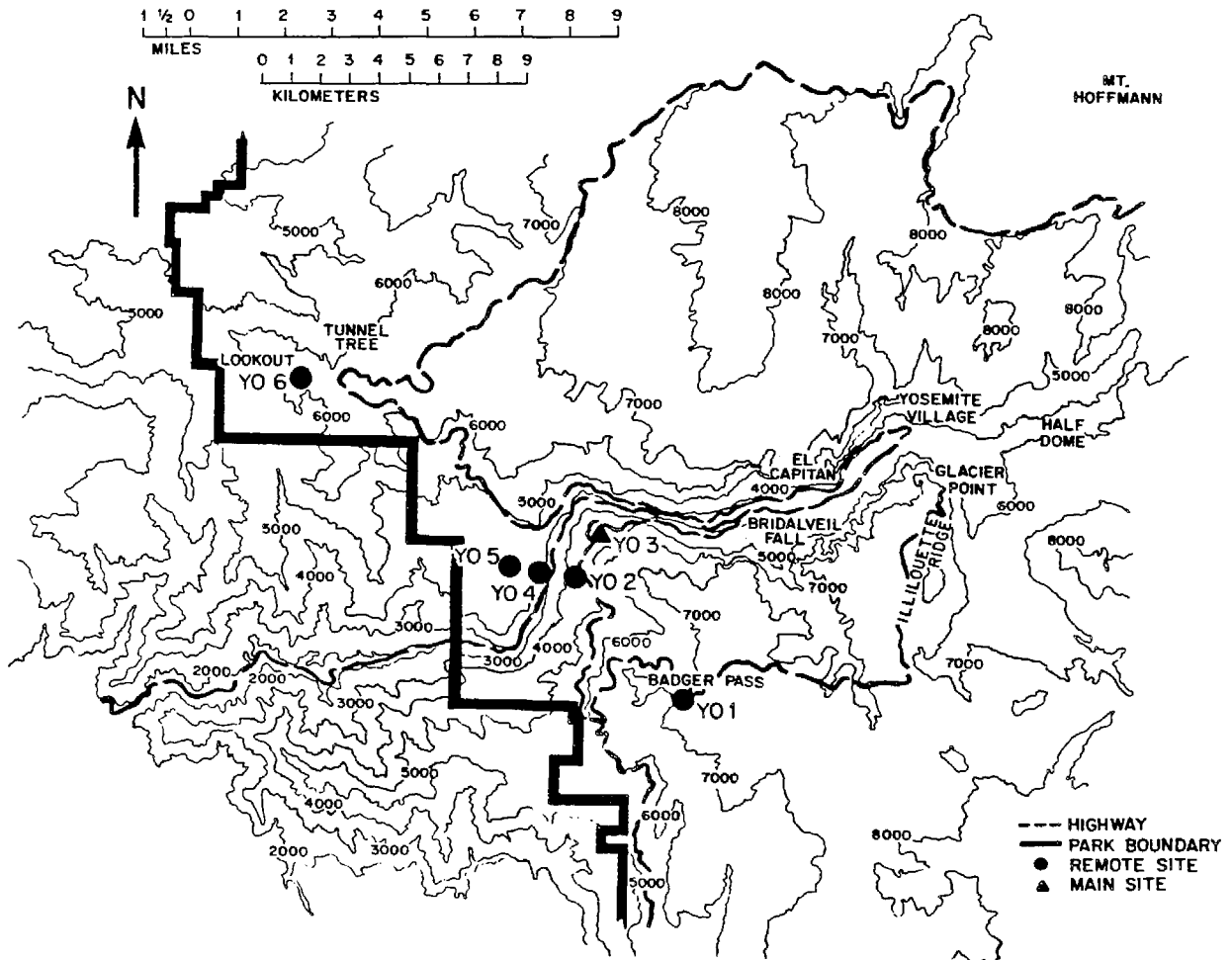


Figure 2. Map of Yosemite National Park indicating the locations of the cloudwater monitoring sites, labeled as remote and main sites. YO3, labeled as a main site, also was utilized to collect cloudwater samples for chemical analysis (see Chapter 2). Contours are labeled in feet.

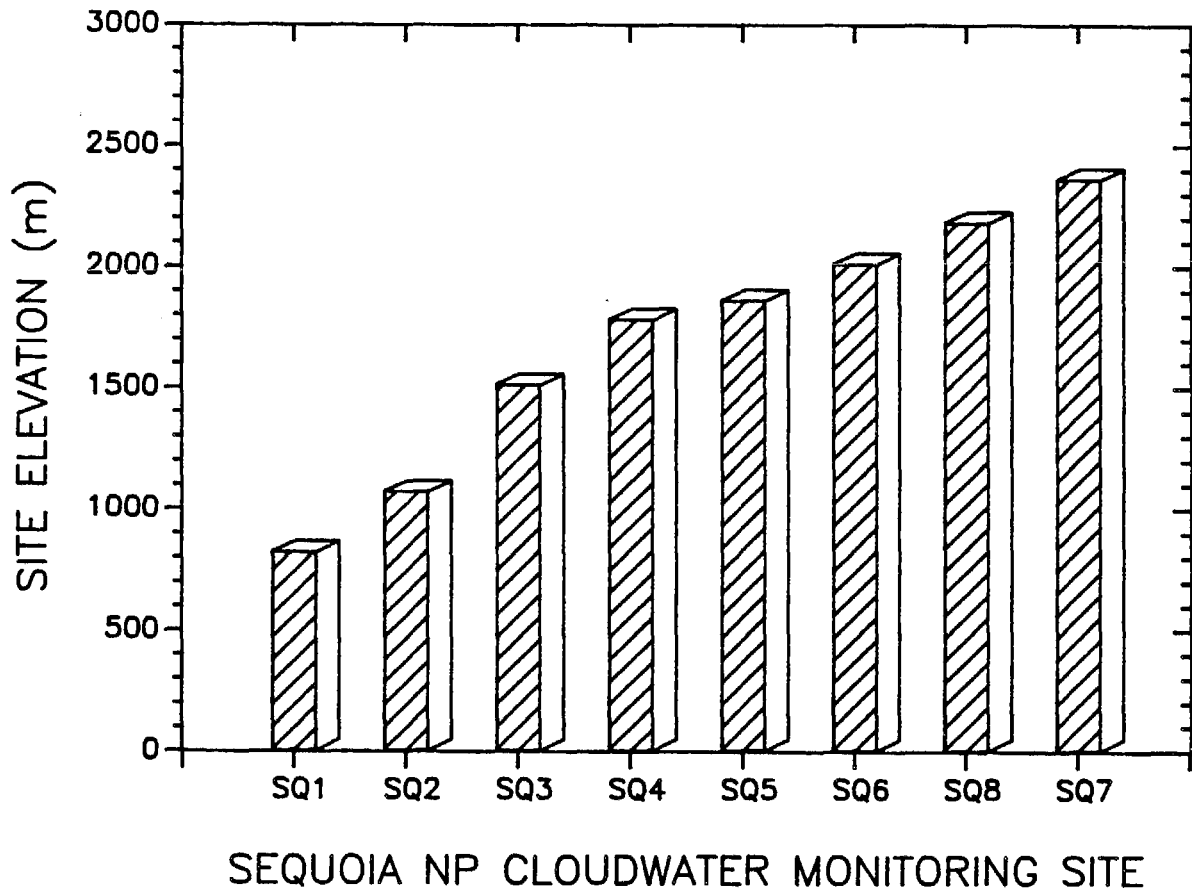


Figure 3. Elevations of the cloudwater monitoring sites in Sequoia National Park.

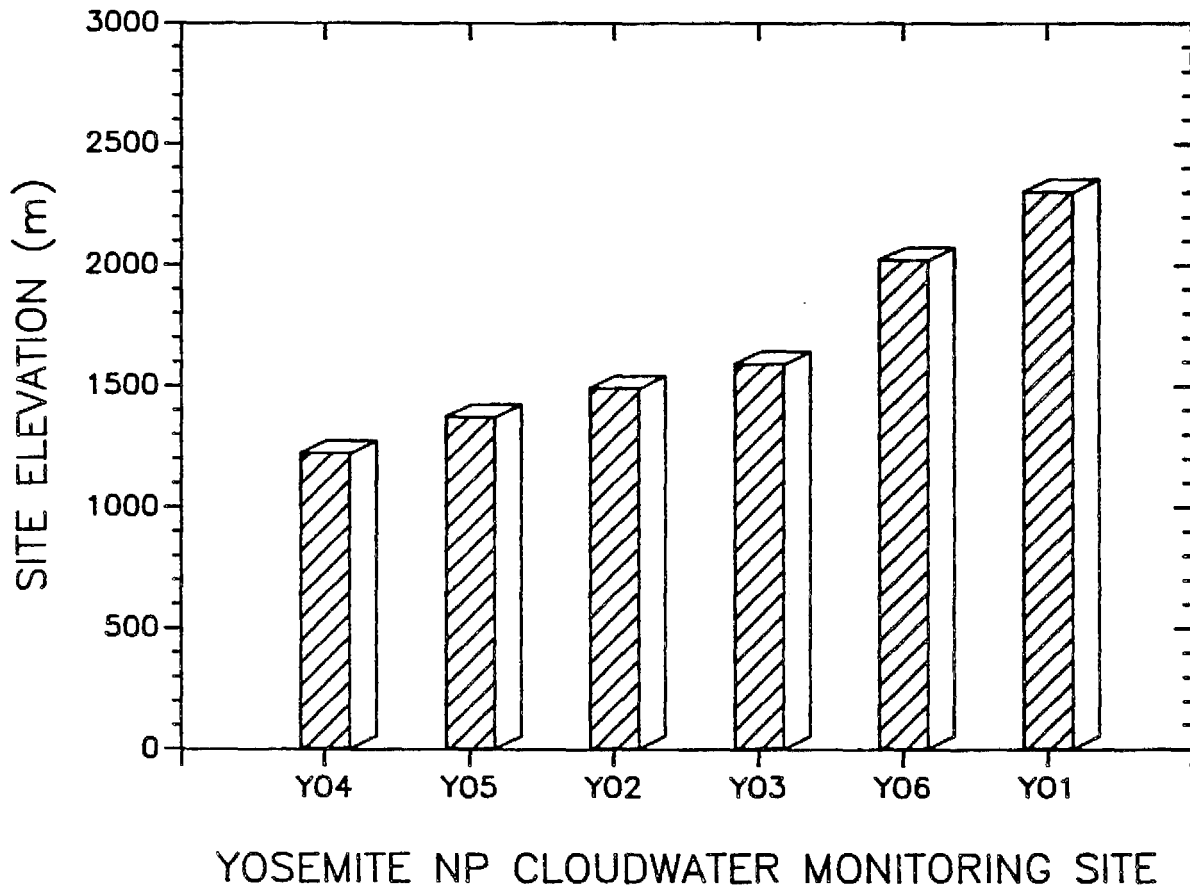


Figure 4. Elevations of the cloudwater monitoring sites in Yosemite National Park.

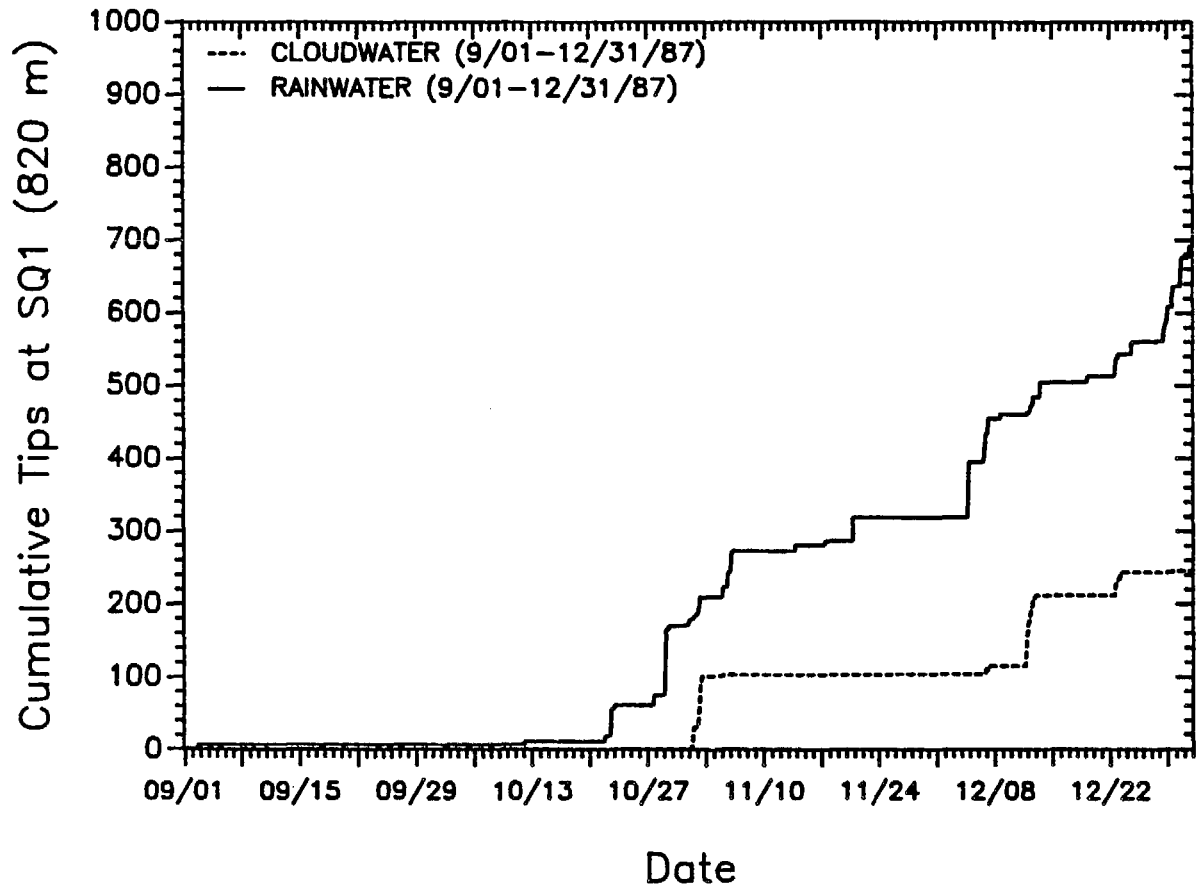


Figure 5. Precipitation and cloudwater deposition at SQ1 (elev. 820 m) during the fall of 1987. Each tip of the rain gauge corresponds to 0.26 mm of precipitation; each tip of the cloudwater gauge corresponds to 0.46 mm of deposited cloudwater.

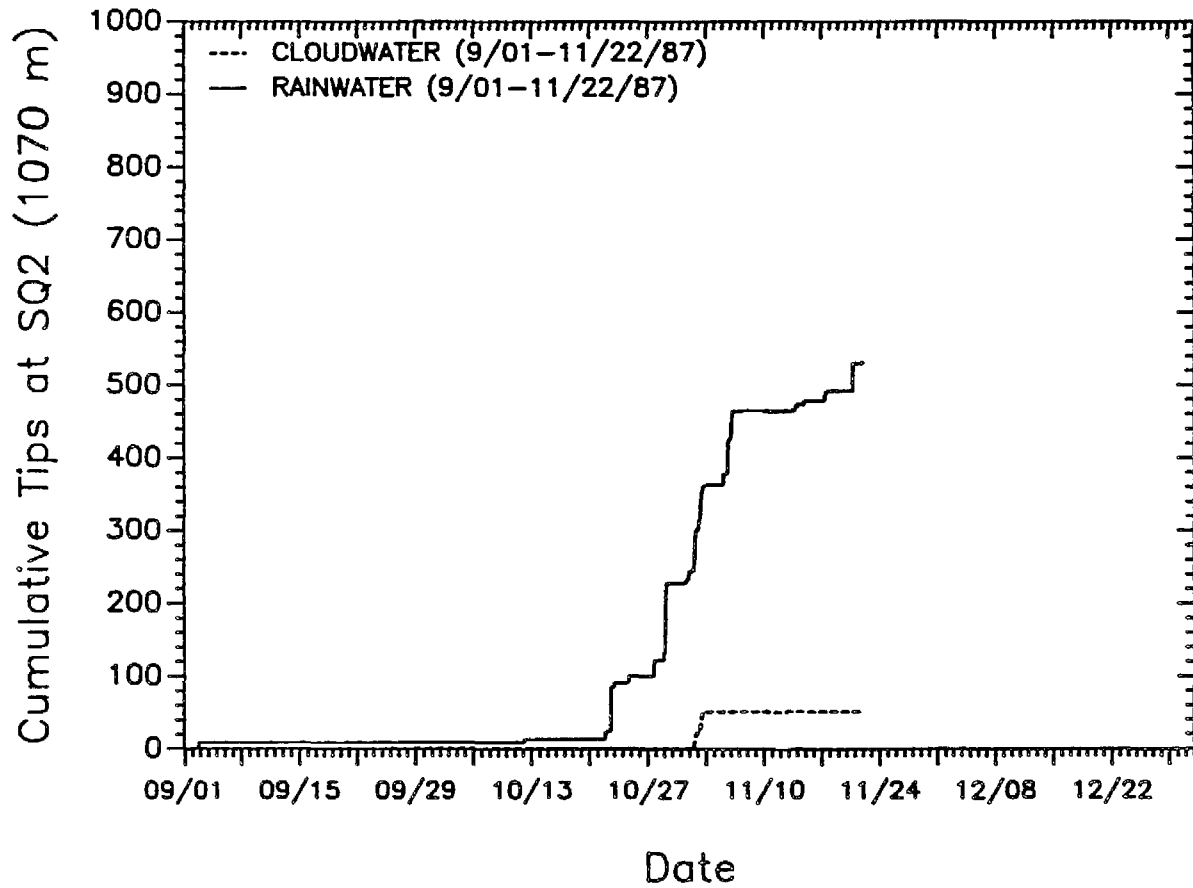


Figure 6. Precipitation and cloudwater deposition at SQ2 (elev. 1070 m) during the fall of 1987. Each tip of the rain gauge corresponds to 0.26 mm of precipitation; each tip of the cloudwater gauge corresponds to 0.46 mm of deposited cloudwater.

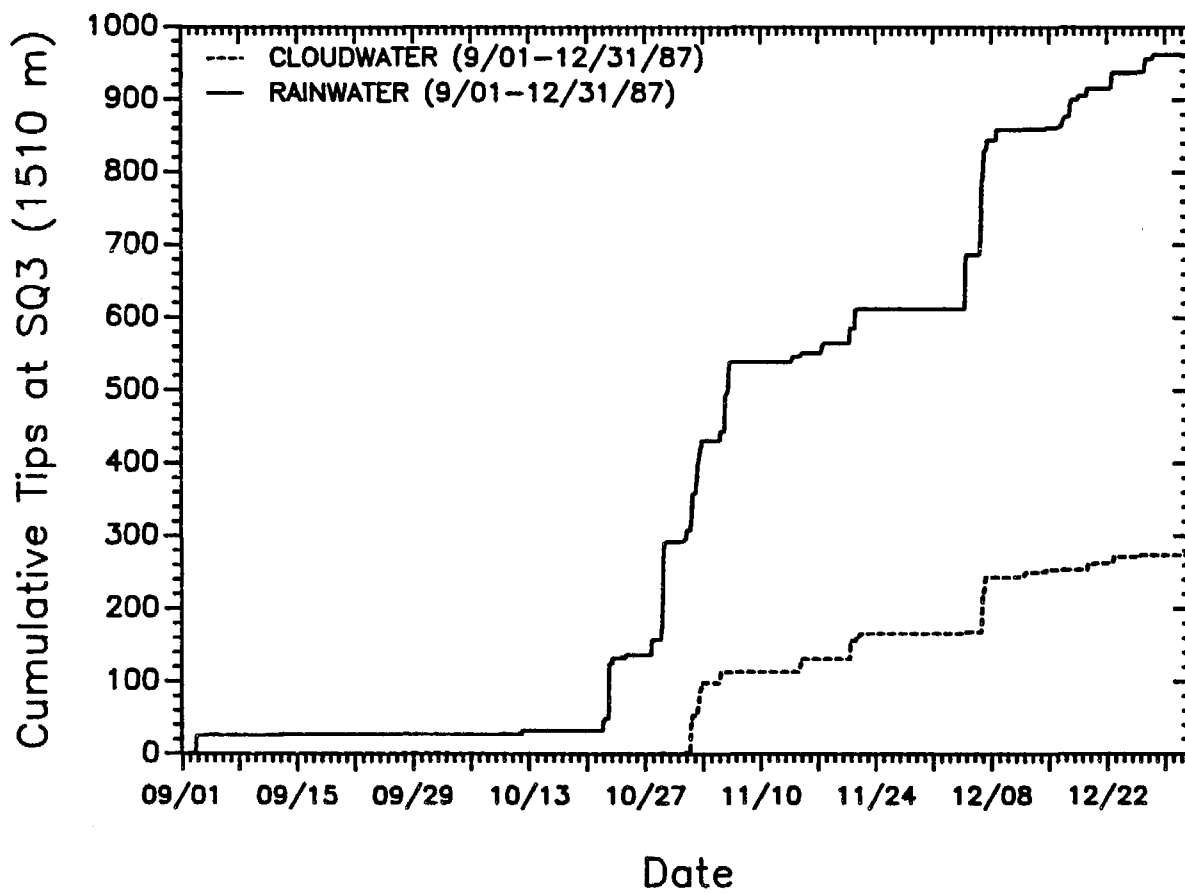


Figure 7. Precipitation and cloudwater deposition at SQ3 (elev. 1510 m) during the fall of 1987. Each tip of the rain gauge corresponds to 0.26 mm of precipitation; each tip of the cloudwater gauge corresponds to 0.46 mm of deposited cloudwater.

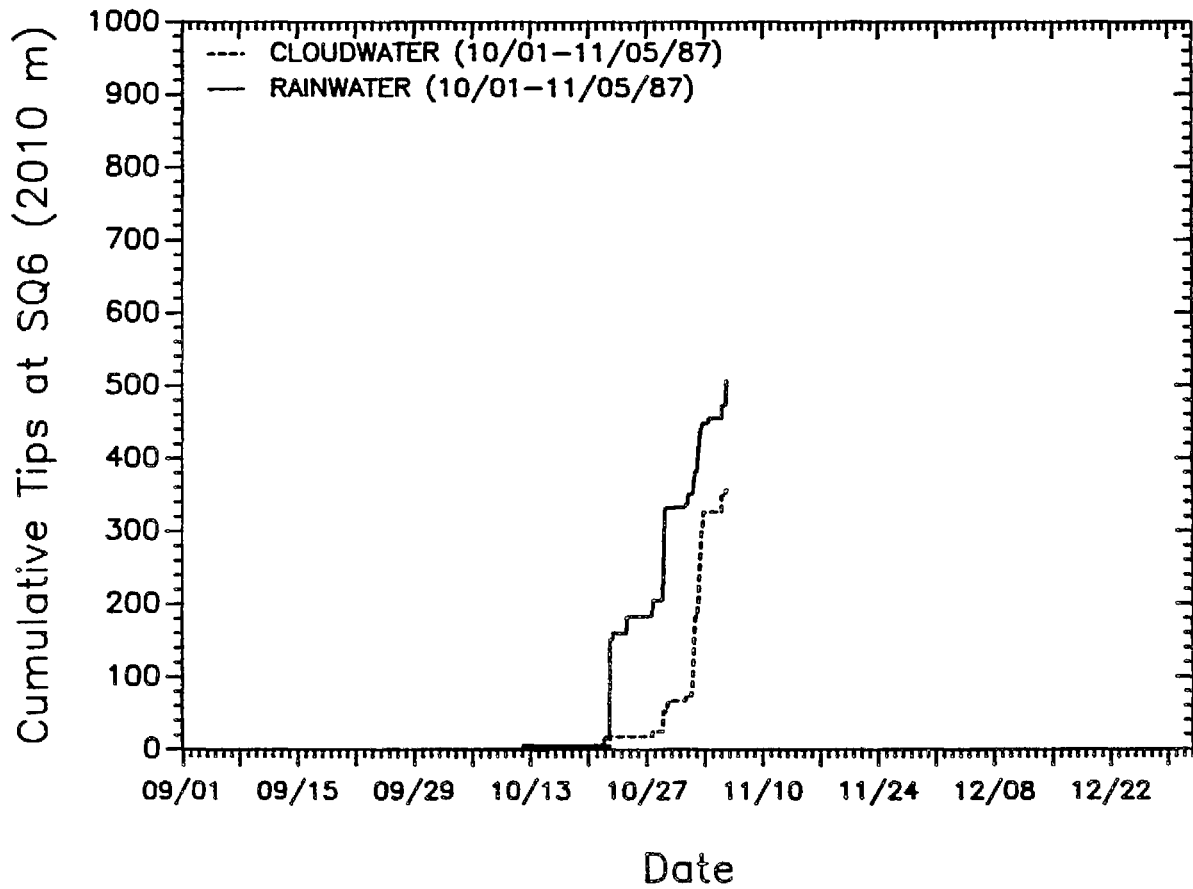


Figure 8. Precipitation and cloudwater deposition at SQ6 (elev. 2010 m) during the fall of 1987. Each tip of the rain gauge corresponds to 0.26 mm of precipitation; each tip of the cloudwater gauge corresponds to 0.46 mm of deposited cloudwater.

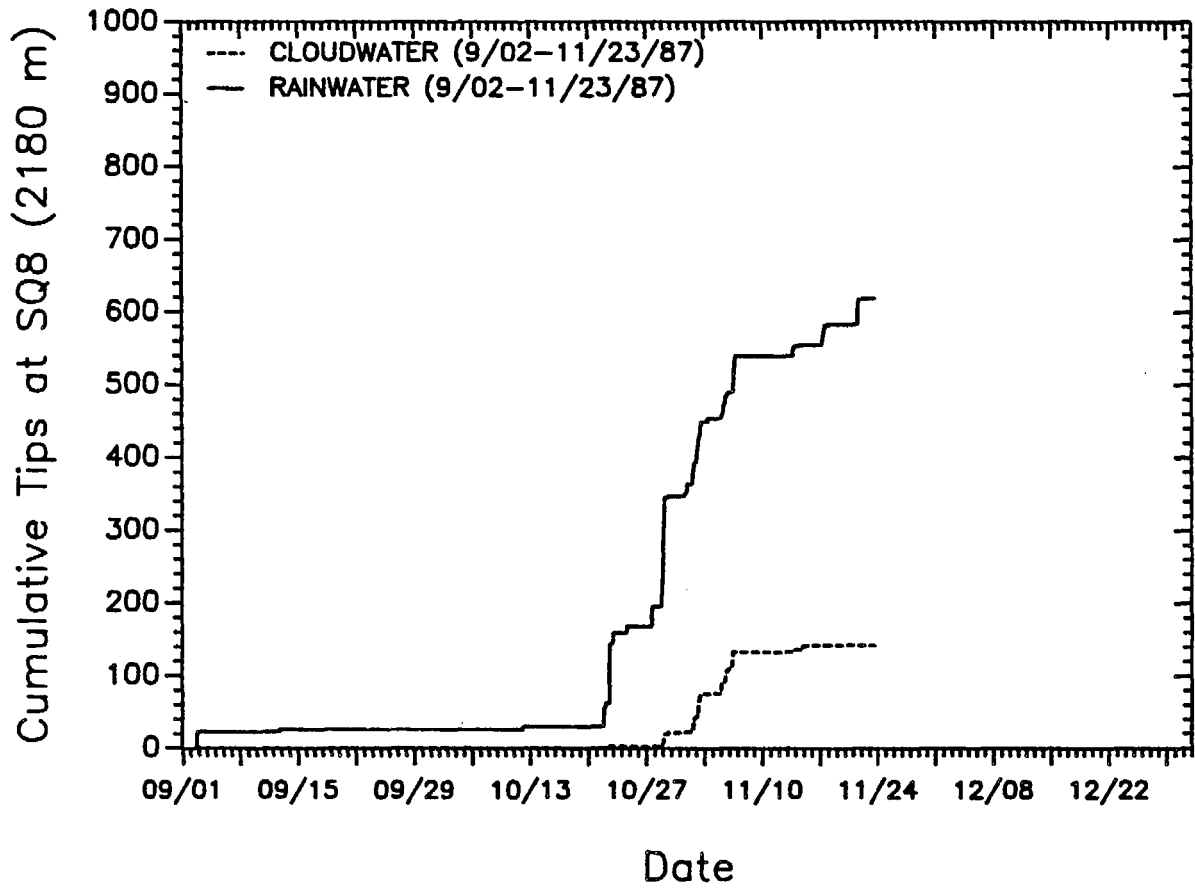


Figure 9. Precipitation and cloudwater deposition at SQ8 (elev. 2180 m) during the fall of 1987. Each tip of the rain gauge corresponds to 0.26 mm of precipitation; each tip of the cloudwater gauge corresponds to 0.46 mm of deposited cloudwater.

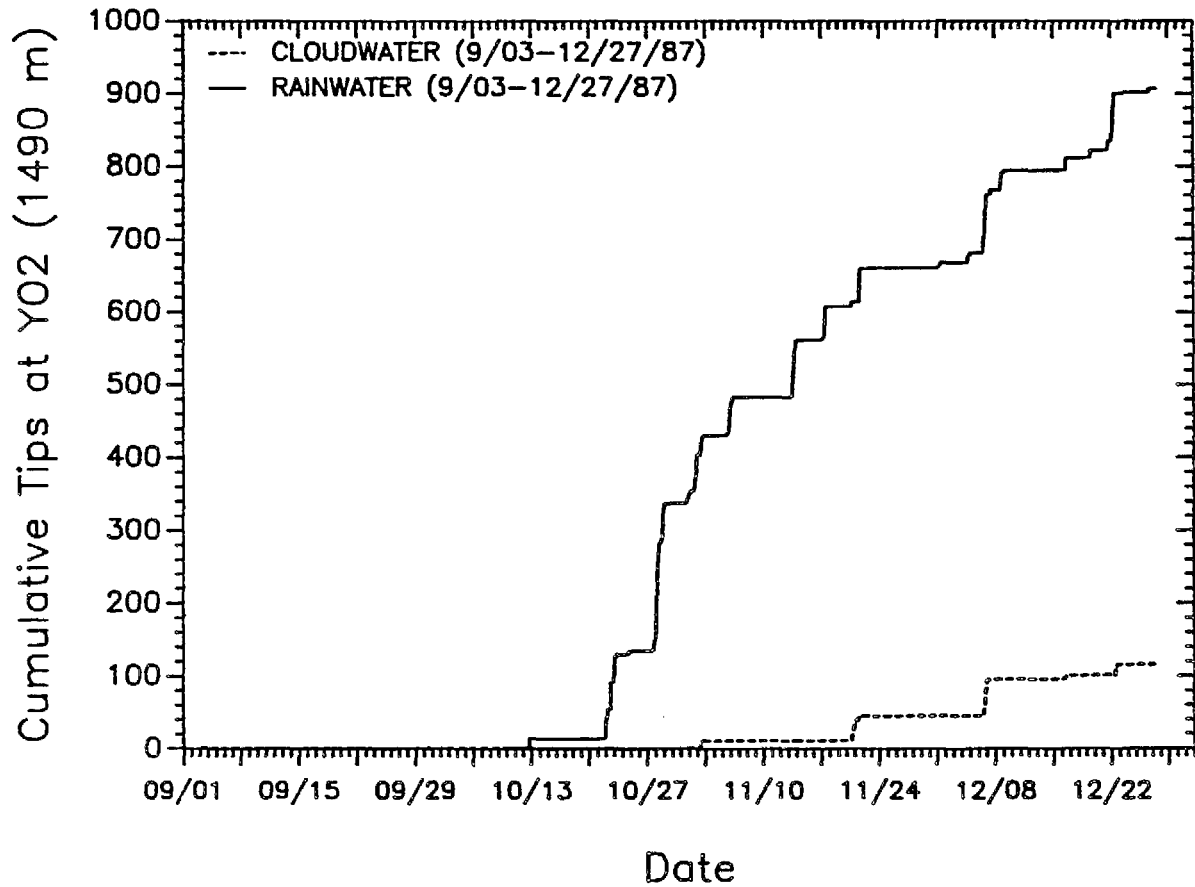


Figure 10. Precipitation and cloudwater deposition at YO2 (elev. 1490 m) during the fall of 1987. Each tip of the rain gauge corresponds to 0.26 mm of precipitation; each tip of the cloudwater gauge corresponds to 0.46 mm of deposited cloudwater.

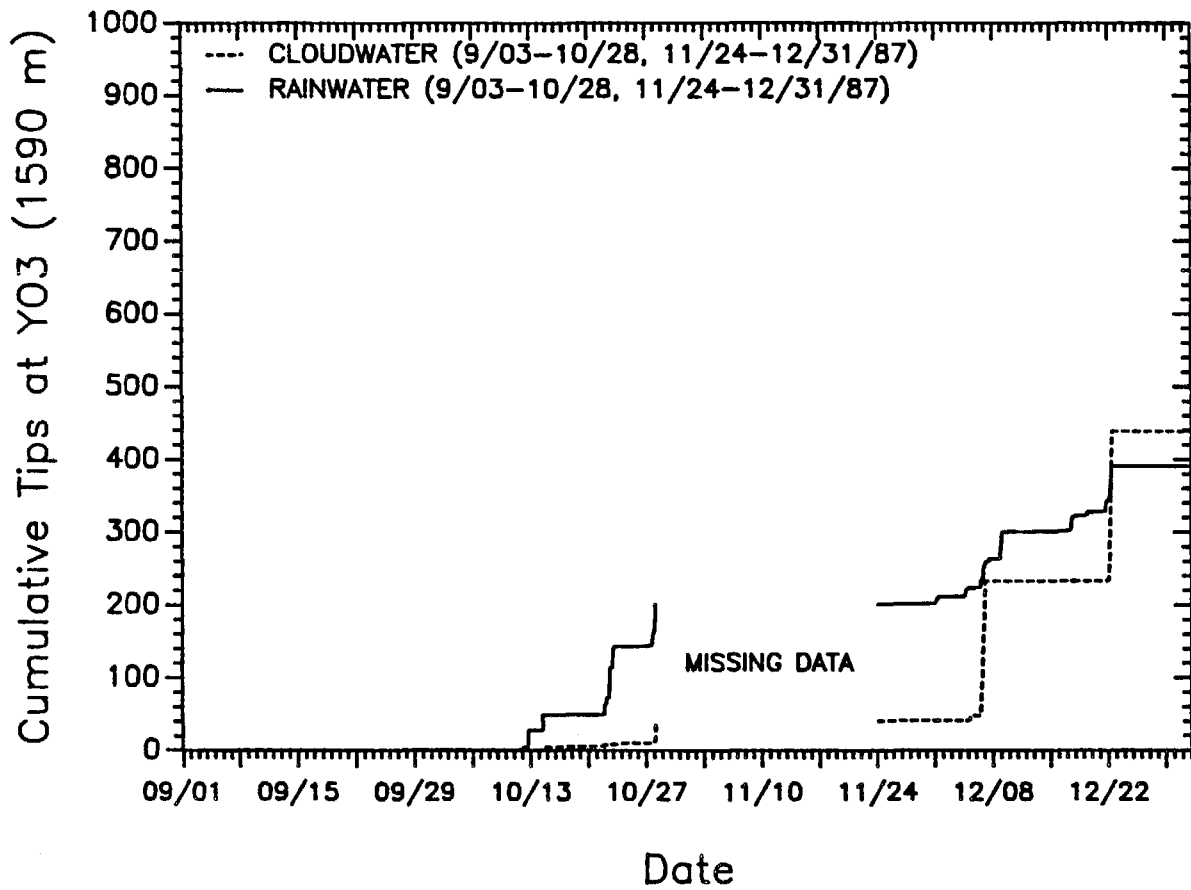


Figure 11. Precipitation and cloudwater deposition at YO3 (elev. 1590 m) during the fall of 1987. Each tip of the rain gauge corresponds to 0.26 mm of precipitation; each tip of the cloudwater gauge corresponds to 0.46 mm of deposited cloudwater.

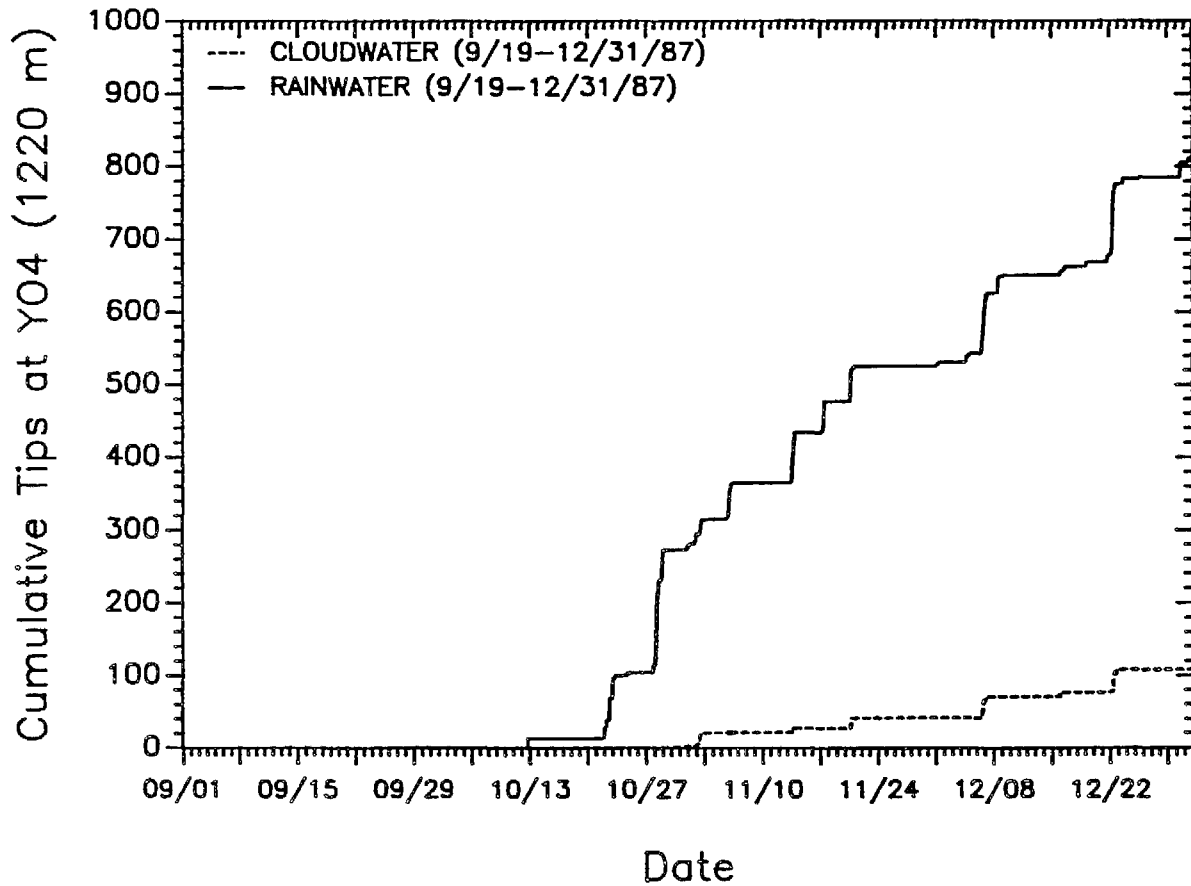


Figure 12. Precipitation and cloudwater deposition at YO4 (elev. 1220 m) during the fall of 1987. Each tip of the rain gauge corresponds to 0.26 mm of precipitation; each tip of the cloudwater gauge corresponds to 0.46 mm of deposited cloudwater.

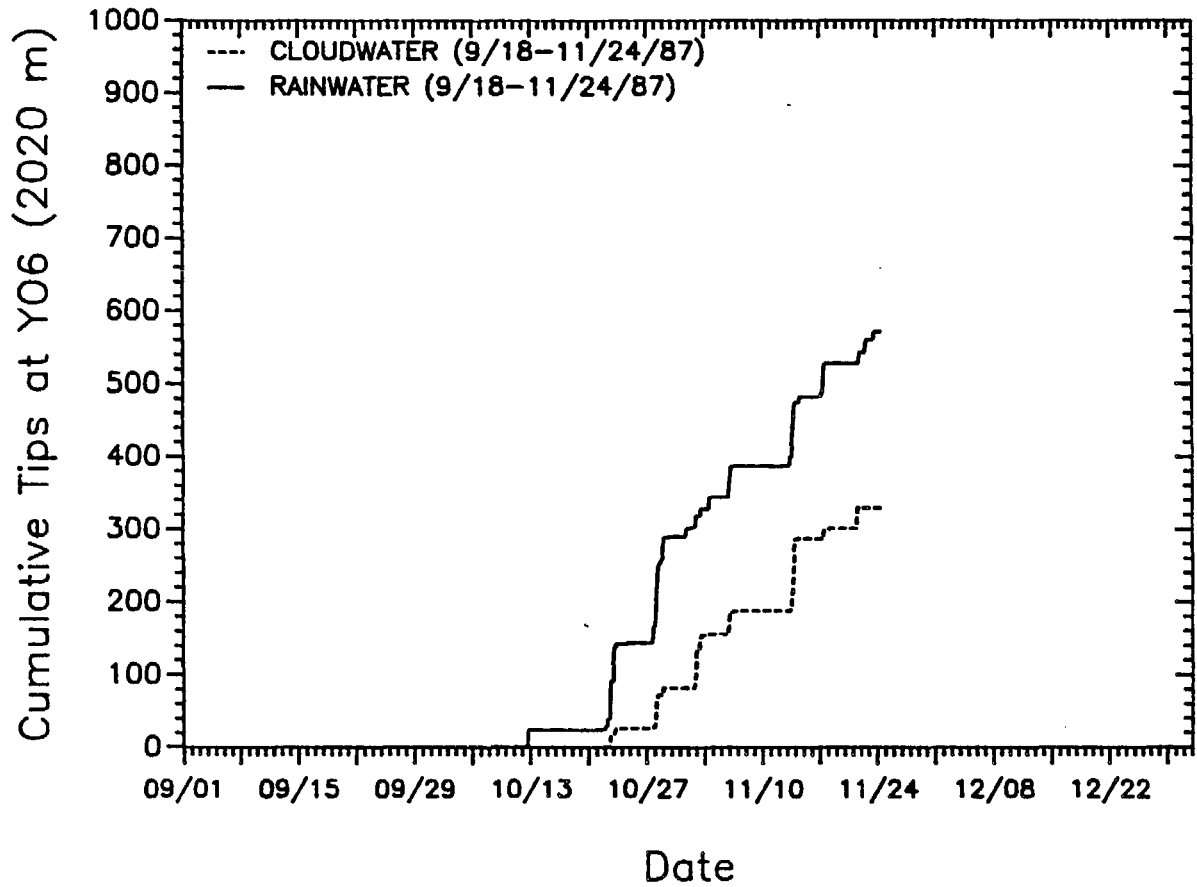


Figure 13. Precipitation and cloudwater deposition at YO6 (elev. 2020 m) during the fall of 1987. Each tip of the rain gauge corresponds to 0.26 mm of precipitation; each tip of the cloudwater gauge corresponds to 0.46 mm of deposited cloudwater.

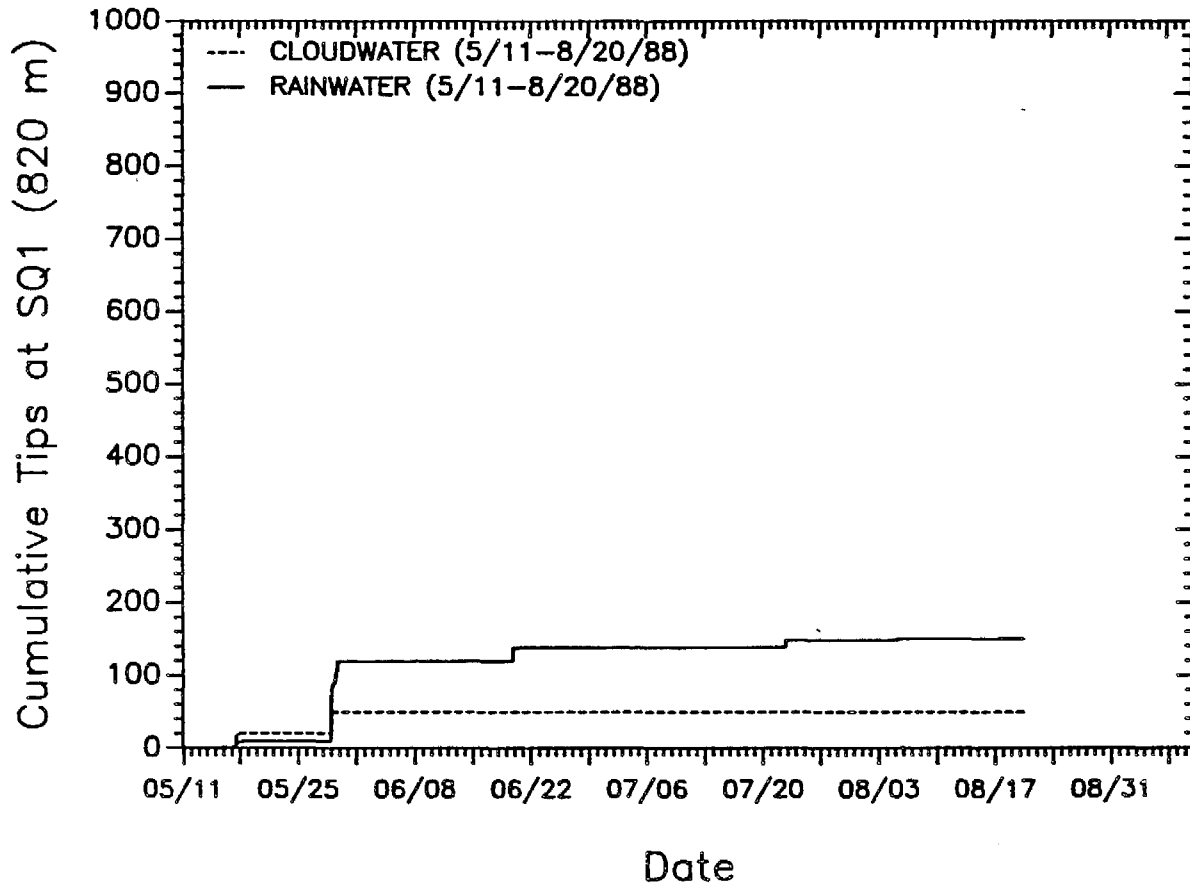


Figure 14. Precipitation and cloudwater deposition at SQ1 (elev. 820 m) during the spring and summer of 1988. Each tip of the rain gauge corresponds to 0.26 mm of precipitation; each tip of the cloudwater gauge corresponds to 0.46 mm of deposited cloudwater.

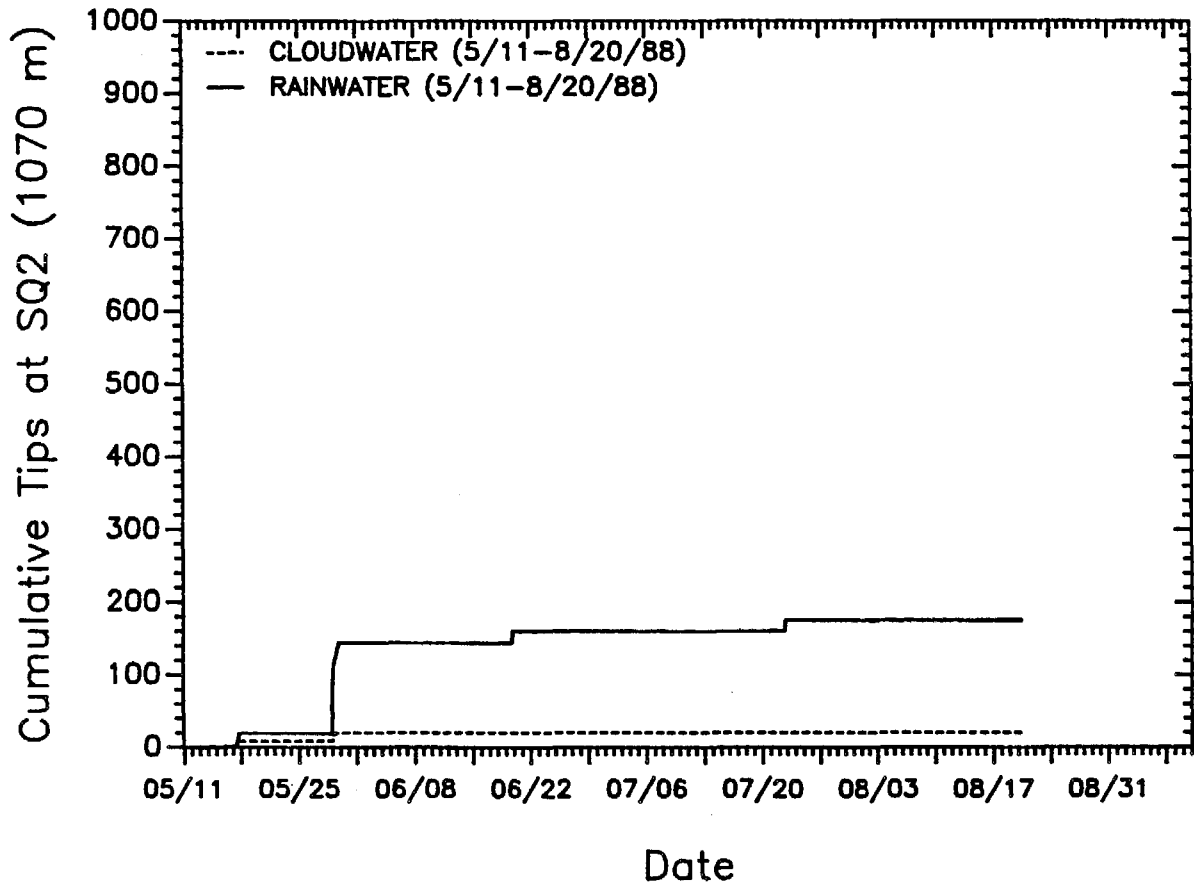


Figure 15. Precipitation and cloudwater deposition at SQ2 (elev. 1070 m) during the spring and summer of 1988. Each tip of the rain gauge corresponds to 0.26 mm of precipitation; each tip of the cloudwater gauge corresponds to 0.46 mm of deposited cloudwater.

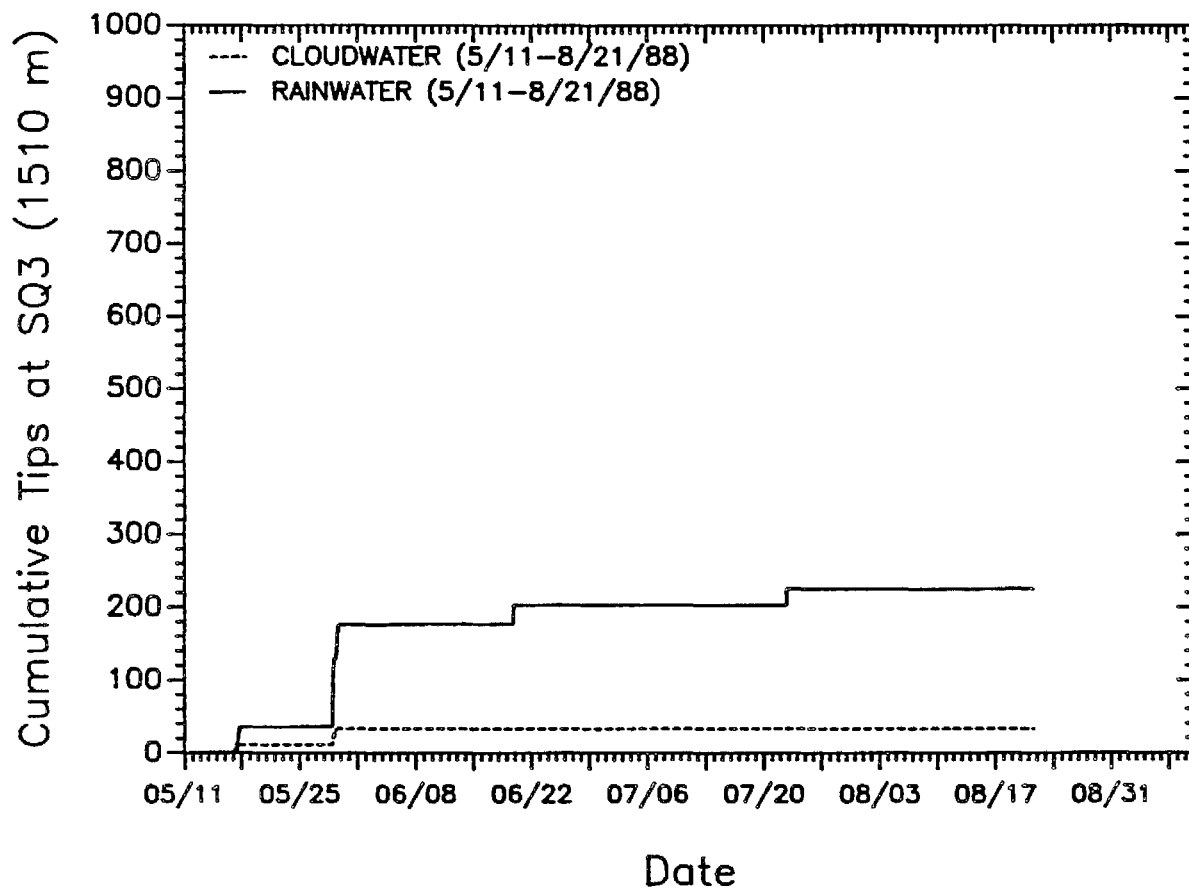


Figure 16. Precipitation and cloudwater deposition at SQ3 (elev. 1510 m) during the spring and summer of 1988. Each tip of the rain gauge corresponds to 0.26 mm of precipitation; each tip of the cloudwater gauge corresponds to 0.46 mm of deposited cloudwater.

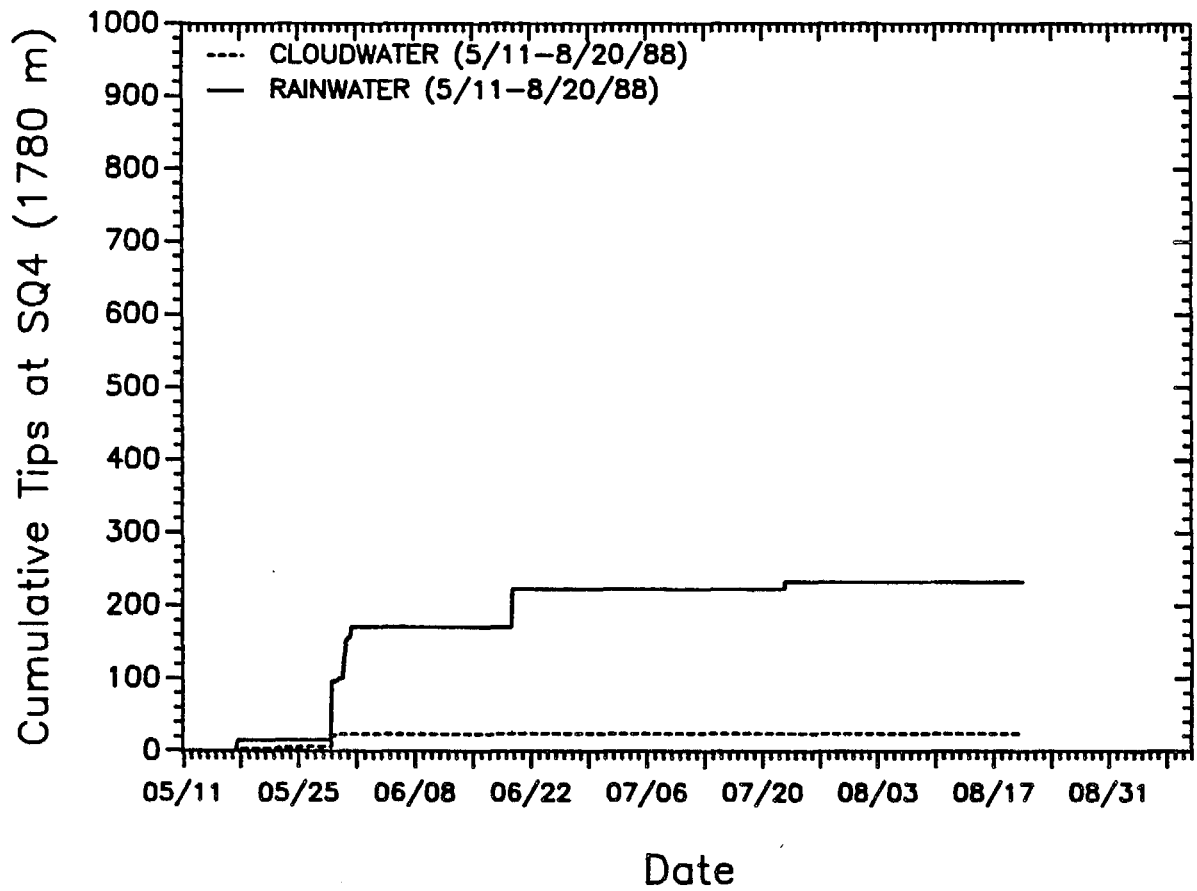


Figure 17. Precipitation and cloudwater deposition at SQ4 (elev. 1780 m) during the spring and summer of 1988. Each tip of the rain gauge corresponds to 0.26 mm of precipitation; each tip of the cloudwater gauge corresponds to 0.46 mm of deposited cloudwater.

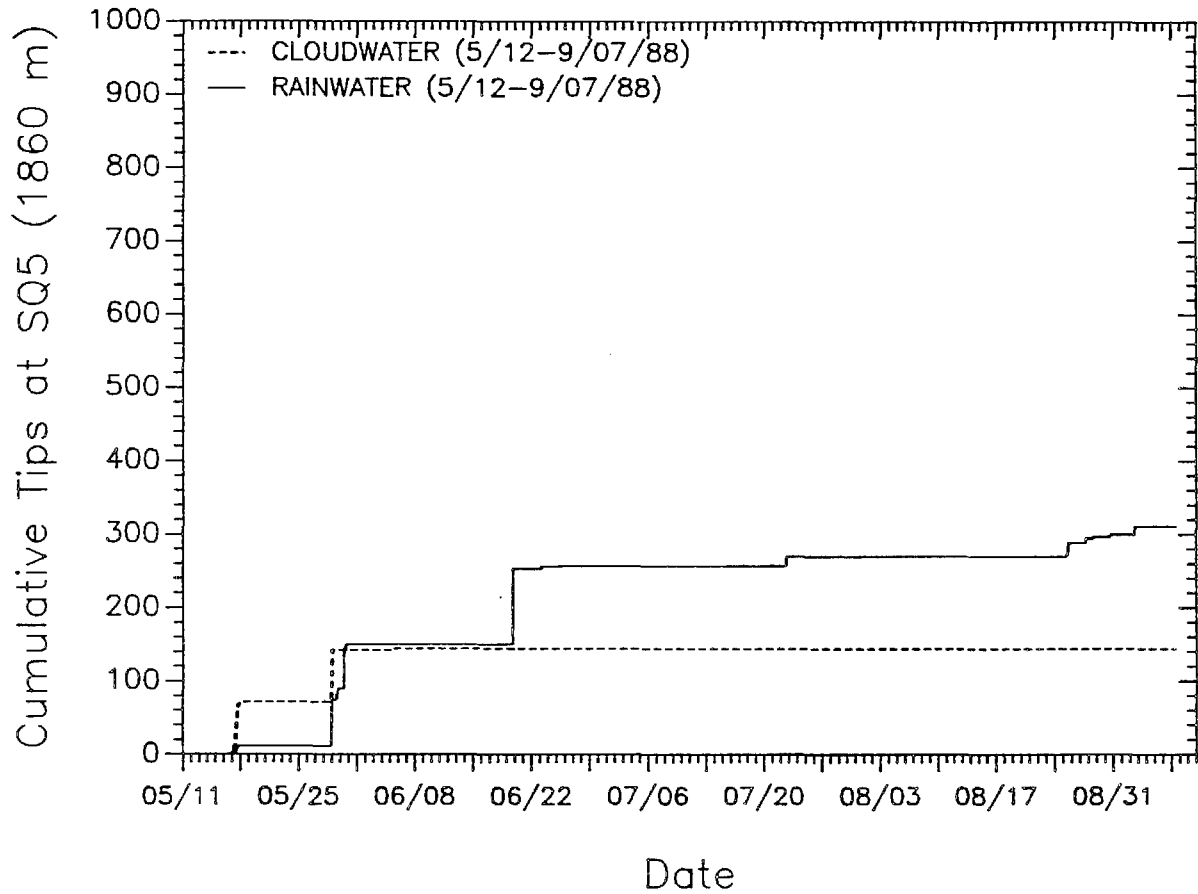


Figure 18. Precipitation and cloudwater deposition at SQ5 (elev. 1860 m) during the spring and summer of 1988. Each tip of the rain gauge corresponds to 0.26 mm of precipitation; each tip of the cloudwater gauge corresponds to 0.46 mm of deposited cloudwater.

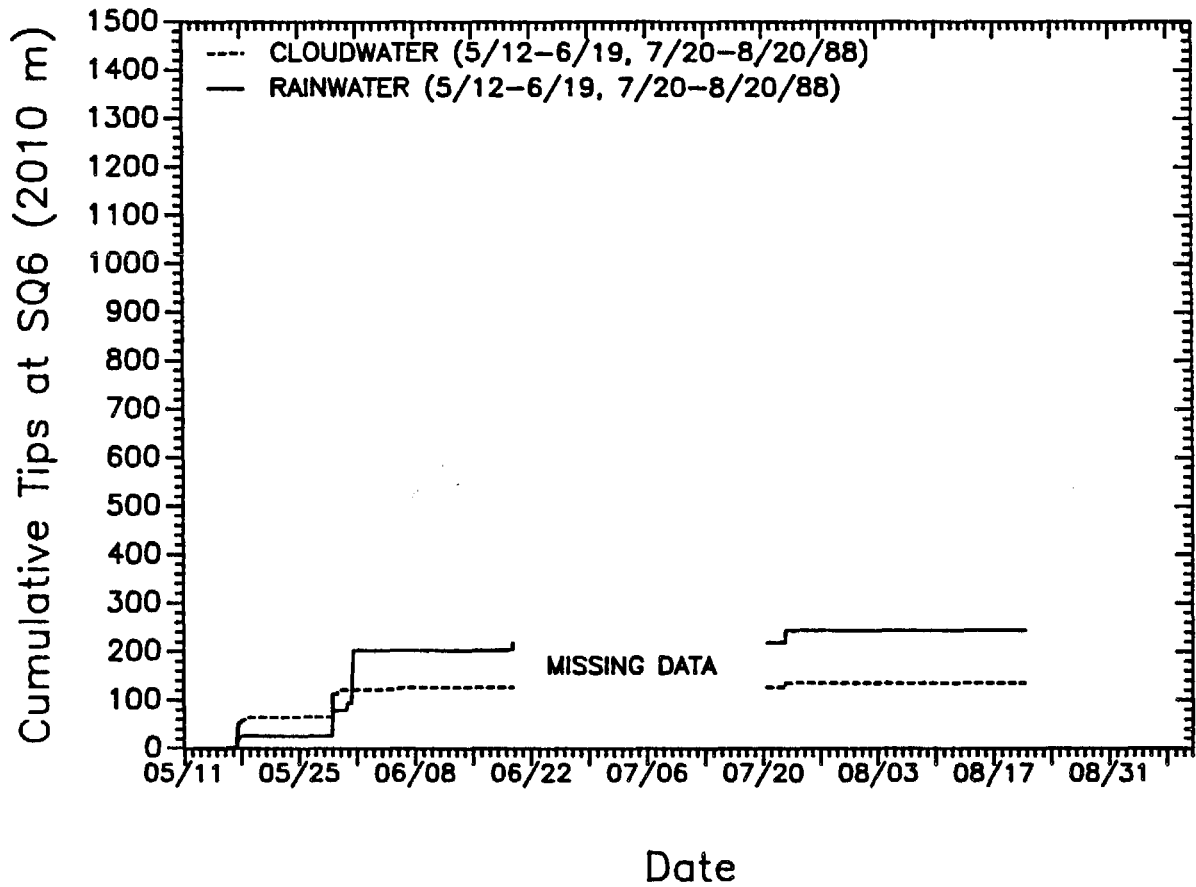


Figure 19. Precipitation and cloudwater deposition at SQ6 (elev. 2010 m) during the spring and summer of 1988. Each tip of the rain gauge corresponds to 0.26 mm of precipitation; each tip of the cloudwater gauge corresponds to 0.46 mm of deposited cloudwater.

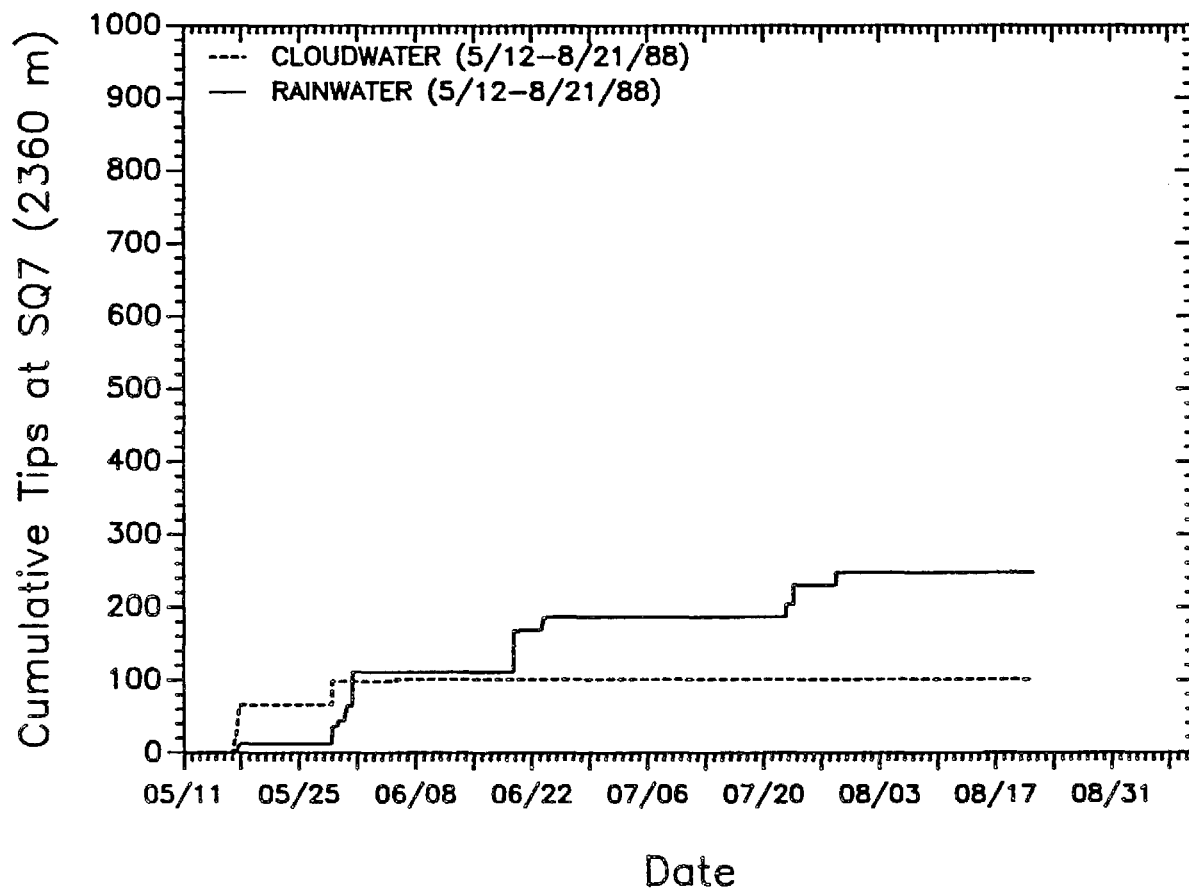


Figure 20. Precipitation and cloudwater deposition at SQ7 (elev. 2360 m) during the spring and summer of 1988. Each tip of the rain gauge corresponds to 0.26 mm of precipitation; each tip of the cloudwater gauge corresponds to 0.46 mm of deposited cloudwater.

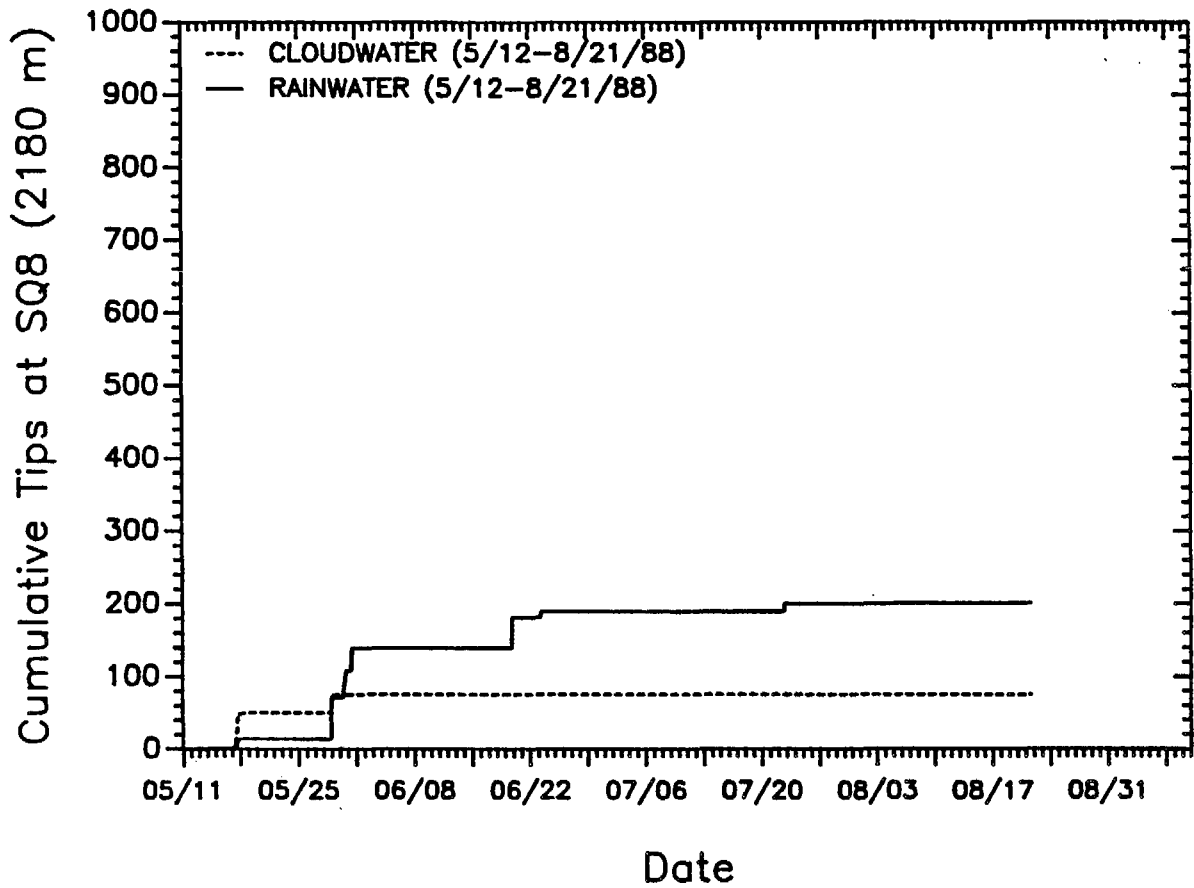


Figure 21. Precipitation and cloudwater deposition at SQ8 (elev. 2180 m) during the spring and summer of 1988. Each tip of the rain gauge corresponds to 0.26 mm of precipitation; each tip of the cloudwater gauge corresponds to 0.46 mm of deposited cloudwater.

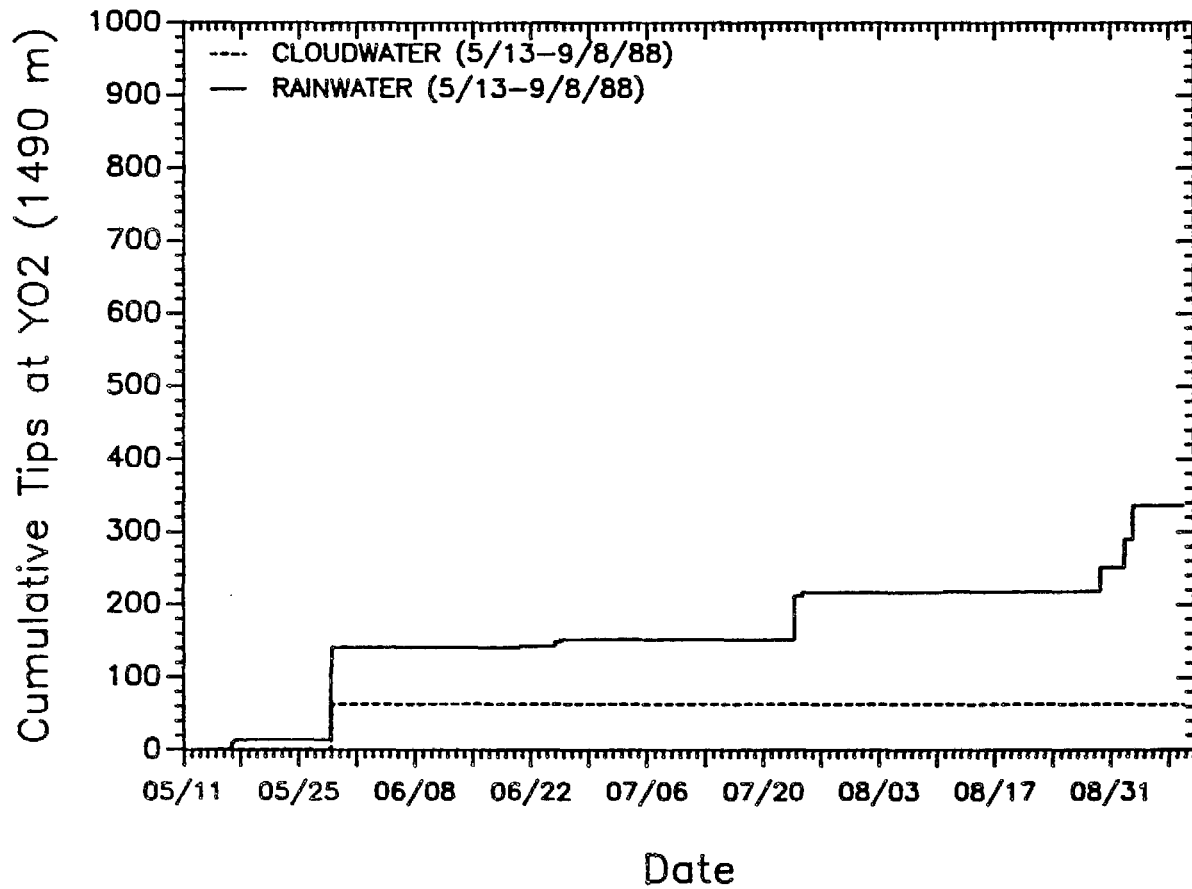


Figure 22. Precipitation and cloudwater deposition at YO2 (elev. 1490 m) during the spring and summer of 1988. Each tip of the rain gauge corresponds to 0.26 mm of precipitation; each tip of the cloudwater gauge corresponds to 0.46 mm of deposited cloudwater.

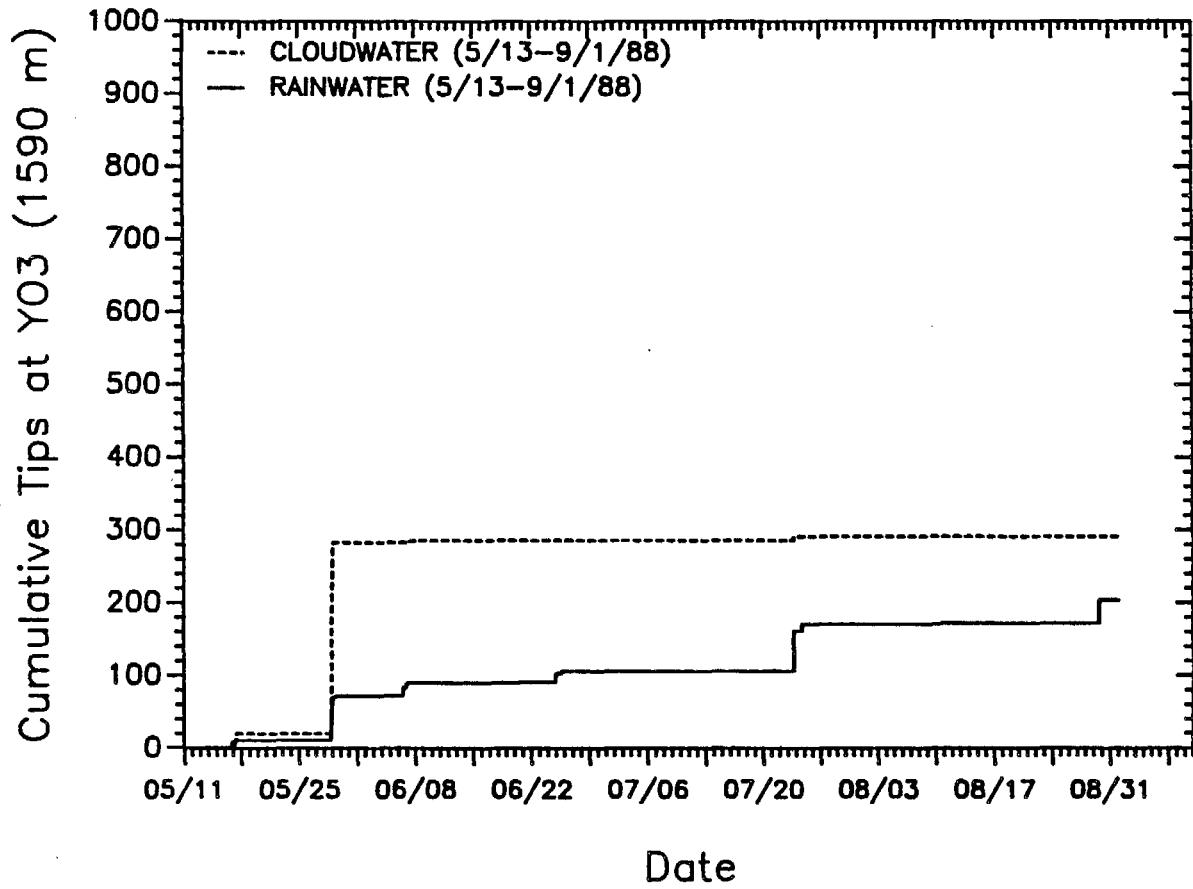


Figure 23. Precipitation and cloudwater deposition at YO3 (elev. 1590 m) during the spring and summer of 1988. Each tip of the rain gauge corresponds to 0.26 mm of precipitation; each tip of the cloudwater gauge corresponds to 0.46 mm of deposited cloudwater.

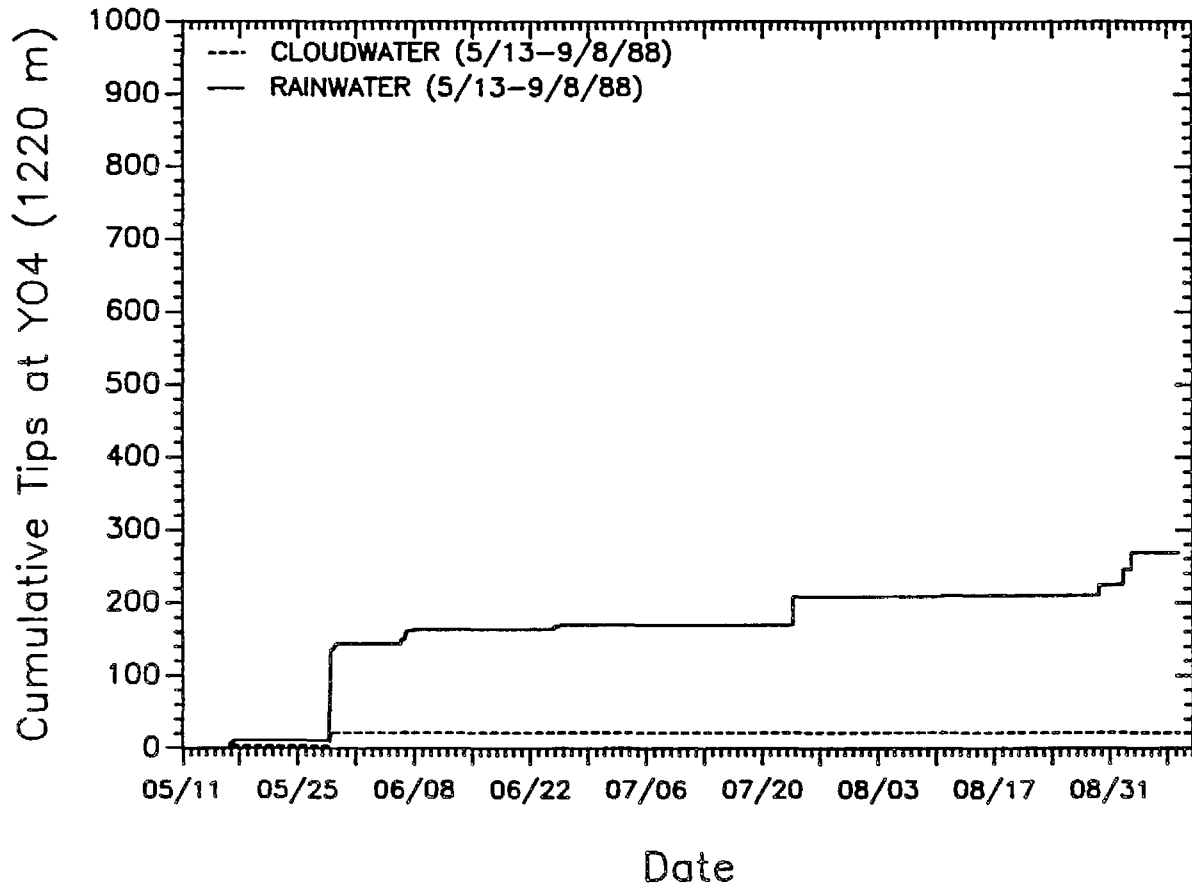


Figure 24. Precipitation and cloudwater deposition at YO4 (elev. 1220 m) during the spring and summer of 1988. Each tip of the rain gauge corresponds to 0.26 mm of precipitation; each tip of the cloudwater gauge corresponds to 0.46 mm of deposited cloudwater.

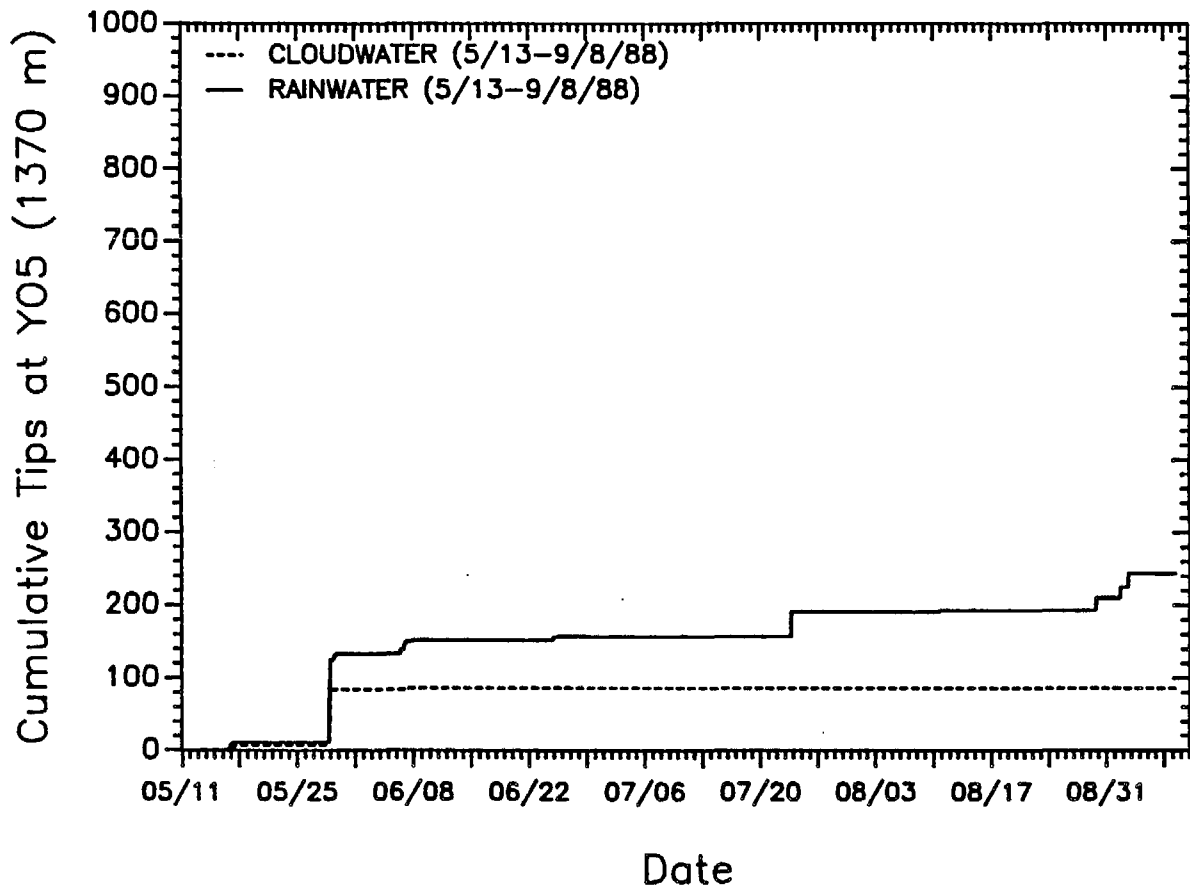


Figure 25. Precipitation and cloudwater deposition at YO5 (elev. 1370 m) during the spring and summer of 1988. Each tip of the rain gauge corresponds to 0.26 mm of precipitation; each tip of the cloudwater gauge corresponds to 0.46 mm of deposited cloudwater.

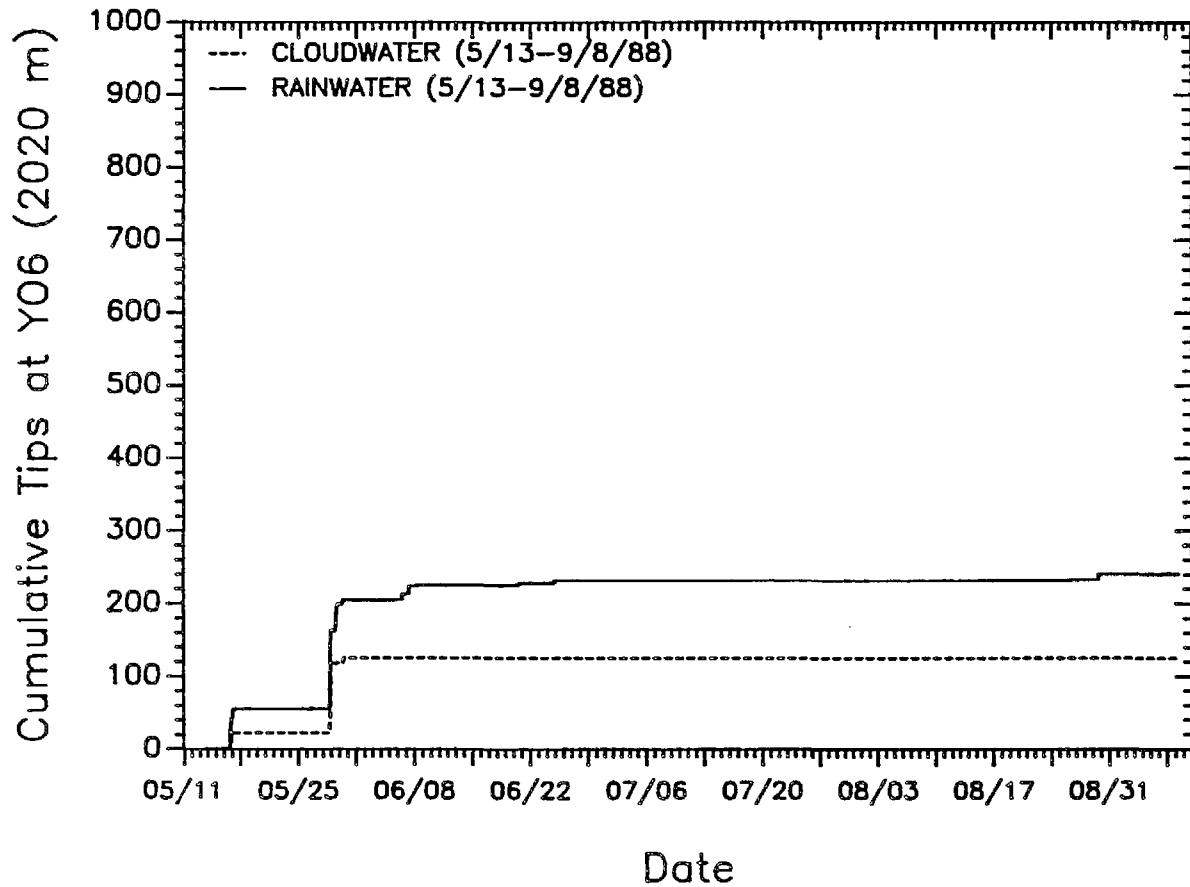


Figure 26. Precipitation and cloudwater deposition at YO6 (elev. 2020 m) during the spring and summer of 1988. Each tip of the rain gauge corresponds to 0.26 mm of precipitation; each tip of the cloudwater gauge corresponds to 0.46 mm of deposited cloudwater.